
[All ETDs from UAB](#)

[UAB Theses & Dissertations](#)

2005

Development of the designer diamond anvils and study of structural and electrical properties of f-electron metals at ultra-high pressures.

Nenad Velisavljevic
University of Alabama at Birmingham

Follow this and additional works at: <https://digitalcommons.library.uab.edu/etd-collection>

Recommended Citation

Velisavljevic, Nenad, "Development of the designer diamond anvils and study of structural and electrical properties of f-electron metals at ultra-high pressures." (2005). *All ETDs from UAB*. 5479.
<https://digitalcommons.library.uab.edu/etd-collection/5479>

This content has been accepted for inclusion by an authorized administrator of the UAB Digital Commons, and is provided as a free open access item. All inquiries regarding this item or the UAB Digital Commons should be directed to the [UAB Libraries Office of Scholarly Communication](#).

DEVELOPMENT OF THE DESIGNER DIAMOND ANVILS AND STUDY OF
STRUCTURAL AND ELECTRICAL PROPERTIES OF f -ELECTRON
METALS AT ULTRA-HIGH PRESSURES

by

NENAD VELISAVLJEVIC

A DISSERTATION

Submitted to the graduate faculty of The University of Alabama at Birmingham,
in partial fulfillment of the requirements for the degree of
Doctor of Philosophy

BIRMINGHAM, ALABAMA

2005

UMI Number: 3201186

INFORMATION TO USERS

The quality of this reproduction is dependent upon the quality of the copy submitted. Broken or indistinct print, colored or poor quality illustrations and photographs, print bleed-through, substandard margins, and improper alignment can adversely affect reproduction.

In the unlikely event that the author did not send a complete manuscript and there are missing pages, these will be noted. Also, if unauthorized copyright material had to be removed, a note will indicate the deletion.

UMI[®]

UMI Microform 3201186

Copyright 2006 by ProQuest Information and Learning Company.

All rights reserved. This microform edition is protected against unauthorized copying under Title 17, United States Code.

ProQuest Information and Learning Company
300 North Zeeb Road
P.O. Box 1346
Ann Arbor, MI 48106-1346

ABSTRACT OF DISSERTATION
GRADUATE SCHOOL, UNIVERSITY OF ALABAMA AT BIRMINGHAM

Degree Ph. D. Program Physics

Name of Candidate Nenad Velisavljevic

Committee Chair Yogesh K. Vohra

Title Development of the Designer Diamond Anvils and Study of Structural and
Electrical Properties of *f*-electron Metals at Ultra-High Pressures

There is great interest in developing a method that can be used to perform multiple measurement tasks at static high pressures, because of the close relationship between the changes in electrical and structural properties of many materials. Designer diamond anvils, used for electrical resistance measurements, have electrical microprobes built into the diamond so they do not interfere with x-ray diffraction experiments. In order to test and develop these anvils, electrical resistance measurements were performed on three test samples, GaAs, CsI, and CsCl, using a diamond anvil cell. The first experiment showed that the electrical resistance of GaAs decreases by more than six orders of magnitude at 17 GPa, which is reversible during decompression, and offers a convenient way of testing each designer diamond anvil prior to performing additional experiments. CsI and CsCl were used to test anvils above 100 GPa. Under applied pressure, both samples were observed to have a continuous decrease in electrical resistance as the proposed metallization pressures of 115 GPa and 280 GPa, respectively, was approached. These experiments show that the mechanical strength of the designer diamond anvils is not compromised by having the microprobes embedded into the diamond.

This technology was also applied for studying light lanthanide metals Pr and Nd. Electrical resistance measurements showed an abrupt drop of 53% at 20 GPa in Pr and a

continuous decrease of 38% between 100-152 GPa in Nd. Simultaneous electrical resistance and energy and angle dispersive x-ray diffraction experiments showed that this change occurred as Pr and Nd underwent a phase transition to an α -U structure. Observation of this structure in Pr and Nd has long been suspected of indicating a localized→delocalized change in the 4*f*-electrons. In addition to the change in electrical resistance at 20 GPa in Pr, another change was observed at 150 GPa and was shown to be a result of another phase transition to a primitive orthorhombic structure (space group $P2_12_12_1$), which is stable up to at least 313 GPa. These studies demonstrate the close connection between the electrical transport properties and the crystal structures at the 4*f*-shell delocalization in lanthanide metals.

DEDICATION

To my wife, Ivanka, my daughter, Natalija, and my parents, Filip and Snežana.

ACKNOWLEDGEMENTS

First and foremost, I would like to thank God for always looking over my family and for giving me the opportunity to meet and work with some wonderful people throughout my graduate study. As a result I have learned a great deal and hope that I will be able to pass this knowledge on to others as generously as it has been passed on to me.

Whatever I have chosen to do in my life my family has always been there for me. I am grateful to my father, Filip, for teaching me many important things about life and for always making sure that I was never absent from school or work. I thank my mother, Snežana, for her unconditional love and support, and for all of the sacrifices she has made for me and my sisters. My wife, Ivanka, has encouraged me and supported me from the day I met her, and I will continue to do the same for her as she strives toward reaching her goals in life, as well. Regarding my daughter, Natalija, all I can say is that there has not been a happier day in my life than the day she was born. Although I cannot name all of my family here, I would just like to say to them: Thank you for all that you have done for me.

I would like to thank all of the members of the UAB physics faculty who have helped me over the years, especially my thesis adviser, Professor Yogesh K. Vohra. I have never met a more caring person. Some the best times I have had in graduate school are those when Professor Vohra and I worked together at the synchrotron sources. He is a tireless worker who leads by an example, and I thank him for constantly teaching and

encouraging me. Along with Professor Vohra, I would also like to thank Professor Krishan K. Chawla, Professor Joseph Harrison, Professor Murli H. Manghnani, and Dr. Gary N. Chesnut for willing to share their time and expertise while serving on my thesis committee.

I thank Mr. Jerry Sewell for his help and diligence in making many of the tools used in my experiments. I am likewise grateful for all of the help and support that I have received from the present and former students, too many to name here, who have worked in our research group. I especially thank Paul Baker for his dedication to the designer diamond anvil project. Thanks go to the office staff for all of their help and patience.

Last, but certainly not least, I thank all of the hard-working taxpayers and the National Science Foundation (NSF) Division of Materials Research-Metals Program for supporting this research, under Grant No. DMR-0203779. Research was conducted (in part) at the National Synchrotron Light Source, Brookhaven National Laboratory, which is supported by the U.S. Department of Energy, Division of Materials Sciences and Division of Chemical Sciences, and at the Advanced Photon Source, Argonne National Laboratory, which is supported by the U.S. Department of Energy, Office of Science, Office of Basic Energy Sciences, under Contract No. W-31-109-ENG-38.

TABLE OF CONTENTS

	<i>Page</i>
ABSTRACT.....	ii
DEDICATION.....	iv
ACKNOWLEDGMENTS	v
LIST OF TABLES	ix
LIST OF FIGURES	x
LIST OF ABBREVIATIONS.....	xiii
INTRODUCTION	1
INSTRUMENTATION AND TECHNIQUES.....	6
Introduction.....	6
Diamond Anvil Cell.....	8
DAC design.....	9
Diamond anvil selection and alignment.....	11
Experimental preparation.....	14
Pressure measurement.....	17
X-Ray Diffraction	18
Synchrotron x-ray source.....	21
Energy dispersive x-ray diffraction	23
Angle dispersive x-ray diffraction	25
Data analysis	28
Designer Diamond Anvils.....	30
Fabrication	31
Application for electrical resistance measurements.....	33
Comparison to traditional technique.....	38
Interpreting electrical resistance measurements	40
Summary	41
RARE EARTH METALS.....	42

LIST OF TABLES

<i>Table</i>		<i>Page</i>
1	The pressure gradient measured over the CsI sample at various pressures by ruby fluorescence technique	66
2	Summary of six high-pressure experiments on Pr, documenting the electrical resistance drop at 20 GPa.....	81

LIST OF FIGURES

<i>Figure</i>	<i>Page</i>
1	Schematic of a sample compressed in a diamond anvil cell.....7
2	Design of diamond anvil cell used at the University of Alabama at Birmingham10
3	The elastic scattering of X-rays by crystallographic planes having interplaner spacing d20
4	Insertion device used by third-generation synchrotron sources, like the Advanced Photon Source at Argonne National Laboratory in Chicago22
5	Illustration of energy dispersive x-ray diffraction in a diamond anvil cell.....24
6	ADXRD spectra of CeO ₂ calibration standard, collected by an image plate detector.....27
7	Two types of designer diamond anvils; the one on the left side is used for electrical resistance measurements and the one on the right side is used for magnetic measurements32
8	Close-up view of the designer diamond anvil used for electrical resistance measurement34
9	External electrical leads attached to the microprobes at the base of the designer diamond anvil, using a conductive two-step epoxy35
10	Crystal structures exhibited by various rare earth metals at ambient pressures44
11	Six-probe designer diamond anvil used in the GaAs experiment.....53
12	Change in electrical resistance of GaAs during compression and subsequent decompression.....55
13	Change in the appearance of GaAs when viewed under a microscope with a normal illumination.....58

LIST OF FIGURES (Continued)

<i>Figure</i>	<i>Page</i>
14	Reversible change in the reflectivity of GaAs viewed under a microscope in normal illumination.....59
15	Result of two compression cycles of GaAs. In both cases, a large decrease is observed in electrical resistance above 15 GPa during compression60
16	CsI in transmitted light at ambient conditions in a diamond anvil cell64
17	Change in the electrical resistance of CsI under applied pressure.....67
18	CsI in transmitted light at $P_C = 35.6$ GPa and $P_{OC} = 38.4$ GPa69
19	CsI in transmitted light at (a) $P_C = 48.3$ GPa and $P_{OC} = 54.2$ GPa and (b) $P_{OC} = 77.3$ GPa71
20	Six-probe designer diamond anvil used for the CsCl experiment73
21	Change in electrical resistance of CsCl with increasing compression load angle measured using various probe combinations, as indicated74
22	Photomicrograph of the Pr sample in an eight-probe designer diamond anvil, with the direction of the current (I) flow and polarity of the voltage (V) leads of four-probe configuration79
23	Electrical resistance of Pr during compression up to 179 GPa, observed in experiment 6.....82
24	Electrical resistance measured during decompression cycle of experiment 183
25	The copper pressure-volume equation of state (EoS) used in pressure measurements in this thesis.....86
26	Energy dispersive x-ray diffraction pattern of Pr sample and a Cu pressure marker at various pressures to 313 GPa.....88
27	The energy dispersive x-ray diffraction pattern for the Pr sample and Cu pressure marker at 158 GPa ($2\theta = 13^\circ$), in an extended energy range89
28	Distortion of α -U structure, indicated by the blue and black arrows, that leads to a new structure $P2_12_12_1$ above 147 GPa91

LIST OF FIGURES (Continued)

<i>Figure</i>	<i>Page</i>
29	Change in the interplaner spacing, d_{hkl} , of the $P2_12_12_1$ structure of Pr with increasing pressure, in the range of 155-315 GPa92
30	Linear compression of the three axes of the $P2_12_12_1$ phase, a/a_0 , b/b_0 , and c/c_0 , normalized to lattice parameters at 158 GPa.....93
31	Anisotropic compression of b-axis and c-axis leading to almost equal value above 260 GPa94
32	The pressure-volume curve of Pr in the 155-315 GPa range.....96
33	ADXRD spectra ($\lambda = 0.3683 \text{ \AA}$) of Nd showing the C2/m and α -U phases at 100 GPa and 118 GPa, respectively.....101
34	Development of α -U structure of Nd above 100 GPa, as indicated by a continuous increase in the peak intensity of the (111) peak of this structure ($\lambda = 0.3683 \text{ \AA}$).....103
35	Change in electrical resistance of Nd metal with increasing pressure, showing a gradual decrease of 38% in the pressure range between 100 GPa and 153 GPa.....105
36	Observed changes in the intensity of the (111) and (021) peaks of the α -U phase of Nd with increasing pressure106
37	Change in the y-positional parameter of the α -U phase of Nd108

LIST OF ABBREVIATIONS

ADX	Angle Dispersive X-Ray Diffraction
DAC	Diamond Anvil Cell
EDX	Energy Dispersive X-Ray Diffraction
EoS	Equation of State
GPa	Giga-Pascal
P-V	Pressure-Volume
RTP	Room Temperature-Pressure

INTRODUCTION

High-pressure research may be classified into two separate, but not all together independent, fields. The classification of the two as dynamic and static is based on the experimental techniques used to generate pressure and the time scale of compression. A dynamic high-pressure field is based on generating a shock wave, using such methods as high explosives, lasers, and pulsed magnetic fields, and studying the propagation of the wave through a substance.¹ Pressure generated by dynamic methods is substantially larger than what one may obtain using static methods, but at the expense of having a much shorter observation time and accompanying heating of the sample during the shock compression process. The static pressure generation technique relies on an opposing anvil design to “squeeze” a sample and thus observe structural and other changes associated with increases in sample density.² There are various instrument designs for static pressure generation, such as the large anvil press, the sapphire anvil cell, and the diamond anvil cell (DAC). All of the high-pressure experiments presented in this thesis were performed with a DAC. The mechanical properties of diamonds, the advantage of using them as the anvils, and various aspect of DAC design will be described in more detail.

In 1959 DAC was first applied for generating static high pressure.^{3,4} Since then, due to a number of successive improvements and the development of new and innovative techniques for studying a wide range of material properties, DAC has become the most widely used tool for static high-pressure experiments. Although DAC has only been

around for about 45 years, the importance of pressure as a thermodynamic variable was realized much earlier. In 1660 Robert Boyle declared that “perhaps the pressure of the air might have an interest in more phenomena than men have hitherto thought” in his famous treatise *Touching the Spring of the Air*, and in the early 1900’s the first experimental evidence was produced by Percy Bridgman at Harvard University that showed drastic changes occurring in condensed matter at high pressure. Bridgman won the Nobel Prize in physics for his work and thus paved the way for the growth and development of high-pressure research.

The Bridgman era was dominated by the Bridgman anvil and piston-cylinder devices, which were developed for electrical resistance and compressibility measurements up to 100 kilobar pressure, where $1 \text{ bar} = 10^5 \text{ Pascal (Pa)} = 0.9869 \text{ atmosphere (atm)}$. The introduction of diamonds as anvils in the design of DAC allowed this pressure range to be significantly increased. Diamond is the hardest known material, with a high shear strength and the capability to sustain large pressures, which is a special case of generalized stress. In 1959 DAC was used to achieve pressures of up to 10 GigaPascal (GPa), where $1 \text{ GPa} = 10^9 \text{ Pa}$. In the years since, with the introduction of the metal gasket to contain the sample, the perfect alignment of the anvils, and the introduction of the beveled anvil, achievable pressure has increased to over 400 GPa.⁵ Besides the modifications that needed to be made to the DAC in order to achieve and study materials at ultra-high pressures, techniques for probing material properties at these conditions have also been a limiting factor.

Pressure is defined as force per unit area, and in order to achieve ultra-high pressures one needs to either decrease the area, i.e., the contact area of the anvils, or increase

the applied force. In theory high pressure may be achieved by either increasing the force or decreasing the contact area, without preference for one over the other. However, increasing pressure in a laboratory is much harder to achieve by increasing the force than by decreasing the diamond anvil contact area. As a result the maximum pressure using DAC has been achieved by decreasing the contact area. A decrease in the contact area ultimately determines the sample volume that may be studied experimentally. In general the contact area of a 200- μm diameter tip, where $1 \mu\text{m} = 10^{-6} \text{m}$, would result in a maximum pressure of about 100 GPa. By decreasing the flat to 35 μm in diameter and going to beveled diamond geometry, one may obtain pressures of 300 GPa and above. At the same time the sample volume of 50 μm in diameter and 20 μm thickness would be reduced to 20 μm in diameter and 5 to 10 μm thickness when going from a 200- μm -tip anvil to a 35 μm tip. Due to the small sample volume, the majority of the performed experiments, and what is understood about material properties at high pressure, has been the result of x-ray diffraction and micro-optical spectroscopy studies. These techniques have produced valuable information about phase transformation, pressure-volume relation, and other sample characteristics as a function of pressure; however, information about low temperature-high pressure superconductivity or the predicted insulator metal transition in many materials has been harder to obtain. One of the major obstacles, as mentioned earlier, is the sample geometry. In order to perform electrical resistance measurements one would have to connect at least two electrical probes to the sample. However, in most cases this is not sufficient either, since the resistance of a metallic sample for example is usually on the order of milliohms, where 1 milliohm ($\text{m}\Omega$) = 10^{-3} Ohm (Ω), and as a result one would need at least four probes so that the four-probe elec-

trical resistance method may be used. In the last decade a collaborative project between the University of Alabama at Birmingham and Lawrence Livermore National Laboratory has produced what has been termed as the designer diamond anvil.⁶ With this technique the electrical probes, which are used to perform electrical resistance and magnetic susceptibility measurements as well as Ohmic heating, are embedded into the diamond. This technique is still new, and therefore the development and testing of designer diamond anvils for constantly performing measurements at ultra-high pressures will be the subject of the first half of this study.

The drive to develop a technique for reliably measuring electrical properties of materials at ultra-high pressures has been going on since the first application of DAC. When subject to external pressure, which increases the inter-atomic interaction, many materials exhibit a rich phase diagram, large volume changes, and considerable change in electrical conductivity.⁷ These are usually not independent of each other, but rather the observed change in one property may go hand in hand with another. However, due to the difficulty of observing and experimentally measuring many of these changes, we are still unable to conclusively describe many of the material properties at high pressures.

One prime example is the lanthanides, more commonly referred to as the rare earth metals. Both $4f$ -electron metals (lanthanides) and $5f$ -electron metals (actinides) have received attention from the high-pressure community as well as theoretical physicists. Rare earths are of particular interest because of their f -shell electrons, which are considered localized and noncontributing to the bonding and formation of room temperature-pressure (RTP) structures.⁸ Under applied pressure it has been predicted, based on the observation of low symmetry crystal structure by x-ray diffraction techniques, that

these electrons become delocalized and thus start participating in bonding. Furthermore, the localized→delocalized f -electron change is also expected to contribute to the number of electrons in the conduction band and therefore significantly increase the electrical conductivity. Still, up till now, no direct evidence has been produced to confirm this. The invention of designer diamond anvils, with the ability to conduct four-probe electrical resistance measurements, may be the perfect tool to measure over this pressure range and study changes in electronic behavior.

After concentrating on the development of designer diamond anvils for ultra-high pressure electrical resistance measurements, the remainder of this study will be dedicated to experiments carried out in order to gain a better understanding of the f -electron metals at high pressures.

INSTRUMENTATION AND TECHNIQUES

Introduction

The continuous development of new experimental techniques and successive improvements made to the DAC, since it was first applied over 50 years ago has made it the most widely used tool for generating static high pressure. Initially only capable of pressures up to 10 GPa or less, today that mark has been increased by more than an order of magnitude. The main parts of the DAC are the two diamond anvils, which compress a metal gasket with a hole in which a sample is placed (Fig. 1). Due to being the hardest known material and having transparency over a wide spectral range, diamond is suitable for generating large pressures while still allowing many material properties to be studied. Initially designed for x-ray powder diffraction³ and infrared absorption measurements⁴, today there are multiple designs of DAC in use. Some of these are the Piermarini and Block,⁹ Mao and Bell,¹⁰ Merrill and Bassett,¹¹ and Syassen-Holzapfel.¹² The cells are designed for performing such experiments as energy and angle dispersive x-ray diffraction, single crystal diffraction, Brillouin scattering, Raman spectroscopy, and neutron scattering, as well as for application at low and high temperatures. At the University of Alabama at Birmingham, the DAC used is a variation designed for achieving maximum pressures over 300 GPa. This design also allows for easy integration of designer diamond anvils, used for electrical resistance measurements, as well as the use of energy and angle dispersive x-ray diffraction for high-pressure crystallographic experiments. In the

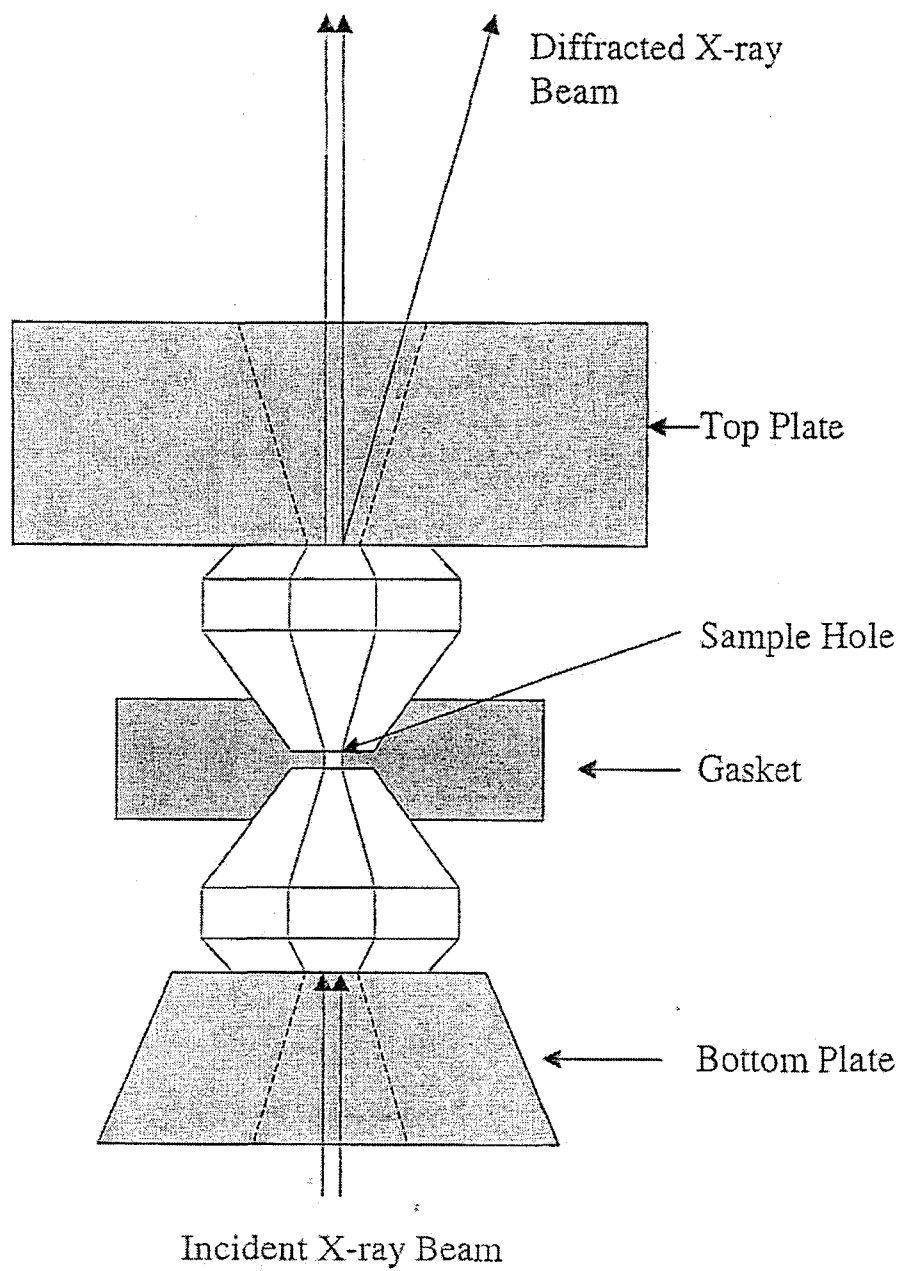


FIG. 1. Schematic of a sample compressed in a diamond anvil cell.

following sections these techniques, their application, and the design of DAC will be described in more detail.

Diamond Anvil Cell

There are a number of important improvements made to DAC design over the last 50 years that have significantly increased the range of static pressures. In the initial application of DAC, the sample was compressed directly between the two anvils. Under applied pressure the sample was not well contained and would squeeze out, resulting in the two anvils coming into contact and breaking at relatively modest pressures. In order to address this problem, a metal gasket, which sits between the two anvils and has a drilled hole for containment of the liquid or solid sample (Fig. 1), was introduced.² Use of the metal gasket was the first major improvement and has played an important role in the evolution of DAC. Not only does it serve as a chamber for sample containment, but it also prevents the anvils from making contact and breaking at low pressures. Following the introduction of metal gasket, an adjustment to the alignment of the anvils was made.¹³ The two anvils are aligned such that the flat of one anvil is overlapping and parallel with the flat of the opposing anvil. The modification to the alignment and use of metal gasket has extended the achievable pressure up to 40 GPa. Other significant improvements, such as the calibration of the ruby pressure gauge¹⁴ and the use of methanol-ethanol hydrostatic medium,¹⁵ followed. Both of these inventions are significant in that the pressure may easily and accurately be determined by measuring ruby fluorescence, while the methanol-ethanol mixture provides hydrostatic conditions up to 10 GPa, but major increase in achievable pressure did not come about until 1978 when the beveled anvil was

first introduced.¹⁶ A beveled anvil is designed so that there is an additional angle between the edge of the flat and the pavilion. At high pressures, the anvils deform in a concave manner, leading to increased stress near the edges. By beveling the edges the stress is reduced, allowing for pressures as high as 400 GPa to be achieved.⁵ It is important to note that all of the improvements described are not unique to any of the DAC designs, but are implemented in all of the DACs in order to achieve and sustain high pressures.

In the following sections we will describe the DAC in greater detail and how the described modifications, from the metal gasket all the way to the beveled anvil, played a role in our experiments. In addition, designer diamond anvil technology will also be described. The invention of the designer diamond anvil may be considered as the latest significant contribution to the development of static high-pressure research.

DAC Design

The version of DAC used at the University of Alabama at Birmingham (Fig. 2) is designed for achieving ultra-high pressures and has been used for experiments above 300 GPa. The primary components are the diamond anvils, which are mounted with a two-part epoxy onto hardened M4 tool steel backing plates. The top plate is then secured to the support plate by two vertical 3/8-in. cap screws. In addition to the two larger screws, there are also four smaller screws that run through the top of the support plate and contact the top of the top plate. These four screws are used for adjusting the parallel alignment of the anvils by the tilting of the top plate, as described in the following paragraphs. The bottom backing plate, which is in the shape of a pyramid, sits in a recess on the top of the piston. The pyramid plate is secured by four screws that provide translational alignment.

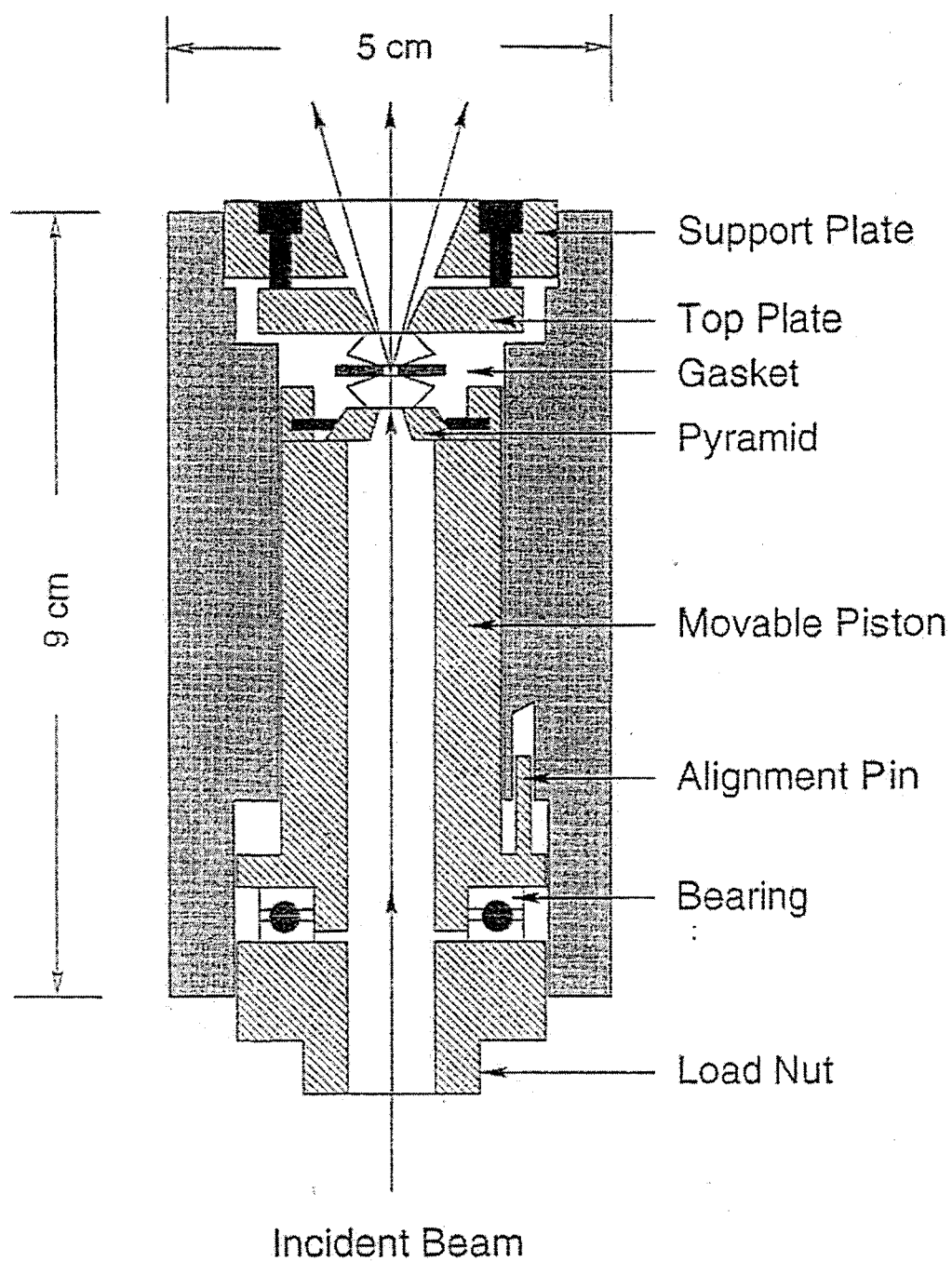


FIG. 2. Design of diamond anvil cell used at the University of Alabama at Birmingham.

The top and bottom backing plates have a hole drilled at the center. The top backing plate hole is aligned with the opening in the support plate, while the bottom backing plate hole is aligned with the opening that runs along the length of the piston. The holes are used as a window to the sample and allow for x-ray, laser, and visible light to be passed to the sample. When the DAC is assembled, the tolerance between the piston and the body of the DAC must be minimized, usually to less than $5\ \mu\text{m}$, in order to avoid the shifting of the anvils at high pressures. The piston is guided by the alignment pin, which allows for the piston to be removed and placed back in a reproducible manner. It also prevents the rotation and shifting of anvils, with respect to one another, while under pressure.

After assembling the DAC, the pressure is generated by turning the 1-in. (40 threads/in.) load nut at the base of the cell. The fine threading of the load nut allows for fine control and a smooth increase of pressure as the load nut pushes the piston containing the bottom anvil against the top anvil. Remarkably, today we are capable of applying pressures on the order of 1 million atmospheres by turning the load nut on a DAC with an average size wrench in a laboratory.

Diamond Anvil Selection and Alignment

In general diamond anvils are selected based on application and in order to achieve maximum pressure. Consideration of the properties of diamond anvils is therefore important in the selection process. Single-crystal gem quality and inclusion-free anvils with low birefringence are used, as any inclusion may result in the development of cracks. Diamonds are usually cut with 8 or 16 faces and range in size from $1/8$ to $1/2$

carat, with 1/3 carat being the most used. Depending on the desired pressure either a flat culet anvil or a beveled anvil may be selected. Most commonly for pressures below 100 GPa a flat culet anvil of 200 μm to 300 μm is used. Above this pressure a beveled anvil with a flat size of 20 μm to 75 μm is needed. The beveling angle has been optimized in order to achieve the highest pressure.¹⁶ For achieving the highest pressure the culet is generally selected to be at least three times larger than the flat, with the bevel angle of 7-8.5°. Although the beveled anvil is preferable due to its ability to sustain higher pressures, it has a downside in that it cannot be reused if compressed to ultra-high pressures. Due to a large deformation of the anvils, failure is observed in the form of ring cracks, which develop on the culet face during pressure release. Therefore, in order to reuse a beveled anvil one must repolish it after each high-pressure experiment above 50 GPa.

In addition to the selection of size and bevel versus flat anvil, the physical and mechanical properties of diamonds are also important. Pure diamonds (type IIa) are desirable because they are transparent over a broad range of electromagnetic spectrum, but they are rare. Natural diamonds have impurities that affect their optical and mechanical properties.^{17,18} One of the main impurities is nitrogen. A study of impurities in diamond shows that nitrogen forms different defects. The scope of defects in diamonds is outside the realm of this study and will not be considered in great detail, but it is important to understand that diamond impurities play a significant role in achieving high pressure and limit the number of experiments that may be performed. In our case, where the interest is to perform high-pressure electrical resistance measurements and x-ray diffraction studies, type Ia diamonds are used. Defects forming type Ia diamonds do not pose a significant problem for performing x-ray diffraction and electrical resistance measurements, and fur-

thermore the existence of some nitrogen defects is expected to increase the hardness of diamond. For other high-pressure studies, specifically at high temperatures, diamonds must be selected with great care.

In addition to a careful selection of diamonds and a solid DAC design, the perfect alignment of anvils has to be achieved in order to maximize the pressure. In most cases, cracks and other damage to the diamonds occur not because of improper selection or even high pressure, but instead because of improper alignment. Initial alignment is performed after the anvils are glued to the plates and placed in the DAC. First, by viewing the anvils from the side under a microscope, a rough alignment of the anvils is performed by adjusting the screws, which translate the anvil attached to the piston. This translation in the plane parallel to the flat of the diamonds ensures that the anvil flats of the top and bottom diamonds are not offset. Next, the parallel alignment is adjusted by using a sodium (Na) lamp and observing Newton's rings. Newton's rings are formed when the monochromatic light from the Na lamp is reflected from the flat of the bottom diamond and interferes with the light reflected from the flat of the top diamond. By observing the number of interference fringes, one may adjust the offset angle between the planes of the diamond flats. The adjustment is made by turning the four small screws in the support plate. The goal of adjustment is to reduce the offset angle, as seen by the reduction of the number of interference fringes. Care should be taken as the adjustments to the parallel alignment may also require translational adjustment. This process is repeated until only one large interference fringe is observed. In most cases, once the perfect alignment is achieved, it remains stable and no additional adjustment needs to be made even after performing multiple experiments.

Experimental Preparation

Preparation for performing a high-pressure experiment begins with the selection of a gasket, followed by gasket pre-indentation, drilling of the sample hole, loading the sample, and choosing a proper pressure marker. Each of these steps is just as important as the selection of diamonds and the alignment in achieving the maximum pressure and being able to collect useful data. In choosing a gasket, for example, the type of material one wants to use as a gasket, a consideration of the type of sample being investigated, and the type of experiment that will be performed play major roles. Typically the material of choice has to have a sufficiently high yield strength to maintain a reasonable gasket thickness at high pressure and at the same time be ductile, to allow for plastic flow and provide support to the anvils. As mentioned earlier, the primary purpose of the gasket is to contain the sample between the two diamond anvils, but it also prevents the edges of anvils from coming into contact and breaking. Brittle materials are therefore inadequate in most cases, as they do not flow well under pressure. Typically plastic materials, such as spring steel or rhenium, are used in ultra-high pressure experiments. Other materials may be used, as in the case where a nonmagnetic or electrically insulating gasket is desirable and also when working with reactive materials. In the present work the latter was not a concern and spring steel is used as the gasket material for all of the experiments. It is important to point out that because designer diamond anvils are used for all of the electrical resistance measurement experiments presented in this study we are still able to use a metallic gasket, as opposed to the traditional electrical resistance measurement techniques where the use of electrically insulating gaskets is a requirement.

After the material used for the gasket is selected, the gasket is then preindented before the experiment. Initially the gasket, which sits on the top of the bottom diamond and is attached to the piston by two screws, has a thickness of 250 μm . Preindenting the gasket reduces this thickness because of plastic deformation and, as a result, a more stable sample chamber is formed at high pressure. Preindentation is performed by closing the cell and compressing the gasket by 135°-155° for flat diamond anvils, while a compression of 155°-165° is used for beveled diamond anvils. After preindentation the thickness of the gasket is reduced to 20-50 μm . Following the preindentation the gasket is removed so that a sample hole may be drilled. Additionally, after removing the gasket, the alignment of the diamond should also be checked by observing the interference fringes, as described in the previous section. If the alignment does not need adjustment then the hole is drilled, otherwise alignment is first adjusted and another gasket is preindented. Holes may be drilled using a mechanical drill or, in the case of an electrically conductive gasket, an electro-erosion technique may be used. The size of the sample hole depends on the flat size of the anvil used. For experiments below 100 GPa, where the diameter of the flat is 100 μm to 300 μm , the hole diameter is usually one third that of the diameter of the flat. However, in the case of a much smaller flat used for ultra-high pressure experiments, drilling a hole that is one third of the flat diameter results in inadequate sample volume and difficulty in data collection. In this case a hole with a diameter as large as two thirds of the diameter of the flat is used. After drilling, the gasket is cleaned and then positioned back on the piston diamond so that the sample may be loaded.

Generally there is no blueprint for sample loading. In most cases it depends on the type of sample as well as the experience of the person loading. However, regardless

of the experience or sample or any other factors, it is important to take the greatest care in performing this step. Due to a very small sample volume, even small contamination is a concern. In most cases the samples loaded for high-pressure experiments are polycrystalline and in some cases single crystals. Loading, as well as performing high-pressure experiments with a single crystalline sample, requires the use of specialized single-crystal x-ray diffraction techniques. Loading a polycrystalline sample is done in two ways. The sample may either be cut or shaved into a fine powder and then placed in the hole, or a piece the size of the hole may be cut and placed in the hole. Independent of the method used it is important that enough sample be loaded. If too much sample is placed in the hole it may actually squeeze out under the gasket as the pressure is applied. If there is not enough sample, than the gasket hole may close due to the flow of the gasket and there may not be enough sample to make a measurement. Unfortunately it is sometimes only by trial and error that “enough” may be defined. However, after subsequent sample loadings one develops a better idea of how much sample needs to be loaded.

In addition to placing a sample in the gasket hole, a pressure marker is also loaded. Various pressure markers are used, as will be described in the following section, and are chosen depending on the experiment, pressure range of the experiment, and sample type. In some cases a pressure medium is also placed in the hole before the cell is closed. Pressure media is sometimes used to reduce the pressure gradient across the sample and provide better hydrostatic conditions.^{15,19} Typically pressure media works at lower pressures and is desirable for harder samples, where large pressure gradients are expected for samples with high yield strength.² Although pressure media may be helpful in some

cases, care should be taken due to possible sample reaction with the media and also in cases where electrical contact needs to be established with the sample.

Pressure Measurement

Various gauges have been developed to conduct pressure measurement simultaneously with the experiment. Most of the pressure gauges may be classified into two categories, the pressure markers that may be measured by optical spectroscopy, and the pressure markers with a known pressure-volume (P-V) equation of state (EoS). Development of optical pressure gauges allows for pressure to be conveniently measured in a laboratory by use of routine, commercially available spectroscopy techniques. For example Raman shift of ^{13}C diamond thin film has been calibrated to high pressures,^{20, 21} and Sm:YAG and ruby have a well-studied pressure-dependant fluorescence spectra^{22, 23} as well. In the present experiment ruby was used as the optical pressure gauge. Ruby, which is Al_2O_3 doped with Cr^{3+} , has two characteristic fluorescence lines called R_1 at 694.25 nm and R_2 at 697.7 nm. The R_1 fluorescence pressure shift has been calibrated to 100 GPa by Mao *et al.* (Ref. 23) against copper (Cu), molybdenum (Mo), palladium (Pd), and silver (Ag), which have a well-known EoS from shock-wave data. The calibration may be described by Eq. (1):

$$P(\text{GPa}) = 380.8 \left[\left(\frac{\lambda}{\lambda_0} \right)^5 - 1 \right], \quad (1)$$

where P is the pressure, λ is the measured wavelength, and λ_0 is the ambient condition wavelength of R_1 line, 694.25 nm. By measuring the shift of the R_1 line and using Eq. (1), pressures up to 100 GPa can be determined in a laboratory. Above this pressure the in-

tensity of the R lines decreases significantly, as the absorption band of ruby shifts and higher energy laser lines are needed to excite fluorescence.²⁴ Furthermore complicating the problem is the shift of the absorption edge of diamond anvils to the visible region, which makes the pumping efficiency even lower.²⁵ Because of the mentioned reasons, it is desirable to use a pressure marker with a known EoS above 100 GPa. If the EoS is known, pressure may be obtained by measuring the volume by x-ray or neutron diffraction experiments. Common materials for this type of pressure marker are platinum (Pt) and gold (Au), as well as Cu, which is used in the ultra-high pressure experiments reported in this study.

To determine pressure, a small piece of Cu marker, usually 10 μm in diameter and 5 μm thick, is placed in the gasket hole along with a sample before closing the DAC. The cell is then taken to a synchrotron source where the unit cell volume of the Cu pressure marker is measured by x-ray diffraction and pressure is calculated from the known EoS of Cu. In order to get the most accurate pressure measurement, Cu P-V shock wave data reported by (McQueen *et al.*, Ref. 26) to 270 GPa and (Holmes *et al.*, Ref. 27) to 1000 GPa was used to obtain an EoS.

X-Ray Diffraction

Due to small sample volume and because the sample is contained in a gasket between the two diamond anvils, techniques for studying materials at high pressures are limited. The ability to generate high-energy x-rays that can penetrate the diamond anvils by synchrotron radiation sources, has made x-ray diffraction one of the most powerful tools used to perform DAC experiments. X-rays have wavelengths comparable to the inter-

atomic spacing of many solids and thus may be applied for structural determination. Application of x-ray diffraction for studying materials has been around since before the invention of DAC. In 1912 William Bragg was able to mathematically express the necessary conditions for the diffraction of x-rays by a crystal. Bragg explained that when x-rays strike a crystal they are reflected by the parallel planes of atoms (Fig. 3) and, depending on the interplaner spacing, the reflected waves will interfere in such a way that they will only be observed for specific angles of incidence and wavelength. This is described mathematically by Bragg's law:

$$\lambda = 2d \sin \theta , \quad (2)$$

where λ represents the incident wavelength, d the interplaner spacing, and θ the angle of incidence measured between the beam and the crystal plane.

In addition to the restriction described by Bragg's law, the positions of the atoms in the unit cell, experimental equipment, sample crystallinity and texturing, and the type of diffraction performed also influence the diffraction pattern. The majority of the DAC x-ray diffraction experiments are performed on polycrystalline powder samples. Single crystalline samples are difficult to study because any nonhydrosticity in the pressure will destroy the single crystallinity of the sample and also due to the inability to orient the DAC and get the diffraction pattern at various Bragg angles. The X-ray diffraction experiments presented in this literature were all performed on powder samples using energy-dispersive and angle-dispersive techniques by application of synchrotron x-ray sources.

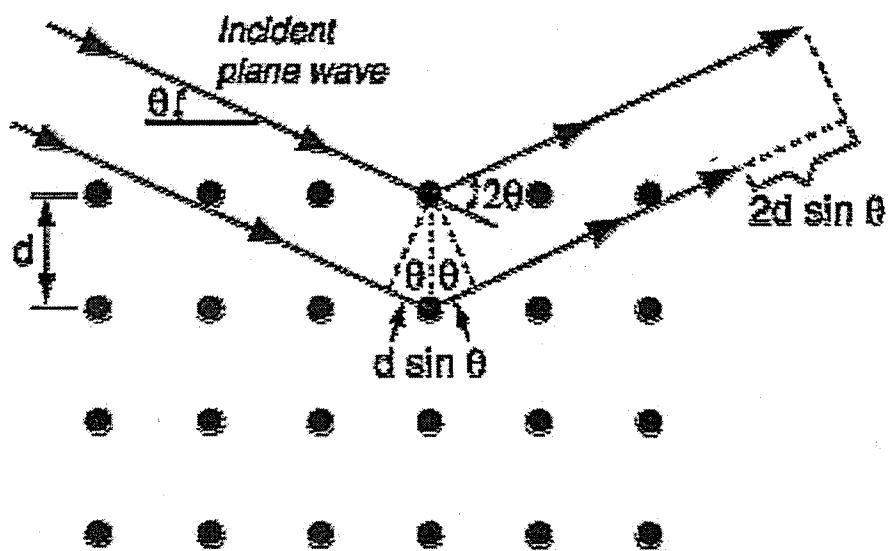


FIG. 3. The elastic scattering of X-rays by crystallographic planes having interplaner spacing d .

Synchrotron X-ray Source

The commercially available laboratory x-ray sources, such as those generated by high voltage tubes or rotating-anode devices, have an insufficient flux and energy for performing x-ray diffraction on samples contained in a DAC. Synchrotron radiation sources, on the other hand, are capable of producing more intense and brighter x-ray beams, with energy greater than 10 keV. X-ray photons with energy greater than 10 keV can penetrate diamond anvils and illuminate samples in a DAC. Initially synchrotron radiation was looked at in connection with radiation emitted from high-energy particle accelerators. High-energy particle accelerators are designed to have a very large radius, as it is known that any deceleration by a charged particle results in a loss of energy by emission of radiation. What is considered as a negative by high energy scientists was applied as a useful research tool. This type of synchrotron radiation is now referred to as the first-generation source. The second-generation source was then built to optimize radiation by use of bending magnets. An example of a second-generation source is the National Synchrotron Light Source (NSLS) at Brookhaven National Laboratory (BNL). In addition to second-generation sources, third-generation sources have been built and are in use today. Third-generation sources, such as the Advanced Photon Source (APS) at Argonne National Laboratory (ANL), have been built in order to further optimize synchrotron radiation by using insertion devices. Insertion devices are periodic magnetic arrays with alternating fields that force the particles to oscillate as they pass through the device (Fig. 4).

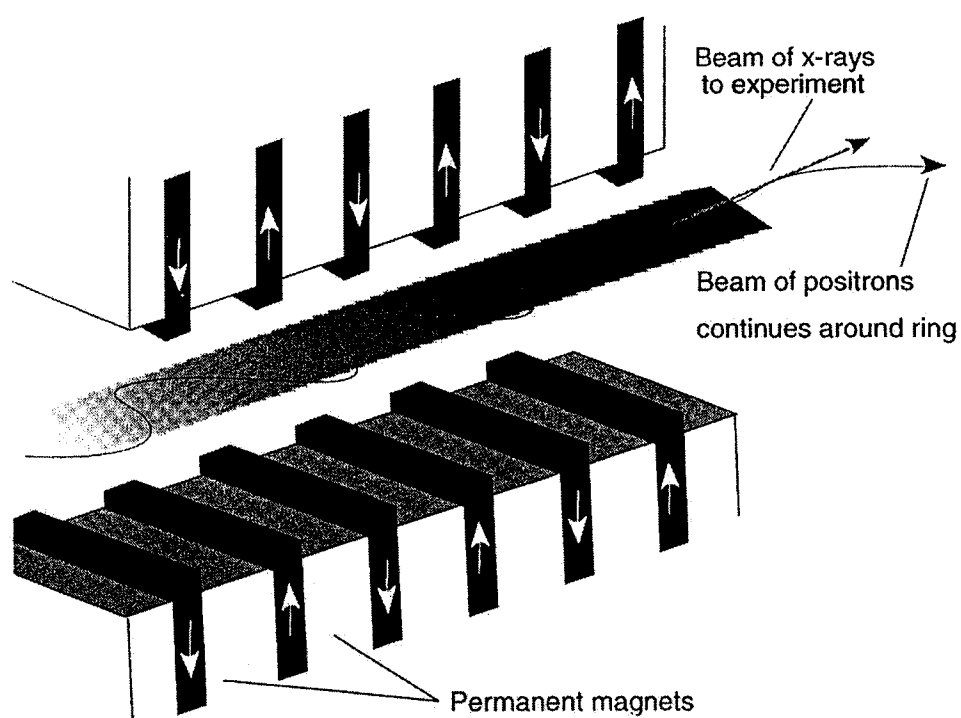


FIG. 4. Insertion device used by third-generation synchrotron sources, like the Advanced Photon Source at Argonne National Laboratory in Chicago.

Energy Dispersive X-ray Diffraction

The energy dispersive x-ray diffraction (EDXD) experiments were performed at the X-17C beamline at NSLS. A polychromatic beam with energy up to 80 keV is produced by a 4.2 Tesla (T) superconducting wiggler magnet. The beam is then collimated to a diameter from 50 μm down to 15 μm , depending on the sample size. Because of the limited openings in a DAC, EDXD has been one of the most used methods for determining the structure of the sample. In this technique the beam enters the DAC, mounted on a mechanical stage, through the piston and is diffracted by the sample through the opening on top of the DAC (Fig. 2). The diffracted beam is then collected by a solid-state germanium (Ge) detector, which sits at a constant angle, 2θ , with respect to the input beam (Fig. 5). The Ge detector, which is able to measure over a wide range of energies, can discriminate photons of different energies and thus record a spectrum. From Bragg's law, Eq. (2), it is understood that for a constant angle there is a corresponding wave length and d spacing that will satisfy the equation. By using energy wavelength relation, $E = hc/\lambda$, where h is Planck's constant and c is the speed of light, Bragg's law may be rewritten as follows:

$$E = \frac{hc}{2d \sin \theta} \quad \text{or} \quad Ed = \frac{6.1993}{\sin \theta} \text{ keV\AA} \quad (3)$$

By rewriting Bragg's law in terms of energy, we see that when the detector is set at a fixed angle, θ , the product of energy, E , and interplaner spacing, d , is constant. The Ed value at a given detector angle is obtained by using a calibration standard, such as gold (Au), that has a well-known crystal structure and for which the pressure dependence of the lattice parameter is well established. The Ed value obtained from the Au standard is then used for data analysis of other spectra collected at the same angle. Although the

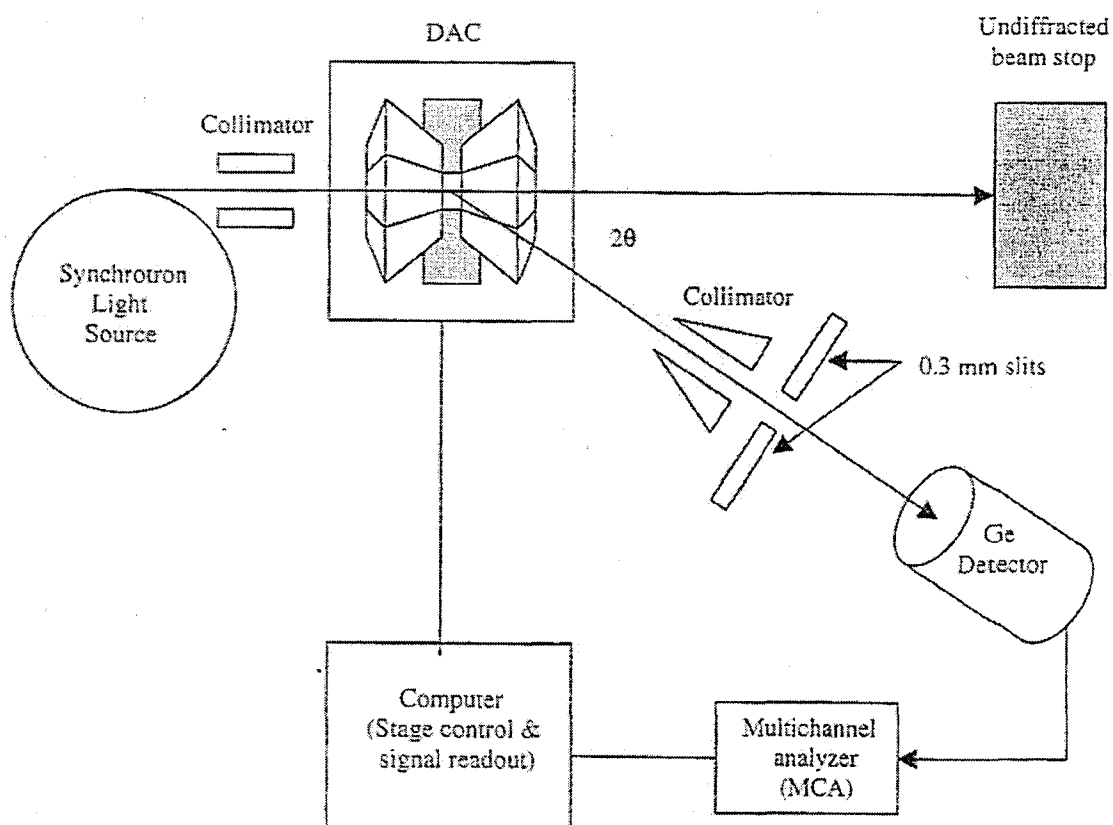


FIG. 5. Illustration of energy dispersive x-ray diffraction in a diamond anvil cell. This setup is employed at the National Synchrotron Light Source at Brookhaven National Laboratory.

EDXD technique has been successfully deployed studying the crystal structure of many materials, one may encounter some problems in studying the phase transitions and P-V relations.

In the case of EDXD, where the detector sits at a constant angle, only a small portion of the whole diffraction cone is measured. As a result, any preferred crystal orientation and grain growth effects that influence peak intensity are hard to detect, and precise structural refinement may be difficult. Furthermore, when x-rays strike the sample, in addition to diffraction, fluorescence peaks arise due to atomic excitation. Fluorescence peaks occur when an inner shell electron is ejected or promoted to a shell with a larger principal quantum number leaving a vacancy. The vacancy is, however, quickly filled by an electron transition from an outer shell. This transition is accompanied by emission of energy and, depending on the shells involved, different amount of energy is emitted. Fluorescence peaks are well studied and the energies emitted during the decay between various shells, which are labeled as K_{α} , K_{β} , L_{α} , L_{β} , and so on, are well documented and therefore it is not difficult to exclude them from structural refinement. However, the fluorescence peaks can cause the same problem in that it may overlap with diffraction peaks from the sample and hence complicate the structural refinements of the EDXD data. However, fluorescence peaks can be separated from the diffraction peaks by changing the diffraction angle.

Angle Dispersive X-ray Diffraction

Development of new synchrotron sources and x-ray detectors, as well as the improvements in the design of DAC, have all contributed to the development of angular

dispersive x-ray diffraction (ADX) for studying samples at high pressures. The ADXD experimental setup is similar to that of EDXD. A DAC is placed on a stage; an x-ray beam enters through the opening in the piston and is diffracted by the sample through the opening at the top of the support plate. However, in the case of ADXD a monochromatic beam rather than a polychromatic beam is used for EDXD. This is possible because the detector in ADXD is placed along the beam path and is able to detect the whole diffraction cone. In order to select a monochromatic beam of a certain wavelength, a polychromatic beam produced by the synchrotron source is incident onto a monochromator. A monochromator is a large, perfect single crystal, typically silicon or germanium, and in some cases synthetic diamond. Silicon and germanium are usually used as they are readily available due to their use in semiconductor industry. By orienting the crystal so that the incident beam strikes at a certain angle θ and is reflected by a chosen crystal plane with a known interplaner spacing d , then by Bragg's law, Eq. (2), only a certain wavelength, λ , will be selected. Silicon and germanium crystals are also cooled to cryogenic temperatures in order to reduce thermal gradients, which may distort the crystal and change the wavelength. ADXD experiments are carried out with a wavelength that is kept fixed throughout the experiment. For collecting the diffracted beam, as in the case of the beamline 16ID-B HPCAT at APS where all of our ADXD experiments were performed, an image plate detector is used. The image plate consists of a photosensitive material that can be read by scanning a laser beam across the plate and recoding the emitted light. A typical diffraction image collected by the image plate detector may be seen in Fig. 6. The Deby-Sherrer rings shown in Fig. 6 are that of CeO_2 calibration standard.

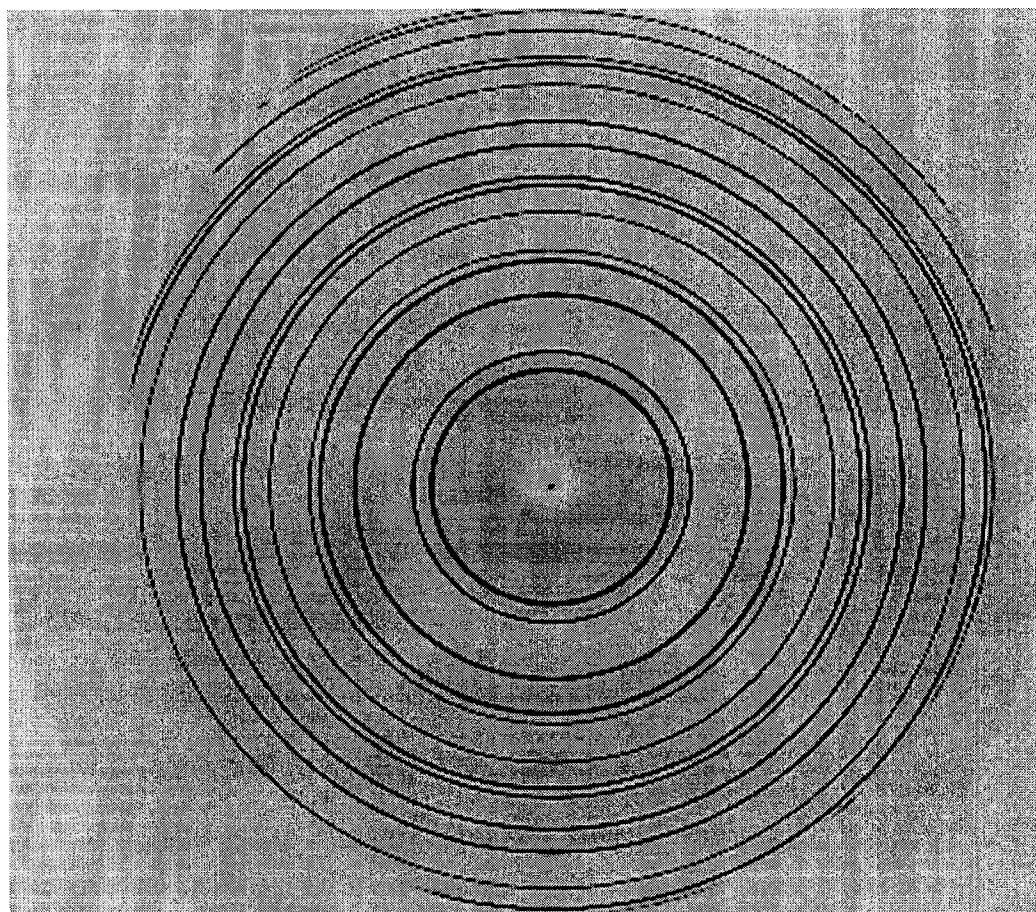


FIG. 6. ADXD spectra of CeO_2 calibration standard, collected by an image plate detector.

The diffraction pattern of the standard is taken prior to performing a high-pressure experiment in order to determine the sample-to-detector distance. Since CeO₂ has a well-known crystal structure and lattice parameter, diffraction angle for a given wavelength can be calculated precisely. Sample to detector distance is then calculated as follows:

$$s = \frac{r_{hkl}}{\tan(2\theta)}, \quad (4)$$

where s is the sample to detector distance, r_{hkl} is the radius of the selected ring, and 2θ is measured between the input beam and the diffracted beam of the selected ring. The detector distance, along with the wavelength, remains constant for the duration of the performed experiments. The main advantage of using ADXD is that the whole diffraction cone is observed and the ring pattern may be analyzed for any texturing effects and the preferred orientation of the crystal. In addition to being able to detect the diffracted beam over a whole solid angle, fluorescence peaks can be eliminated with ADXD as well.

Data Analysis

Data collected using the EDXD and ADXD methods are analyzed using the XRDA²⁸ and GSAS²⁹ structural refinement programs. In order to use the two programs certain information is needed. In the case of EDXD, where the detector angle is held constant, the Ed value is first determined from the Au calibration standard, as described previously. The calculated Ed value is then loaded into the refinement program in order to perform a structural calculation. The refinement program also requires that the peak indexing, assignment of atomic positions, and selection of Bravais lattice type be entered manually. The program is then able to determine the lattice parameter, observed interplaner spacing (d_{obs}), calculated interplaner spacing (d_{cal}), observed peak intensity (I_{obs}),

and calculated peak intensity (I_{cal}) of each peak. For high-pressure experiments two major things are usually observed to occur as pressure is increased. First is that the peaks move to high energies. This is obviously the result of pressure-driven decreases in interplaner spacing, d . Since Ed is constant a decrease in d results in an increasing E value. The second thing that may be observed is the appearance or disappearance of peaks. This usually indicates a structural phase transition. At this point new peak indexing, atomic positions, and Bravais lattice type must be entered. By performing the refinement we are able to minimize the difference between observed and calculated interplaner spacing and between the observed and calculated diffraction intensities.

ADXD refinement is done in a similar fashion, with a few exceptions. Raw data collected by the image detector must first be converted to a graphical output appropriate for the refinement programs. For this step a program called FIT2D³⁰ is used. This program is specifically designed for the calibration and correction of detector distortions and the conversion of raw data for refinement. This is done by first opening the file from the CeO₂ standard in FIT2D. Next, the wavelength used must be entered, so that the sample to detector distance, s , can be calculated by Eq. (4). Once s is determined it is used for future file conversions. Files are converted and output as intensity versus 2θ . The output files can then be analyzed, in the same manner as with EDXD, by providing the wavelength, λ , rather than the Ed value.

Both XRDA and GSAS programs allow for crystal structure refinement and lattice parameters and interplaner spacing to be determined; however, XRDA was designed mainly for use with EDXD, while GSAS was designed for use in both EDXD and ADXD, as well as, neutron diffraction analysis. The difference between the two x-ray diffraction

techniques, as mentioned earlier, is that ADXD allows for more accurate measurement of diffracted peak intensity. As a result, when EDXD spectra are analyzed using the XRDA program, certain information, such as atom position, must be entered, and Miller indices must be assigned to a minimum number of peaks, depending on the Bravais lattice, in order for the program to assign all of the peaks to a given structure and determine lattice parameters. XRDA also reports the calculated and observed peak intensity; however, in order to minimize the difference between the two, such factors as lattice parameters must be varied manually. GSAS allows for structural refinement to be done automatically. When the diffraction spectra are input into GSAS, information about the structural space group and atomic position must also be entered. Once this information is supplied the program automatically refines the spectra using the Rietveld method of minimizing the weighted sum of squared difference between observed and calculated peak intensity.²⁹ Both programs ultimately allow for structural refinement and the difference between observed and calculated peak intensity to be minimized and, typically, both programs may be used to verify the calculated results.

Designer Diamond Anvils

Electrical resistance measurements at high pressures are not as common as x-ray diffraction experiments. As mentioned earlier, this has been in large part due to the sample geometry and the difficulty in placing the multiple electrical probes needed to perform the measurement. For a typical electrical resistance measurement at least two electrical probes are needed, one for the input signal and the other for the output signal. However, for very good conductors and especially for samples with small volumes, as in

the case of the samples in a DAC, four probe technique needs to be applied. The requirement to place four probes in contact with the sample makes it even more difficult to perform electrical resistance measurements on a high-pressure sample. There are also additional problems that must be addressed with the conventional high-pressure electrical resistance measurement technique, as described in the following sections. It is only by addressing these problems and understanding the technical difficulties with the conventional technique that the significance of designer diamond anvils may be understood. Currently there are two types of designer diamond anvils in use. One, as mentioned, is used for performing electrical resistance measurements, as well as for heating samples by using the electrical leads to pass large electrical current through them. The second design of designer diamond anvil is used for measuring the magnetic properties of the sample. Designer diamond anvils are ideal for magnetic measurements because the excitation and pickup coils are placed much closer to the sample. Having the coils closer to the sample helps improve the signal-to-noise ratio and also allows for a low magnetic field, produced by a small sample, to be detected.

Fabrication

Fabrication of the designer diamond anvils⁶ begins with the deposition of the tungsten (W) microprobes on the surface of the diamond anvil. Typical width of the microprobe is 5 μm to 10 μm and is deposited by a lithographic technique. The probes are then encapsulated with a homoepitaxial diamond layer grown by the chemical-vapor-deposition (CVD) process.^{31,32} After the probes are encapsulated with the diamond layer, the anvil is polished in order to expose the probes. Polishing exposes the probes only at

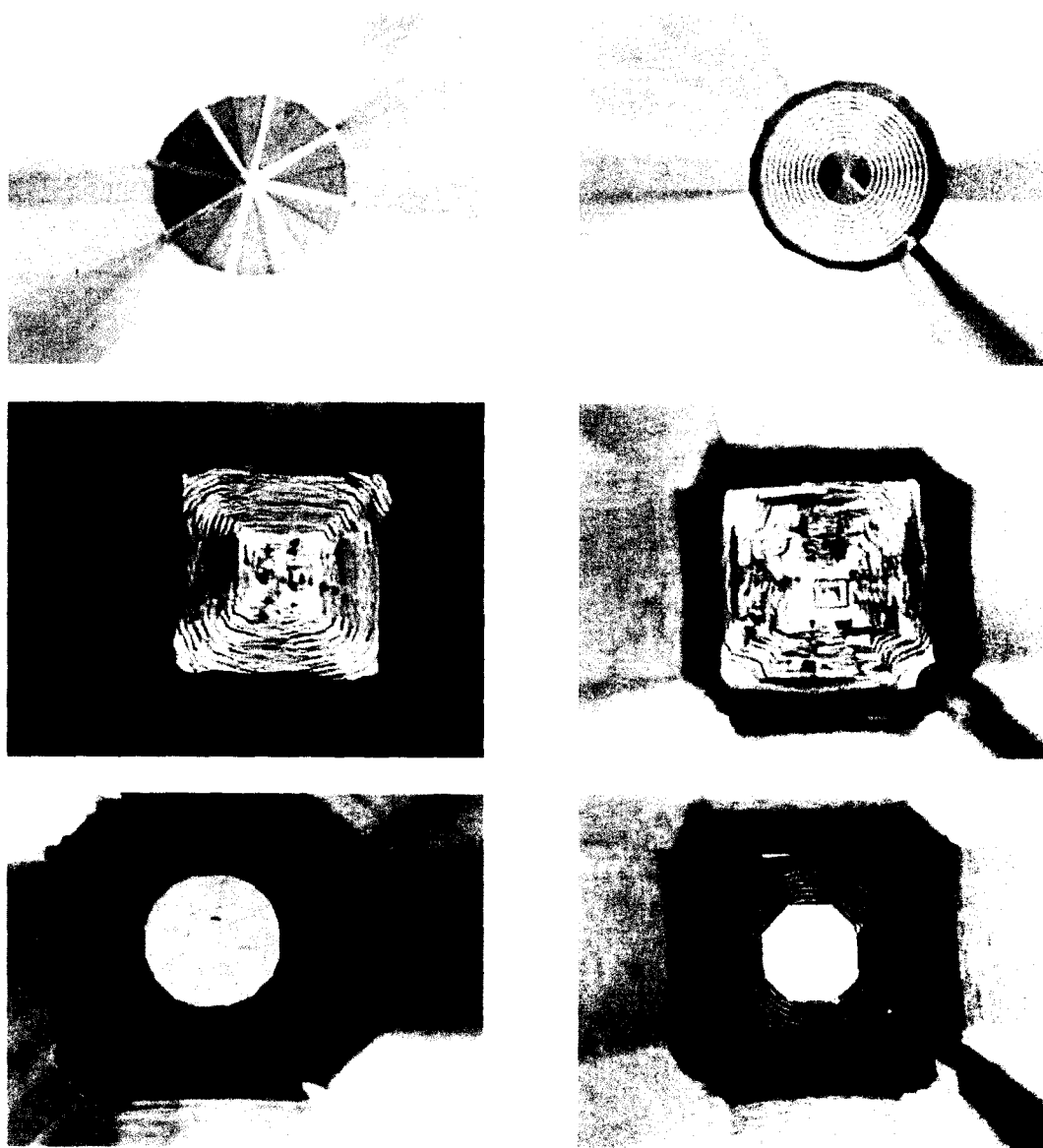


FIG. 7. Two types of designer diamond anvils; the one on the left side is used for electrical resistance measurements and the one on the right side is used for magnetic measurements. Top two pictures show the anvils after deposition of microprobes by lithographic technique. Middle two pictures are of the anvil after CVD. Bottom two pictures are of the final finished designer anvils show electrical probes exposed at the center for making contact with the sample.

the surface, where electrical contact will be made, while the remainder of the probes remains encapsulated by diamond. Figure 7 shows the two types of designer diamond anvils after the successive fabrication steps described previously, while Fig. 8 gives a close-up view of the designer diamond anvil used for electrical resistance measurements. In Fig. 8 the designer diamond anvil is shown in transmitted and reflected light. When viewed in reflected light only the exposed part of microprobes at the surface is observed. On the other hand in transmitted light the length of the probe encapsulated by the diamond is observed.

Application for Electrical Resistance Measurements

In addition to exposing the electrical microprobes at the surface, the desired geometry for the anvil is chosen during the last fabrication step. In the present experiments, the anvil geometry is chosen on the same basis as when choosing a regular diamond anvil. Once the fabrication process is completed, external electrical leads, which are used to connect to the electrical meters and perform the measurement, are attached to the electrical pads of the microprobes. The length of the microprobes extends from the surface, where the contact is made with the sample, through the diamond and comes out near the electrical pads at the bottom of the anvil. At this point external electrical leads are connected by using a conductive two-part silver epoxy (Fig. 9). After this step, the experimental preparation is the same as for a regular anvil. Spring steel is also used as the gasket material for electrical resistance measurements, since the probes are shielded from the gasket by the encapsulating diamond layer. The only possible point of contact between the gasket and the microprobes is at the surface. It is therefore important to drill a

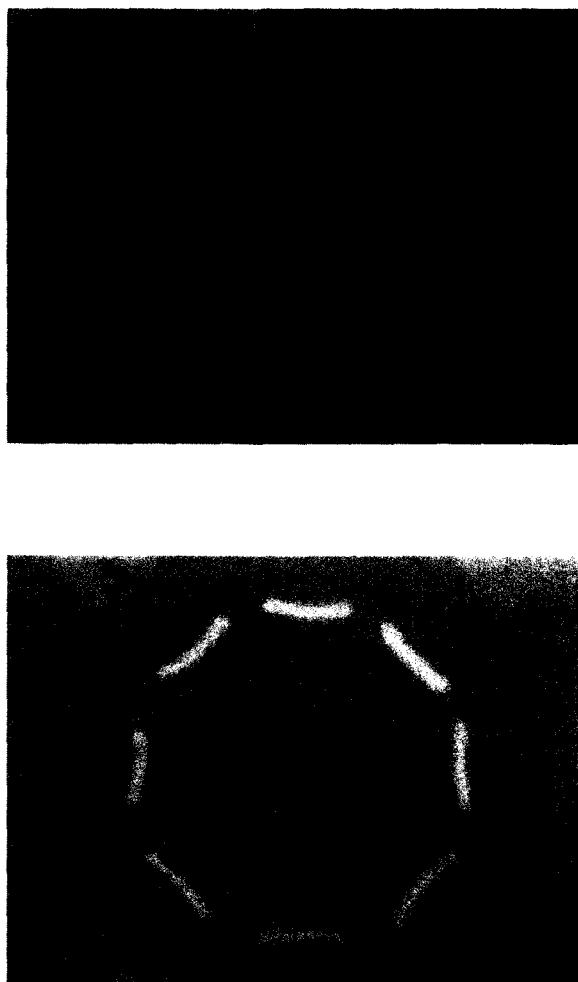


FIG. 8. Close-up view of the designer diamond anvil used for electrical resistance measurement. Top figure shows the anvil in transmitted light with the eight probes embedded in the diamond. Bottom figure is shown in reflected light, with only the part of the probe exposed at the surface reflecting light.

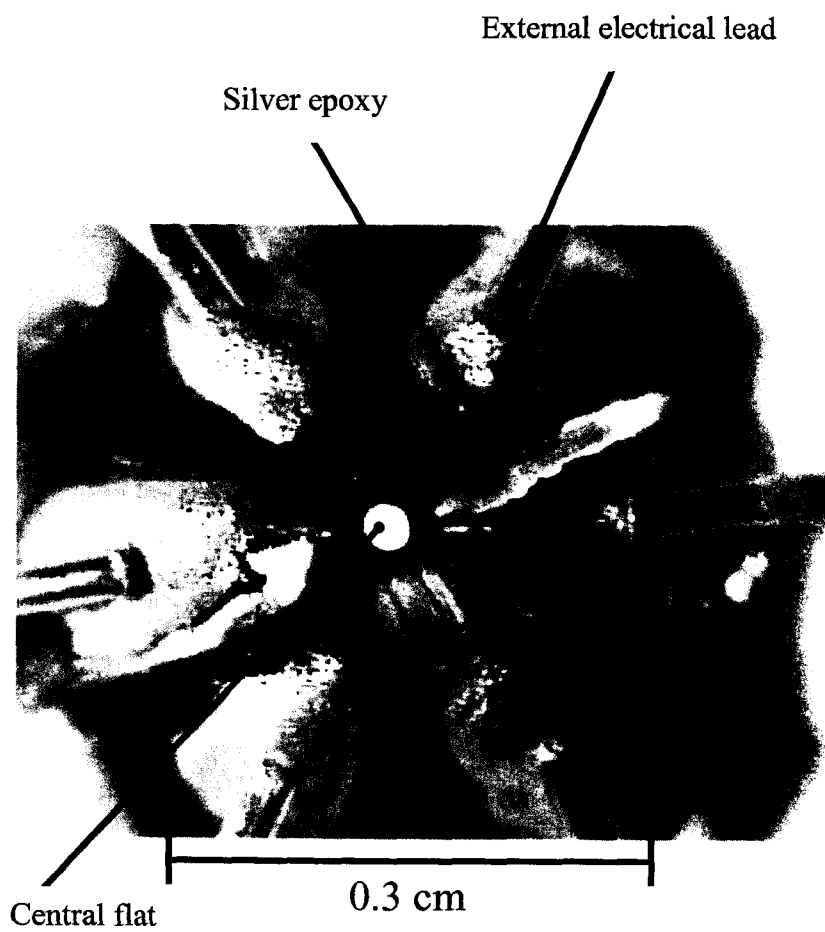


FIG. 9. External electrical leads attached to the microprobes at the base of the designer diamond anvil, using a conductive two-step epoxy.

symmetric hole in the gasket, so that only the sample makes contact with the probes. Choosing a pressure gauge is also done with some additional consideration. Pressure markers such as Cu, and other electrically conducting materials, are not used, as they may contribute to the measured electrical resistance. For determining the pressure, a ruby gauge is used as well as the pressure-volume EoS of the sample studied. Use of the sample EoS may be used in the case where the EoS has been previously determined and when x-ray diffraction is performed in conjunction with electrical resistance measurement. Furthermore, the pressure range of the experiment must be in the range of the established EoS of the pressure standard. Determining the pressure in this manner is ideal as there are no other materials in the sample chamber that would interfere with the electrical resistance measurement of the sample. However, this method may also require additional experiments to be performed in order to establish or even extend the pressure range of the EoS. Ruby is also suitable because it remains electrically insulating throughout the applicable pressure range. The challenge in using a ruby pressure gauge lies in the ability to select a piece of ruby of adequate size. Typically a spherical piece of 10 μm in diameter is desirable for measuring up to the highest pressure of 100 GPa. If it is significantly smaller than this it becomes difficult to excite enough fluorescence and determine pressure above 10 GPa. On the other hand, if the ruby piece is much larger than 10 μm , it may block the probes from making an electrical contact with the sample.

Once a satisfactory pressure gauge is chosen, DAC is closed and a minimum compression of 20° is applied. By applying initial compression the sample is sealed and pressure of 5 GPa is generated, which is required in order to establish a good contact between the sample and the probes. After the contact is achieved electrical resistance is

measured by a two-probe or four-probe technique, depending on the sample resistance. Two-probe measurements presented in this literature are performed with a Hewlett Packard model 34401A multimeter. By sending a small test current, I , through the probes and across the sample, the multimeter measures the total voltage drop, V_T , and computes the resistance, R , by Ohm's law, $R=V_T/I$. Although the test current is small, the total voltage drop is a sum of voltage drop across the sample, V_S , and the two electrical leads, V_{2L} , used to perform the measurement. Therefore the R value reported is also a sum of the sample resistance, R_S , and the two lead resistances, R_{2L} , and by Ohm's law may be expressed as follows:

$$R = \frac{V_T}{I} = \frac{(V_S + V_{2L})}{I} = R_S + R_{2L} \quad (5)$$

When the R_S value is comparable to the R_{2L} value it is difficult to perform an accurate two-probe measurement. For the reported electrical resistance measurements here, a two-probe technique is used when R_S is larger than 500 Ω . Below this R_S value a four-probe technique is applied.

The advantage of the four-probe technique is that the two different sets of leads are used to supply the test current and measure the voltage drop. First, using the KEITHLEY model 2400 current source supply, a steady test current, I , of 1 to 3 milliamps (mA), where 1 mA = 10^{-3} A, is sent through one set of leads and the sample. Then, through the other set of leads, called the sense leads, voltage, V_T , is measured using the KEITHLEY model 2182 nanovoltmeter. Although some current flows through the sense leads, in order to measure the voltage drop, it is on the order of picoAmps (pA), 1 pA = 10^{-12} A. Due to the large difference between the current across the sense leads and the current

across the sample, $V_T = V_S$, where V_S is again the voltage drop across the sample. Then by Ohm's law:

$$R_S = \frac{V_T}{I} = \frac{V_S}{I}, \quad (6)$$

where R_S is the sample resistance. By eliminating the lead resistance, the four-probe technique is better suited for detecting small changes, sometimes in the $m\Omega$ range, in electrical resistance that may occur at high pressures.

Comparison to Traditional Technique

With the conventional technique, used in high-pressure electrical resistance measurements, a set of probes is placed directly between the top diamond anvil and the gasket.^{2,33} Although some data has been collected in this way, the process is very tedious. The probes not only have to be shielded from the gasket by an insulating material or, as is usually done, by a non metallic gasket, but it is also very challenging to make sure that all of the probes are in contact with the sample and yet not in contact with each other. With increasing pressure there are also other problems with this technique that have to be considered. The probes are placed between the diamond anvil and the gasket, so they are exposed to flow stresses and, as a result, there is a large plastic deformation in the probes. Due to the effect of changing probe geometry on the measured electrical resistance, the measured values may be difficult to interpret. The second problem is that the sample flows during compression; as a result the probes tend to shift and one is not able to consistently measure resistance sample region. The plastic deformation of the probes will also result in the change of probe spacing and less reliable electrical resistance data. This problem may be best understood by considering that what is generally measured and re-

ported for high-pressure experiments is the electrical resistance, R , rather than resistivity, ρ , of the sample. The reason for reporting R rather than ρ is due to the difficulty in determining sample geometry at high pressures. Various experiments and computational studies have attempted to describe and determine the geometry, but these results have been estimates at best, and therefore measurements have only dealt with changes in R . From this perspective it is important to consistently measure R over the same region of the sample for comparison of R versus pressure. If there is a considerable shift during increasing pressure, the resulting change in R may be due to the change in the sample region measured rather than the change in the mechanical or electrical property of the material studied.

The development of the designer diamond anvils for high-pressure measurements has reduced some if not all of the problems associated with the conventional electrical resistance measurement technique. By design, electrical microprobes are embedded in the diamond and are only exposed at the surface (Fig. 8). This allows the electrical probes to make contact with the sample while the rest of the probe is insulated from the metallic gasket. Furthermore, the embedding of the electrical probes in the diamond anvil minimizes flow stresses and the plastic deformation of the probes. It also means that the only shift in the relative position of the microprobes with increasing pressure is the result of the deformation of the diamond anvil at high pressure, which is minimal since diamond is the hardest known material. However, because this technique is fairly new, measurements must be made and an experimental technique developed in order to test and develop designer anvils for consistent use in high-pressure electrical studies.

Interpreting Electrical Resistance Measurements

As mentioned in previous sections, one of the main advantages of designer diamond anvils is that the probe position is stable and the electrical resistance measurements are constantly performed over the same sample region. This plays an important role, in that electrical resistance depends on sample geometry and the placement of electrical probes on the sample. For example, if we consider a general case of an electrically conducting wire of length l and cross sectional area A , the resistance, R , of the wire is $R = (l/A)\rho$, where ρ is the resistivity of the wire. In case l or A is changed the measured resistance will change accordingly. On the other hand, ρ does not depend on the sample geometry and probe placement, but rather is an intrinsic property of a material that is determined by $\rho = m/ne^2\tau$, where m is the mass of the conduction electron, n is the number of conduction electrons per unit volume, e is the electron charge, and τ is the collision time of electrons with crystal impurities, lattice imperfections, and phonons. However, under applied pressure, sample resistivity can also change due to the shifting of the energy bands, which can change the number of conduction electrons, and structural phase transitions, which can alter the collision time of electrons. Because the probe spacing with designer diamond anvils remains constant during high-pressure electrical resistance experiments it does not contribute to changes in the measured electrical resistance. On the other hand, in order to determine whether sample geometry or a change in resistivity is responsible for changes in measured electrical resistance, it is important to perform additional measurements, such as x-ray diffraction, simultaneously with electrical resistance measurements at high pressures.

Summary

Over the last 50 years, DAC has evolved into the most dominant device for generating static high pressures. Using innovative techniques and realizing the wealth of information it may produce, researchers have pushed the DAC to pressures in excess of 400 GPa. Advances in synchrotron radiation sources, the ability to produce synthetic diamond that is harder than the natural diamond used in high-pressure experiments today,³⁴ and the development of designer diamond anvils will continue to push the limits of high-pressure research in new and uncharted directions.

RARE EARTH METALS

Introduction

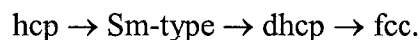
It is well established that when metals are heated their electrical resistance increases, while in semiconductors temperature has just the opposite effect on electrical resistance. In fact, up until the early 1900s, temperature played a greater role than pressure in our understanding of the many physical properties of materials. When subject to external pressure, which increases the inter-atomic interaction, many materials exhibit a rich phase diagram, large volume changes, and considerable changes in electrical conductivity. These are usually not independent of each other; rather the observed changes in one property may go hand in hand with another. However, due to the difficulty of observing and simultaneously measuring many of these properties, we are still unable to conclusively describe many of the material properties at high pressures.

The role of pressure in changing the physical properties of materials is possibly no more evident than in the rare earth metals. At RTP lanthanides are characterized by an unfilled $4f$ -shell and actinides by an unfilled $5f$ -shell. Initially, it is believed that there is virtually no interaction between the spd and f -electrons in lanthanides since f -electrons are localized and the wave functions of the $4f$ -shell do not extend far from the nucleus. On the other hand, the $5f$ -shell extends more spatially and there is an interaction between the f -shell electrons and spd conduction band in light actinides. The result is a formation of low symmetry complex structures in actinides, as opposed to the lanthanides, which

crystallize in the higher symmetry structures at ambient conditions. Lanthanides themselves can further be separated into two groups, divalent and trivalent. At RTP all of the lanthanides are trivalent and are commonly referred to as the regular lanthanides, except europium (Eu) and ytterbium (Yb,) which are divalent.

Regular Rare Earth Metals Under Applied Pressure

A phase diagram of the regular rare earth metals may be separated into two parts. The first part is attributed to pressure-driven $sp \rightarrow d$ electron transfer,³⁵ with no contribution from the $4f$ -shell electrons. The spd valence electrons therefore dominate the bonding initially, and the following structural sequence is observed with increasing pressure^{36, 37}:



This is clearly demonstrated by the observation of the rare earth crystal structural sequence in the transition metal yttrium under applied pressure. Yttrium has the same structural sequence as the lanthanides,³⁸ even though it has no nearby f states. The structural sequence may be viewed as a variant stacking sequence of hcp layers, such ABAB for hcp, ABACACBCB for Sm-type, ABAC for dhcp, and ABC for fcc, as shown in Fig. 10. Another characteristic of the lanthanide metals is that this structural sequence is observed as a function of pressure as well as a change in atomic number. This is explained by considering the valence electrons as being compressed by either externally applied pressure or reducing the atomic number at room pressure.³⁹ At higher pressures, distorted fcc structures (d-fcc), such as the hR24 structure, which is based on doubling the

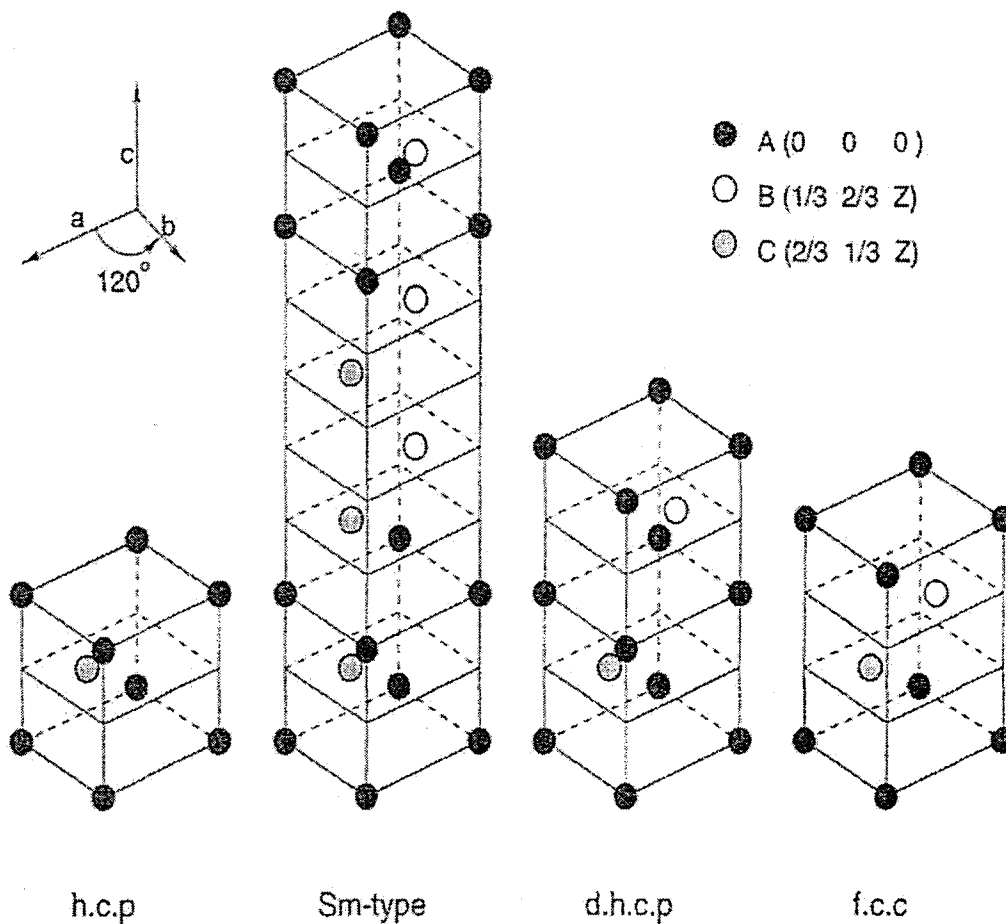


FIG. 10. Crystal structures exhibited by various rare earth metals at ambient pressures. All of the structures may be represented by different stacking of the hexagonal close-packed layers.

hexagonal cell, both a and c lattice parameters, and has 24 atoms per cell, are also observed.⁴⁰⁻⁴²

With increasing compression, as the inter-atomic distance is decreased, the overlap of outer electron increases and the Fermi energy and the energy bands are shifted. As a result, the previously localized $4f$ -electrons are expected at some point to become delocalized and begin to participate in bonding. Observation of low symmetry crystal structures, which deviates from the higher symmetry structures observed at lower pressures, is taken as an indication of this drastic change in the electronic structure and forms the second part of the structural phase diagram of the rare earth metals. Low symmetry structures observed are the body center monoclinic (bcm) structure^{43, 44} with two atoms per cell and an orthorhombic structure referred to as α -Uranium (α -U).^{40, 45} α -U, space group Cmcm, has four atoms per cell. A phase transition to α -U structure has been reported in praseodymium (Pr) at 20 GPa⁴⁶⁻⁴⁸ and in neodymium (Nd) at 110 GPa,⁴⁰ while a bcm structure has been observed in gadolinium (Gd) at 59 GPa⁴⁹ and dysprosium (Dy) at 73 GPa.⁵⁰ Although the observed formation of these structures has been interpreted as being driven by f -electron delocalization there are still some questions. Most notably are those arising from reports indicating the formation of two possible monoclinic structures, space group C2/m, following the d-fcc structure and prior to transition to the α -U structure in Pr and Nd. One of the proposed monoclinic structures has four atoms per cell,^{45, 51, 52} while the other is described by eight.⁵³ These two monoclinic structures are low symmetry structures and have raised the debate as to whether they may indicate the occurrence of localized \rightarrow delocalized f -electron change. Furthermore, based on a comparison of bulk modulus calculated for the monoclinic phase observed in Pr to that of the actinides with

delocalized f -electrons, it is suggested in Ref. 53 that the appearance of the monoclinic phase is indicative of delocalized f -electrons. Delocalized f -electrons in light actinides participate in bonding and increase lattice stiffness, resulting in a larger bulk modulus over the localized regime compared to lanthanides.

Delocalization of f -electrons

Primary evidence of f -electron delocalization in regular rare earth metals is given by the observed formation of lower symmetry crystal structures, such as α -U and bcm, at high pressures. When compressed, lanthanide band occupancy versus volume/atom is comparable to that of the light actinide metals with delocalized $5f$ -electrons.⁸ In these metals, $5f$ -electrons participate in bonding at RTP and contribute to the formation of low symmetry crystal structures,³⁷ such as the ones observed for the compressed lanthanides. In contrast the low symmetry structures are not observed for yttrium (Y). Furthermore, in some of the metals the localized \rightarrow delocalized f -electron transition is accompanied by a large volume collapse, giving further support to a drastic change in electronic behavior. For example in Pr a volume collapse of 9.1% to 16.7% has been reported at 20 GPa during the transition to α -U phase,^{45, 54, 55} and a volume collapse of 11% for Gd⁷ and 6% for Dy⁵⁰ is reported to occur during the transformation to bcm phase. It should also be pointed out that the volume collapse in Pr at 20 GPa is observed regardless of whether the transition to the α -U phase is preceded by a monoclinic C2/m phase⁴⁵ or occurs directly from the d-fcc phase.^{54, 55} On the other hand Nd, which also adopts the α -U structure at 110 GPa, has been shown to transform continuously from the C2/m phase.⁴⁰ The change in f -electron behavior from localized to delocalized is also expected to lead to other sig-

nificant changes, such as an increase in bulk modulus due to *f*-electron participation in bonding and a decrease in electrical resistivity due to additional electrons in the conduction band.⁸ The challenge has been in experimentally verifying some of these changes.

Major obstacles in performing experiments that would further support the proposed *f*-electron delocalization pressure and also measure some of the other expected changes are sample geometry, which is not only constricted in lanthanides but all high-pressure samples, as explained earlier, and the pressure-volume behavior of lanthanides. Lanthanides metals are generally very soft and, when subject to applied pressure, the decrease in volume is significant. Even for Pr, where the proposed localized→delocalized transition occurs at a relatively low pressure of 20 GPa, volume is reduced by almost 50% over this pressure range.⁴⁵ A large reduction in volume with increasing pressure not only makes such measurements as electrical resistance very difficult, but even x-ray diffraction experiments are challenging. As a result x-ray diffraction experiments have not been able to show the existence of low symmetry structures in some lanthanides, and furthermore no post- α -U or post-bcm structural phase transitions have been reported.

Divalent-Trivalent Transition

The major difference between Eu and Yb versus the regular lanthanides is that Eu and Yb are divalent at RTP. This divalent characteristic of Eu and Yb results in larger atomic volume compared to the regular lanthanides and also in the deviation from the common structural sequence, hcp → Sm-type → dhcp → fcc → d-fcc, observed for trivalent lanthanides during compression. Neither Eu nor Yb exhibit this sequence, but rather a structural sequence of bcc → hcp → Eu-III is observed from room pressure to 40 GPa

for Eu,⁵⁶ and fcc I \rightarrow bcc \rightarrow hcp \rightarrow fcc II \rightarrow hP3 structural change has been reported for Yb from room pressure to 202 GPa.⁵⁷ Spectroscopic studies as well as theoretical results have suggested that Yb undergoes a gradual increase in valence occupancy from a divalent state, $4f^{14}(5d6s)^2$, to a trivalent state, $4f^{13}(5d6s)^3$.⁵⁸ This is further supported by the formation of an hP3 structure in Yb at 98 GPa, which is one of the d-fcc structures reported to occur in regular lanthanides, Nd and samarium (Sm). In comparison to Yb, experiments performed on Eu are less common. This is in part due to the rapid oxidation of Eu. Surface oxidation of Eu makes it difficult to establish an electrical contact for electrical resistance measurements, and even x-ray diffraction is challenging due to the appearance of oxidation peaks. In the few reported results for Eu at high pressure, no clear evidence has been given yet regarding a possible divalent to trivalent transition and the pressure range over which it may occur.

TESTING AND DEVELOPMENT OF DESIGNER DIAMOND ANVILS FOR ULTRA-HIGH PRESSURE EXPERIMENTS

Introduction

Preliminary measurements and application of designer diamond anvils in studying such materials as carbon nanotubes, carbon fullerenes, and beryllium have been very positive, in that the data obtained were consistent with the observations made using x-ray diffraction techniques.^{59, 60} Performed measurements were also successful because they showed that the designer diamond anvil may be applied in high-pressure research for electrical resistance measurements. However, the pressure over which the measurements were made is relatively low compared to the ultimate goal of applying this technology for measurements above 100 GPa. In order to apply designer diamond anvils at ultra-high pressures, as well as consistently at lower pressures, further studies need to be performed in order to fully understand the measured results as well as possible problems at high pressure.

In order to develop the designer diamond anvils for consistent use in high-pressure experiments, a systematic test procedure needs to be developed that would be performed on each designer diamond anvil prior to experiment. The goal of developing a standard test is to easily and thoroughly check potential problem that may be encountered when performing high-pressure electrical resistance measurements. Some of the more common problems that may arise are the shorting of the electrical leads during the preparation of the anvil for high-pressure experiments, loss of electrical contact due to possible

damage during the fabrication process of the microprobes, as well as loss of contact due to the deformation of the diamond at high pressure. Testing the anvil for such problems as the shorting of the electrical leads and damaged microprobes may be performed easily prior to performing additional testing and without application of pressure. If the electrical probes are functioning, as would be indicated by the initial tests, the next step is to perform a high-pressure electrical resistance measurement on a sample that would give further insight into the stability of the probes and other problems that may arise at high pressures. For this step, a semiconductor gallium arsenide (GaAs) sample, which has a well-established semiconductor-to-metal transition, is used.

Initial tests and the measurement of electrical resistance of GaAs versus pressure may be performed on all designer diamond anvils prior to an experiment. These tests are a good indicator of potential problems with the anvil; however, another aspect of electrical resistance measurements at high pressures must also be considered. It was explained in the previous chapters that the selection of diamonds, more precisely a flat anvil versus a beveled anvil, is based on the maximum pressure to be achieved. It was also mentioned that although beveled anvils may in general sustain larger pressures, they develop ring crack during the decompression of pressure and can not be reused as is. This same process applies for designer diamond anvils as well. Flat designer anvils, being tested as described previously, may be used to perform multiple electrical resistance experiments without failure. The obtained results may then be compared for consistencies and discrepancies, which would indicate problems with the anvil. On the other hand, since beveled anvils are not reusable, an alternative method must be used in order to develop beveled designer diamond anvils for consistent use at ultra-high pressures. During the fabri-

cation process, the geometry of the beveled designer anvils may be adjusted. By applying designer anvils in an ultra-high-pressure electrical resistance study of cesium iodine (CsI) and cesium chloride (CsCl), this geometry, as well as the ability of designer anvils to sustain large stresses, will be tested.

Initial Tests

Initial testing consists of two steps. The first step is performed on the designer anvil while the anvil is not in contact with the sample. At this point the electrical resistance measurement, using any combination of probes, should yield a very large, greater than 100 MegaOhm ($M\Omega$) resistance value, indicating that the electrical probes are not shorting. If this is the case, the second step is to measure the electrical resistance during the preindentation of the metallic gasket; otherwise, the problem in step one should be addressed first. The gasket in our case is made of spring steel and is a very good conductor. Pressure up to 20 GPa is generated across the gasket during the indentation process. At this point the thickness of the gasket is reduced from 250 micron to approximately 10-25 micron. The four-probe electrical resistance measurement should all be very low, in the milliOhm ($m\Omega$) range, due to the low resistivity, as well as the thickness, of the metallic gasket. Typical values obtained vary between 0.1 – 5 $m\Omega$, depending on the thickness of the gasket. This test is a good indicator of any broken and or damaged micro-probes.

GaAs Test

Introduction

The GaAs sample is chosen as a test sample because it is a semiconductor at RTP and is expected to have a high resistance value, so all of the measurements should be on the order of $M\Omega$. Under applied pressure, GaAs undergoes a first-order phase transition from GaAs I (zinc-blende) \rightarrow GaAs II (orthorhombic) structure above 15 GPa.^{61, 62} Associated with this transition is a 17.2% drop in volume⁶¹ and a large change in electrical resistance from $M\Omega$ down to $m\Omega$.⁶³ The transition pressure over which this large change in electrical resistance occurs is convenient, as it may be measured without damage to either flat or beveled designer anvil.

The electrical resistance versus pressure, during compression and decompression, of GaAs is presented in the following sections. For performing the measurement, a six-probe designer anvil with a flat size of $200\ \mu\text{m}$ is used [Fig. 11(a)]. A spring steel gasket with a drilled sample hole of $80\ \mu\text{m}$ is used to contain the sample [Fig. 11(b)]. All pressure measurements are performed with a ruby pressure gauge and determined by Eq. (1). Because of the broad range of electrical resistance values observed, measurements were performed using both two-probe and four-probe techniques.

Electrical Resistance During First Compression

After placing the GaAs sample and ruby in the drilled gasket hole, a compression of 30° was applied in order to seal the sample and establish a good electrical contact with the microprobes. As a result of the initial compression a pressure of 6.7 GPa, as measured by the ruby, is generated across the sample. At this point the electrical resistance, R ,

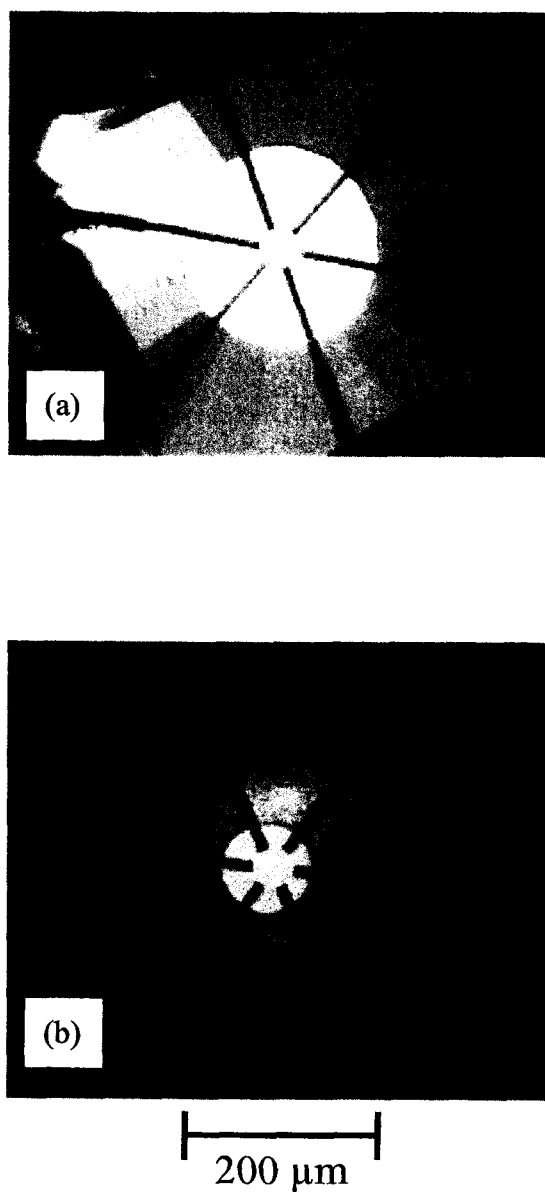


FIG. 11. Six-probe designer diamond anvil used in the GaAs experiment. (a) Shows the anvil prior to use, while (b) shows the anvil with the spring steel gasket mounted on diamond. The central bright region is the hole drilled for sample chamber.

of the sample is measured to be $7.7 \text{ M}\Omega$ using the two-probe technique. Further increases in pressure to 11.2 GPa and then 15.5 GPa result in a steady decrease in R to $3.2 \text{ M}\Omega$ and $1.1 \text{ M}\Omega$, respectively. An increase in pressure above 15.5 GPa to 17.4 GPa results in a large decrease in the R value. Due to the significant decrease in the sample resistance, the four-probe technique is applied at this point by passing a steady 1 mA dc current across the sample and determining R by Eq. (6). A value of $0.924 \text{ }\Omega$ is obtained for R at 17.4 GPa . A further decrease to $12.4 \text{ m}\Omega$ is measured as the pressure is increased to 22.6 GPa . Above this pressure, a steady R value is observed up to the highest pressure of 30.5 GPa . At this point the pressure is released and electrical resistance is measured during the decompression. During the initial decrease in pressure, R values in the milliohm range are measured up to 11.5 GPa , after which the resistance starts to increase as the pressure is further decreased to 6.5 GPa . Although the measurement shows a reversible sample resistance during decompression, showing that the sample is returning to its original state, a clear hysteresis is observed. Figure 12 shows the natural log of the measured electrical resistance, $\ln(R)$, during increase and decrease of pressure. $\ln(R)$ is plotted rather than R for better comparison. The large drop in R , by over six orders of magnitude, coincides with the reported GaAs I (zinc-blende) \rightarrow GaAs II (orthorhombic) structural phase transition above 15 GPa . The hysteresis in the electrical resistance is also consistent with the observed reversibility of the sample to GaAs I (zinc-blende) structure.⁶² This reference reports that the structure is reversible below 10 GPa . The offset in pressure during compression and decompression is a result of the nucleation of the first-order phase transition, where there is a competing difference between the surface energy of the new phase and the volume energy of the old phase as the system minimizes

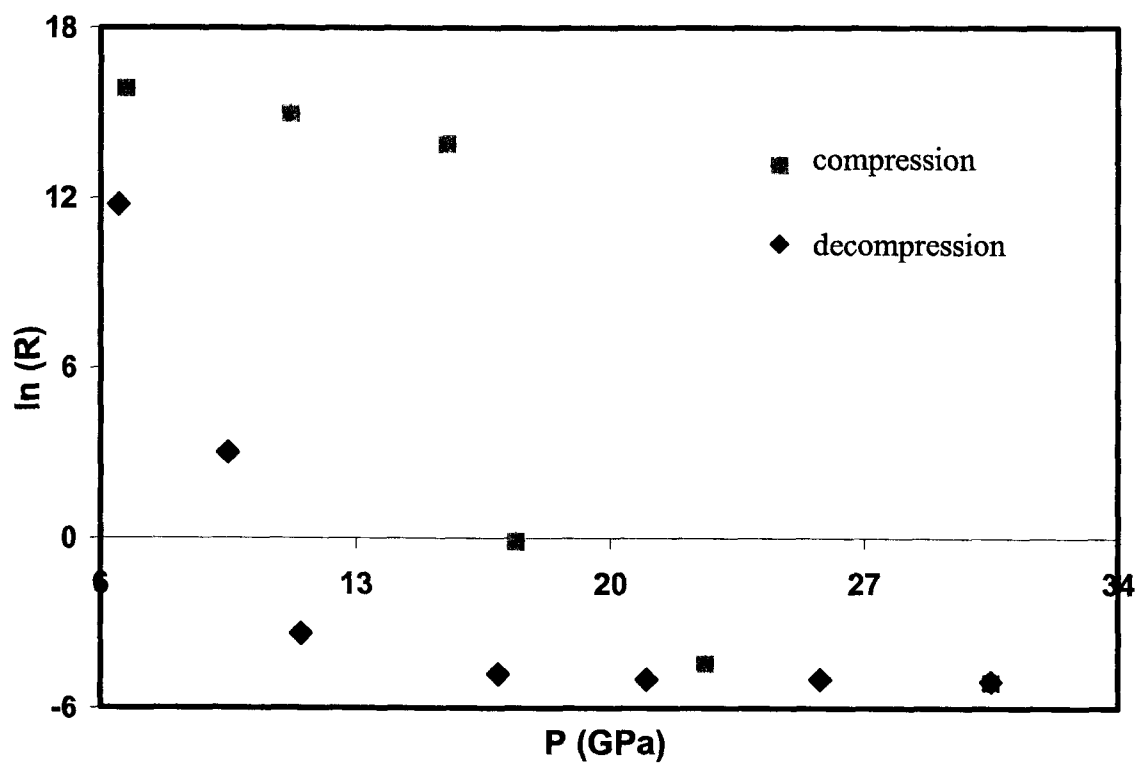


FIG. 12. Change in electrical resistance of GaAs during compression and subsequent decompression. Natural log was calculated from resistance, R , values in units of Ohm.

the free energy with change in pressure. However, the kinetics of this phase transition are not the focal point of the GaAs experiment, but rather the change in electrical resistance and its use in testing the working condition of a designer diamond anvil. A large drop in electrical resistance during increasing pressure and reversibility during decompression, as shown in Fig. 12, offers a convenient way to test an anvil prior to its use in other experiments. When designer anvils were selected for experiments presented in this study, they were all tested using the GaAs sample as a bench mark.

Optical Reflectivity

When performing high-pressure experiments it is instructive to visually observe the sample during subsequent increases in pressure. While the pressure is initially increased, the gasket flows and the gasket hole may get deformed as a result. Deformation of the hole depends on how much the gasket was preindented and on the amount of the sample in the gasket hole. Typically the sample hole becomes smaller as the sample is compressed, but in some cases the sample hole may be deformed significantly as the sample is compressed. This is even more important during an electrical resistance experiment, where the electrical microprobes may come in contact with the metal gasket at the surface. In addition to monitoring for potential problems, valuable information about sample properties may also be obtained. Optical properties of GaAs under pressure have been investigated in much greater detail elsewhere.⁶² However, by simple observation of the GaAs sample under a microscope in reflected light, a comparison may be made with the measured electrical resistance, which could aid in testing of designer anvils.

During the initial pressure increase up to 15.5 GPa, the sample appears dark and easily distinguishable from the metal gasket, as shown in Fig. 13(a) at 15.5 GPa. As the pressure is increased further, due to the shift in the absorption edge,⁶² sample reflectivity increases simultaneously with the observed decrease in electrical resistance. Figure 13 shows the sample as it becomes almost indistinguishable from the metallic gasket. In addition to observing the changes in appearance with increasing pressure, the researcher also monitors the sample during decreasing pressure. Sample appearance is observed to be reversible as the sample is observed to become dark again with decreasing pressure (Fig. 14). The major difference is that during the pressure increase the sample is dark at 15.5 GPa and only appears metallic above 17.4 GPa, whereas during decompression the sample only starts becoming dark at around 11.5 GPa. This is again consistent with the measured electrical resistance (Fig. 12), and the observed hysteresis during the decompression. The clear relation between the change in the electrical resistance and the observed change in the appearance of the GaAs sample under pressure gives a reliable backup method to the ruby pressure measurement and, furthermore, is a good indicator of the expected change in the electrical resistance.

Pressure Cycling

Deformation of the anvil under applied stress leads to possible damage and or failure. In order to check the stability of the designer anvil and verify the observed change in electrical resistance, pressure is cycled and electrical resistance is measured during the second compression and subsequent decompression. Figure 15 shows the electrical resistance measured during the first and the second compressions and

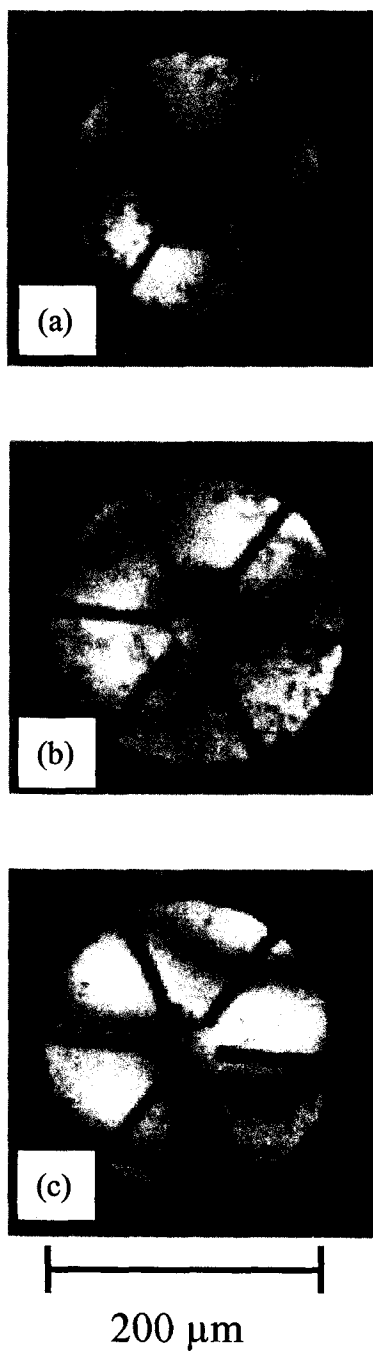


FIG. 13. Change in the appearance of GaAs when viewed under a microscope with a normal illumination. Sample appears dark initially and becomes almost indistinguishable from the metallic gasket as the pressure is increased from (a) 15.5 GPa to (b) 17.4 GPa to (c) 30.5 GPa.

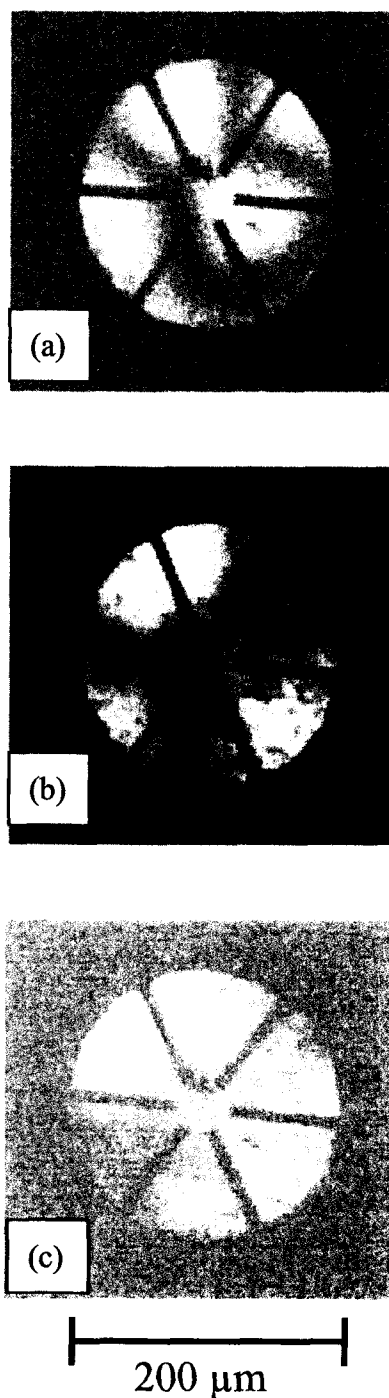


FIG. 14. Reversible change in the reflectivity of GaAs viewed under a microscope in normal illumination. Images are taken during pressure down from (a) 21.0 GPa to (b) 11.5 GPa to (c) 6.5 GPa.

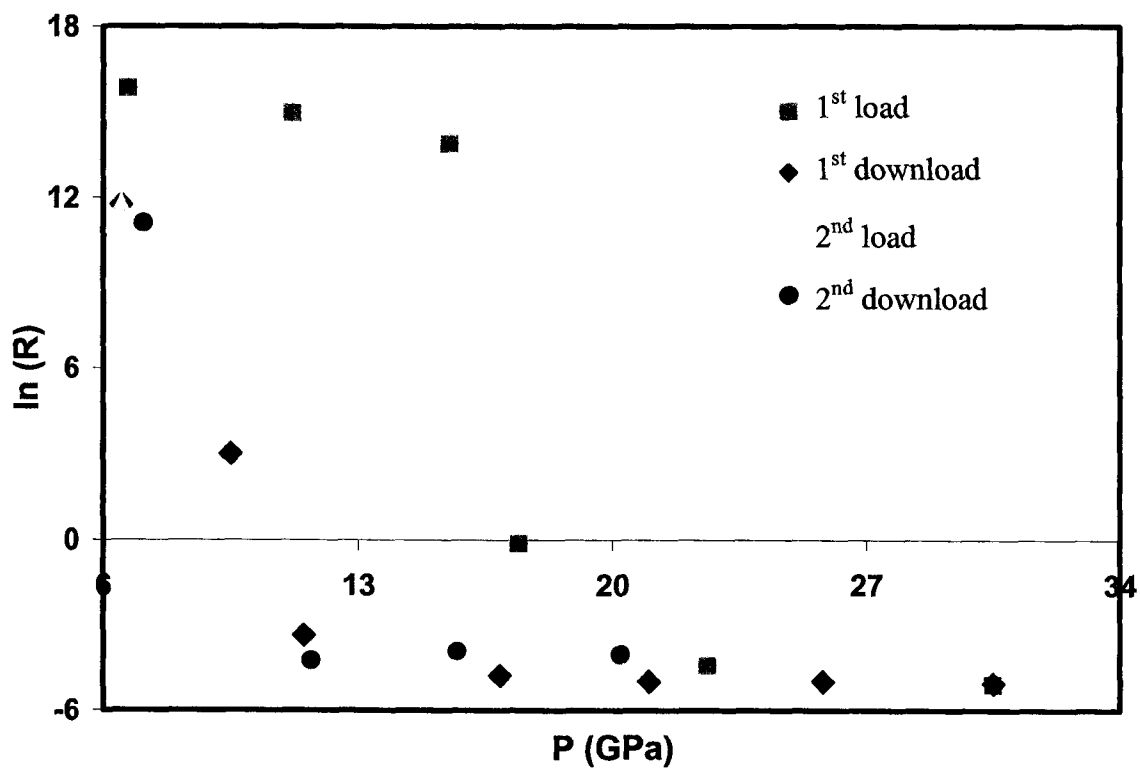


FIG. 15. Result of two compression cycles of GaAs. In both cases, a large decrease is observed in electrical resistance above 15 GPa during compression. Behavior is reversible as the pressure is decreased. Natural log was calculated from resistance, R , values in units of Ohm.

decompression. Once again $\ln(R)$ versus pressure is graphed for comparison. During the second compression, the same behavior is observed as during the first compression. Initially the sample has $M\Omega$ resistance, and a large decrease is observed in the $m\Omega$ range above 15 GPa. Likewise during the second decompression a hysteresis is once again observed as the sample reverts back to the original state. It should be noted that once the GaAs test is completed, another gasket may be indented and electrical resistance measured again through the gasket. The reason for the last step is that in many cases, after a high-pressure experiment, some of the sample may remain on the flat of the anvil itself. In most cases the remaining sample may be removed easily with acetone or sandpaper, but if the sample remains over the part where the probe should be exposed, we would experience interference with the electrical resistance measurement through the metal gasket.

CsI and CsCl High-Pressure Experiments

Introduction

When considering the use of beveled designer anvils for performing ultra-high-pressure electrical resistance studies, two questions must be answered: Will the embedded microprobes jeopardize the mechanical strength of the diamond and cause the anvil to break before achieving maximum pressure, and do the microprobes experience any flow stresses that may lead to a loss of electrical contact or result in unreliable data? In order to answer these questions we selected two anvils with optimal geometry, as in the case of the regular anvils, for achieving pressure in the 100-200 GPa and 200-300 GPa ranges. In addition to selecting the geometry of the anvil, CsI and CsCl were chosen for the experiments. These two samples were chosen because Cs halides, that is CsI, CsBr,

and CsCl, are all characterized by a large energy band-gap of 6.40 eV, 8.36 eV, and 9.03 eV, respectively, at RTP.^{64,65} Optical absorption studies during increasing pressure have shown a decrease in the band-gap and have suggested a possible metallization of CsI above 100 GPa.^{66,67} Using the conventional electrical resistance measurement technique and checking the temperature dependence of resistance, it was later confirmed that the metallization of CsI occurs above 115 GPa.⁶⁸ This reference reports that initially CsI exhibits a steady decrease in electrical resistance, which then levels off at 115 GPa. This is consistent with a continuously decreasing band-gap with increasing pressure that is independent of structural phase transitions. Similar behavior is expected for CsCl; however, due to a significantly larger band-gap, it has been predicted based on a full-potential linear muffin-tin orbital (FP-LMTO) computational simulation⁶⁹ that the metallization of CsCl would occur at a pressure closer to 300 GPa.⁷⁰ Performing ultra-high-pressure electrical resistance measurement on CsI and CsCl therefore gives us the opportunity of possibly determining the insulator→metal transition pressure, while electrical resistance versus pressure data may be monitored for any abrupt changes, discontinuities, and otherwise inconsistent behavior that may suggest problems with the designer anvil at ultra-high pressure.

Metallization of CsI Under High Pressure

In order to measure electrical resistance above 100 GPa a six-probe designer diamond anvil with a 100 μm flat, 10° bevel, and 300 μm culet was used. Prior to loading the CsI sample initial tests, including the GaAs, electrical resistance measurements, were performed with the anvil, as described in the earlier sections. A sample is loaded in a

sample hole $50\ \mu\text{m}$ in diameter, drilled in a preindented spring steel gasket. The exposed microprobes separation at the tip is $25\ \mu\text{m}$, measured as the distance between the opposing probes. Drilling a $50\text{-}\mu\text{m}$ sample hole ensures that the probes are in contact with the sample and not the metal gasket. No pressure media is used because of the interference it may cause with establishing electrical contact with the sample. In order to monitor the effect of any pressure gradient on the change in electrical resistance, two pieces of ruby are placed for pressure determination. As shown in Fig. 16, one piece of ruby, marked P_{RC} , is placed near the center of the flat while the other, marked P_{ROC} , is placed roughly $15\ \mu\text{m}$ from the center. In addition to a ruby pressure gauge, a pressure-volume EoS of CsI is used for determining the pressure. Previous x-ray diffraction experiments show a continuous distortion of the cubic CsI structure, referred to as the B2 structure, to an orthorhombic structure above 15 GPa, which is then stable up to 200 GPa.⁷¹ The measured pressure-volume relation is fit using a universal EoS form.^{71,72}

An initial compression of 15° results in pressure of 9.9 GPa determined from the center ruby, P_C , and 10.6 GPa determined from the ruby that was placed $15\ \mu\text{m}$ off center, P_{OC} . The difference in the pressure is due to a pressure gradient over the sample. A two-probe electrical resistance measurement, using various probe combination, gives values ranging from 204 k Ω to 283 k Ω . Higher electrical resistance of the sample is measured in the area near the P_{RC} using probes 4-7, and decreases as the measurements are made closer to the P_{ROC} using probes 2-5. A further compression increase results in $P_C = 21.6$ GPa and $P_{OC} = 21.9$ GPa. At the same time the measured electrical resistance has a value of 190 k Ω to 229 k Ω . Larger values are once again obtained near the center ruby, an area of lower pressure, than over the higher pressure area of the sample. The observed

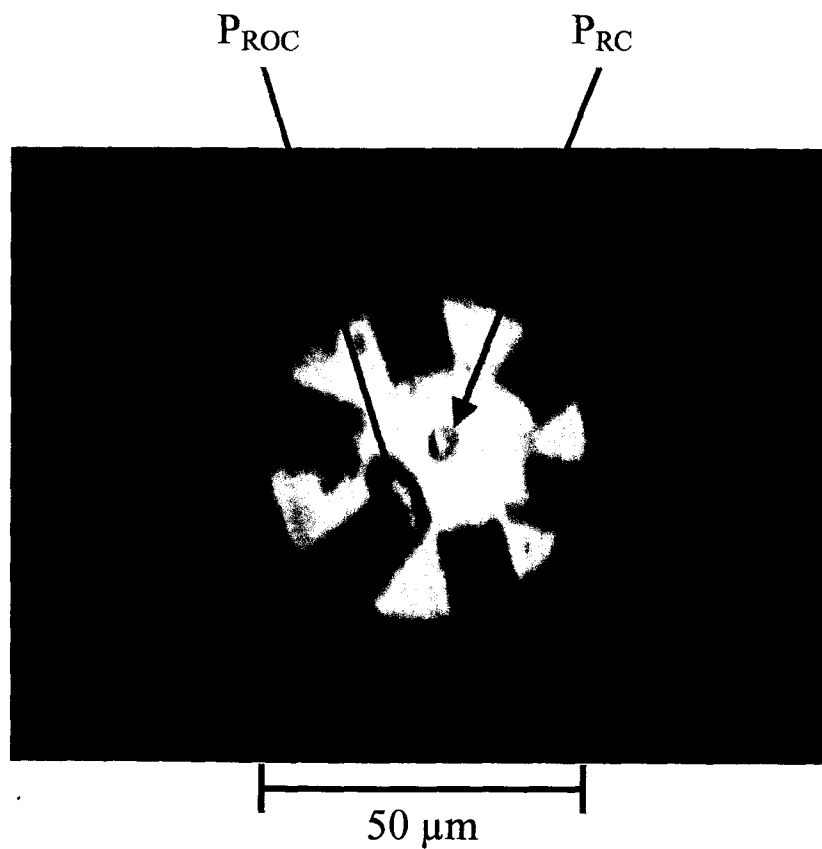


FIG. 16. CsI in transmitted light at ambient conditions in a diamond anvil cell. Also shown are the two ruby pressure markers, marked as P_{RC} and P_{ROC} , used for determining pressure during CsI experiment and the four probes, 2, 4, 5, and 7, used for measuring electrical resistance.

pressure gradient is not unusual and has been a subject of previous experimental and theoretical studies.⁷³ The resulting pressure gradient gives rise to differences in compression of the band-gap across the sample. In the higher pressure region, which has the measured pressure P_{OC} , the band-gap is smaller than in the region of P_C and, as a result, the electrical resistance values of the sample are lower when measured with probe 2-5 than when measured with probe 4-7. The displacement of the highest pressure region from the center of the anvil flat is the result of tolerance in the piston of the DAC. During compression the two anvils are offset with respect to each other and thus the center of the overlapping area is near the off-center ruby. Table 1 shows the measured pressure in the two regions during successive compression. The resulting electrical resistance values are also consistently lower when measured in the area of higher pressure, P_{OC} . The highest pressure obtained for P_C is 48.3 GPa. Under further compression we were not able to detect the ruby signal for pressure measurements in this region and for a comparison of the effect of pressure gradient on electrical resistance. As a result pressure is measured using the off-center ruby only up to a pressure of 77.3 GPa, at which point the ruby signal becomes too weak to measure. Above this pressure, EDXD spectra of CsI is collected, and pressure is determined from the EoS, P_{EOS} .

Due to the observed pressure gradient, only the electrical resistance measured over the same sample region may be compared directly. Figure 17 shows the change in the electrical resistance of CsI up to the highest pressure of 118.2 GPa. Graphed data shows the natural log of electrical resistance, $\ln(R)$, that was consistently measured in the region of the off-center ruby used for determining P_{OC} . The steady decrease in the electrical resistance down to a milliohm range above 100 GPa is consistent with what was

TABLE 1. The pressure gradient measured over the CsI sample at various pressures by ruby fluorescence technique.

Compression	P_C (GPa)	P_{OC} (GPa)
15°	9.9	10.6
4°	21.6	21.9
3°	35.6	38.4
3°	48.3	54.2
2°	*	62.0
2°	*	77.3

*Ruby signal can not be detected.

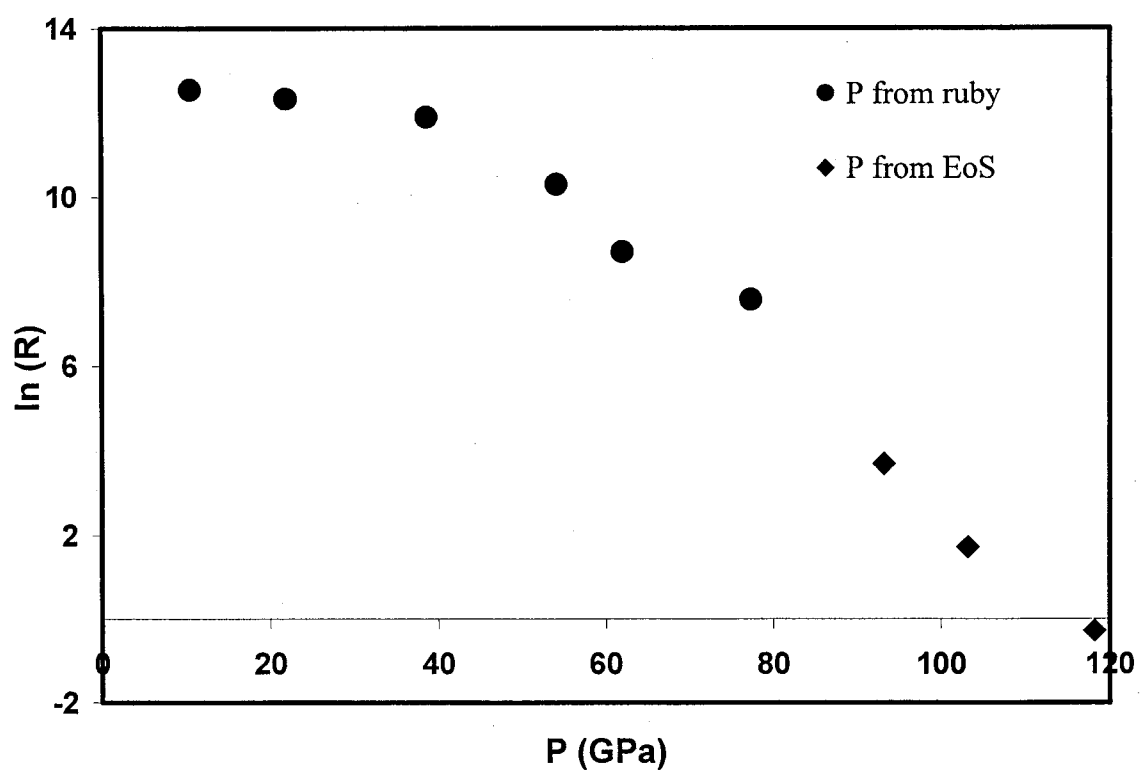


FIG. 17. Change in the electrical resistance of CsI under applied pressure. Natural log was calculated from resistance, R , values in units of Ohm.

reported in Ref. 68. Furthermore, electrical resistance is also consistent in that there are no sudden drops or otherwise anomalous behavior that would indicate problems with the stability of the electrical microprobes at high pressure. The highest obtained pressure of 118.2 GPa also falls within the range of what may be expected with this anvil geometry. Although higher pressure generation could be possible, there are other factors that may influence this limit. One of those is the hardness of the sample. Higher pressures are generally achieved with a given anvil geometry when harder, less compressible samples are used. CsI is considered soft, as shown by the pressure-volume curve,⁷¹ which shows a decrease of almost 50% in volume at 50 GPa. Because of the large decrease in volume, soft samples do not provide as much support between the anvils as the harder samples. As a result diamond anvils may come in contact with each other, leading to failure at high pressure.

Change in Optical Absorption

Initially, when viewed under a microscope in transmitted light, CsI appears transparent (Fig. 16), as expected due to the large band-gap. However, as the band-gap decreases, the absorption edge shifts to visible range and, as a result, transmitted light is absorbed. This leads to a change in the color of the sample from light yellow→dark yellow→orange→red→dark red→opaque with increasing pressure. As observed by measuring ruby at different areas of the sample there is a pressure gradient, which is also evident when the sample is viewed in transmitted light. The constant compression sample area at higher pressures, as measured by P_{ROC} , is at a higher end of the color sequence than the lower pressure sample region, measured by P_{RC} . The observed color change is

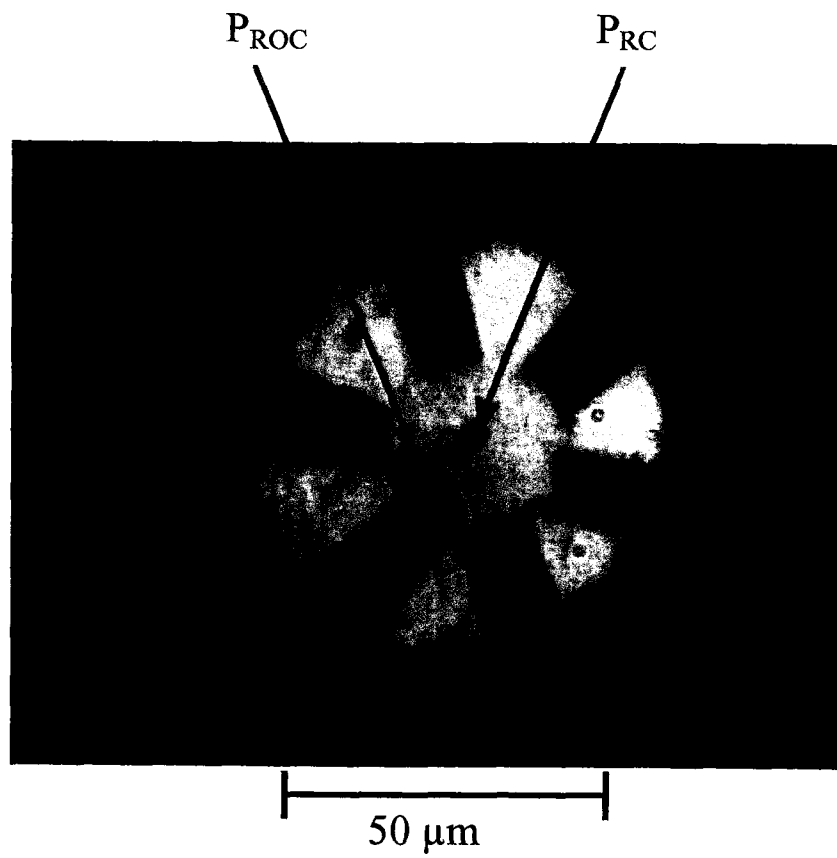


FIG. 18. CsI in transmitted light at $P_C = 35.6$ GPa and $P_{OC} = 38.4$ GPa.

also consistent with the measured electrical resistance. Figure 18 shows the sample at $P_C = 35.6$ GPa and $P_{OC} = 38.4$ GPa. This figure shows that most of the sample is still transparent except for the area near the ruby marked as P_{ROC} , which appears to be light yellow. Electrical resistance measurement at this compression by probes 4-7 gives a value of 189 k Ω , compared to 148 k Ω measured by probes 2-5. The change in color is even more evident during further compression, with measured pressure $P_C = 48.3$ GPa and $P_{OC} = 54.2$ GPa [Fig. 19(a)], and $P_{OC} = 77.3$ GPa [Fig. 19(b)]. A continuous decrease in the band-gap results in more of the sample becoming darker, starting in the area of P_{ROC} and propagating in a radial direction. Successive electrical resistance measurements at a constant compression always result in a lower value when the measurement is made over the darker color region, probes 2-5, than the lighter color region of the sample, probes 4-7.

In addition to observing the change in color due to the absorption of transmitted light, the sample chamber is also observed to have changed with increasing pressure. Initially the sample hole is 50 μm in diameter (Fig. 16); however, as may be seen in Figs. 18 and 19, when the pressure is increased the gasket flows and the diameter of the sample hole is increased. As the sample hole diameter gets larger, there is less support between the anvils. As mentioned in the previous section, in the case of soft samples such as CsI, the sample does not provide enough support and as a result limits the ultimate high pressure that can be achieved.

CsCl Electrical Resistance

By performing the CsI experiment first we are able to get an idea of how the electrical resistance of this sample changes with an increase in pressure and the subsequent

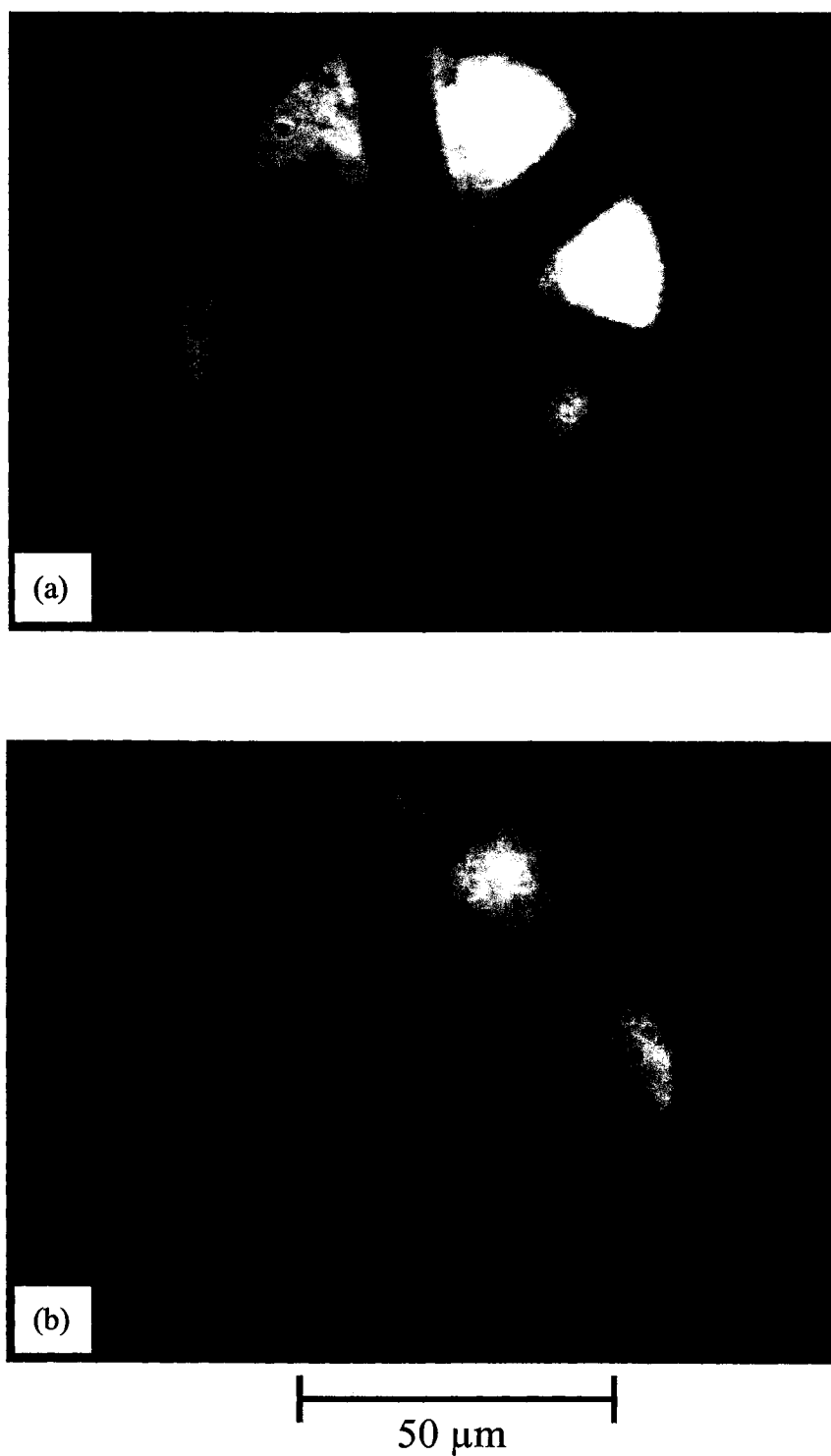


FIG. 19. CsI in transmitted light at (a) $P_C = 48.3$ GPa and $P_{OC} = 54.2$ GPa and (b) $P_{OC} = 77.3$ GPa,

decrease in the band-gap. In order to test the designer diamond anvil at even higher applied stress, a six-probe anvil, with a probe separation of 20 μm measured between the opposing anvils, a 65 μm central flat, an 8.5° bevel, and a 300 μm culet (Fig. 20), is used to measure the electrical resistance versus pressure of CsCl sample. CsCl is suitable for this experiment because it has a band structure similar to CsI, but with a larger band-gap, at RTP.^{67, 74} Under applied pressure CsCl is likewise expected to have a continuous decrease in the band-gap leading to metallization above 280 GPa.⁷⁰ Electrical resistance measurements are performed using a two-probe technique, while EDXD spectra are collected during increasing pressure. Pressure media and pressure gauge are not used in order to reduce possible problems with data collection and subsequent data analysis. In order to monitor electrical resistance over the whole sample area and the effect of the pressure gradient, as observed during the CsI experiment, six different probe combinations are used.

Initially electrical resistance of the sample is very high, as expected due to a large band-gap. The Hewlett Packard model 34401A multimeter used for performing electrical resistance measurements in the experiment has a maximum measurement upper limit of 110 M Ω , and values above this are reported as "Ovld." Initially all of the electrical resistance measurements result in Ovld, as compression is increased in 5° steps up to a total of 50°. As the compression is further increased by 5°, resulting in a total compression of 55°, electrical resistance values decreased below Ovld (Fig. 21). The observed decrease in electrical resistance continues as the compression is increased to the highest value of 103°. Difference in electrical resistance measured between various probes also appears to decrease as the compression is increased. Resistance values measured at the compression

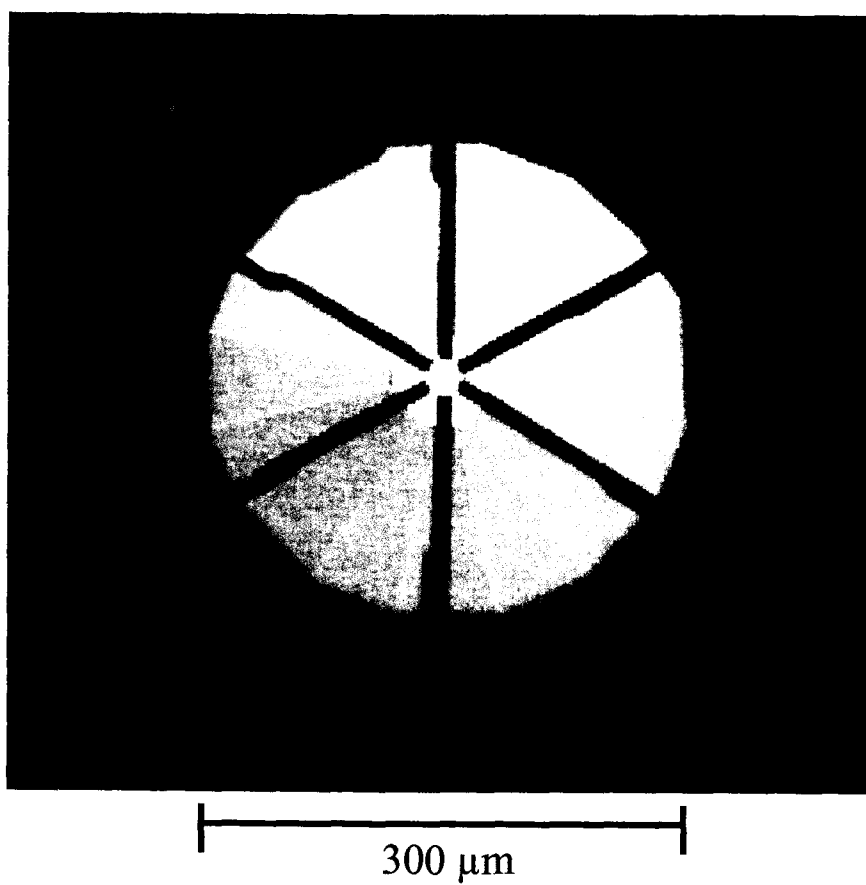


FIG. 20. Six-probe designer diamond anvil used for the CsCl experiment.

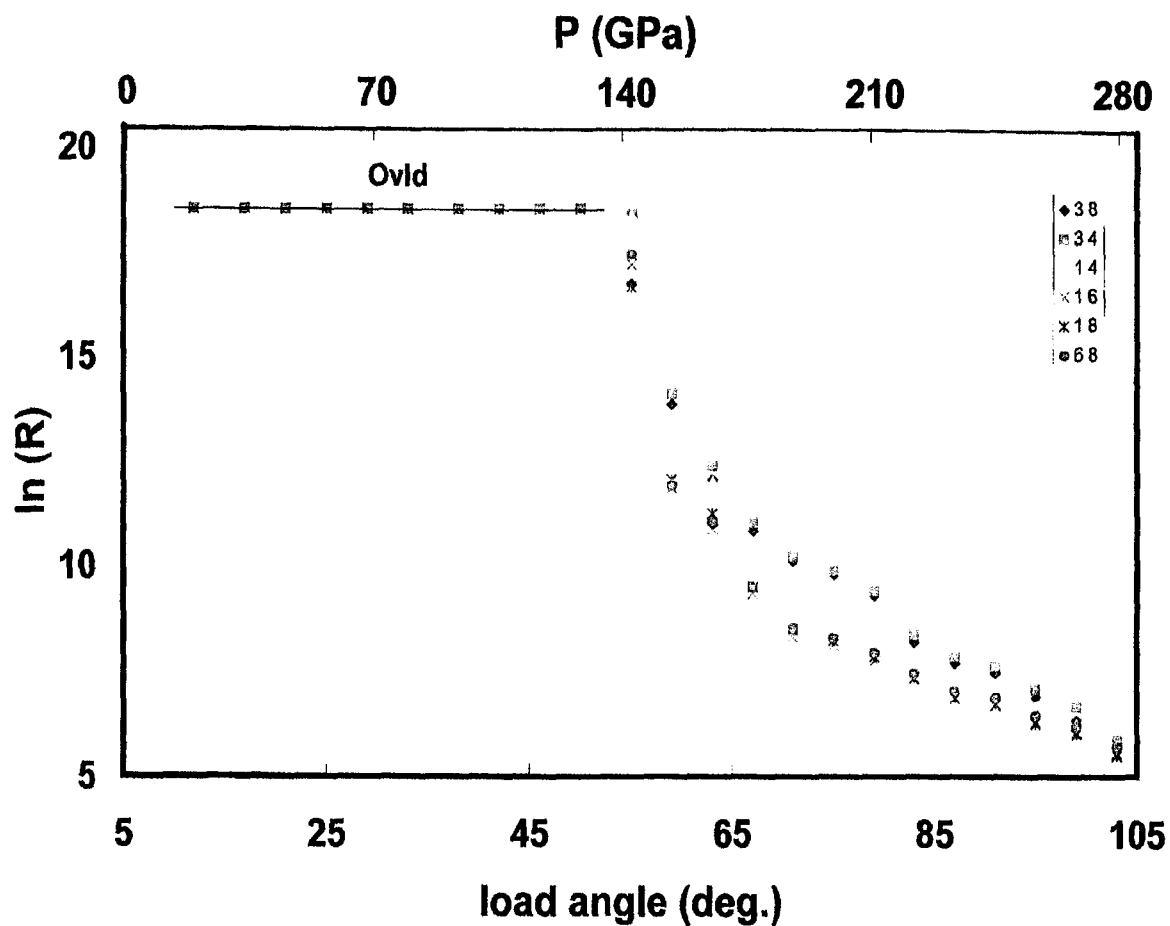


FIG. 21. Change in electrical resistance of CsCl with increasing compression load angle measured using various probe combinations, as indicated. Initially values are above $110 \text{ M}\Omega$, which is the upper measure limit of the multimeter, and are reported as "Ovld." Natural log was calculated from resistance, R , values in units of Ohm.

angle of 55° range from $17 \text{ M}\Omega$ up to $98 \text{ M}\Omega$, at 79° compression measured values range from $3 \text{ k}\Omega$ up to $12 \text{ k}\Omega$, and at 103° compression the difference in the measured values decrease even further, from $251 \text{ }\Omega$ to $366 \text{ }\Omega$. The difference in the measured resistance values can most likely be attributed to a pressure gradient, as in the case of CsI. In addition to giving rise to differences in the band-gap, sample thickness is also influenced by pressure distribution. However, as the sample thins out with increasing compression, the difference in thickness across the diameter of the flat becomes comparably smaller, leading to a smaller spread in the measured electrical resistance values. Figure 21 shows $\ln(R)$ versus compression load angle; estimated pressure from the compression load angle is also plotted on the top axis. Pressure can only be estimated due to the lack of a pressure marker in the sample chamber. Although EDXD spectra are also collected, the pressure-volume EoS is only known up to 40 GPa for CsCl.⁷⁵ Even though pressure cannot be determined exactly, the final pressure estimate is in a good agreement with the predicted decrease in the band-gap and possible metallization above 280 GPa . At this point there is no conclusive evidence, such as a measurement of the temperature dependence of electrical resistance, indicating that the metallization of CsCl has occurred; however, by comparison to CsI (Fig. 17), a decrease in electrical resistance by more than six orders of magnitude may indicate a significant decrease in the band-gap of CsCl. Data collected for CsCl (Fig. 21) is also consistent with CsI data, reported in this study as well as in Ref. 68, in that the resistance decreases continuously with no sharp drops that would indicate potential problems with the probes.

Conclusions

In order to consistently and reproducibly collect any data, the equipment used must be understood and all of the possible problems that may occur during data collection must be addressed. By performing a few simple tests, such as measuring open electrical resistance and the electrical resistance of the metal gasket during indentation, potential problems caused during the fabrication and preparation of designer diamond anvils may be addressed prior to performing an experiment. Furthermore, a change in the electrical resistance in GaAs with increasing and decreasing pressure allows for additional testing to be performed on flat and beveled anvils alike. By performing CsI and CsCl experiments it is also shown that having the electrical microprobes built into the diamond does not compromise the mechanical strength of designer diamond anvils for application in high-pressure experiments.

PRASEODYMIUM

Introduction

Of all the regular rare earth metals, Pr is an ideal candidate for studying changes in the electronic structure induced by applied pressure. The proposed localized→delocalized f -electron transition is predicted to occur at 20 GPa as Pr undergoes a structural phase transition to an α -U structure. This is a relatively modest pressure for diamond anvil cell devices and can be achieved with designer diamonds of 200-300 μm in diameter. The electrical transport data can be readily reproduced for experiments in this pressure range. Furthermore, compared to Nd, Gd, and Dy, where the proposed transition pressures are well above 50 GPa, Pr allows for post-transition properties to be studied over much greater pressure ranges. In particular, it is of great interest to investigate the stability of the α -U structure at extreme compressions.

The extreme compressions are defined as ones where material volume is reduced to one-half to one-third of its volume at ambient pressure. Such volume compressions of 50% to 66% are now possible in ultra-high-pressure diamond anvil cells, and materials can be studied using intense and focused synchrotron radiation beams and designer diamond anvils. Pr adapts the α -U phase at pressures above 20 GPa at ambient temperature, while it is observed in Nd above 113 GPa.^{40, 47, 48} Earlier high-pressure studies on Pr metal had established the stability of the α -U structure to 103 GPa and Nd to 155 GPa.^{40,}
⁴⁵ Density-functional electronic structure calculations have been used to investigate the

high-pressure behavior of Pr.⁷⁵ These calculations reproduce the pressure and volume conditions for the formation of the α -U phase in Pr remarkably well and predict a transformation sequence α -U \rightarrow body centered tetragonal (bct) \rightarrow hexagonal close packed (hcp) with increasing pressure. The α -U \rightarrow bct phase transformation in Pr is predicted to occur at 104 GPa ($V/V_o = 0.40$), while the bct \rightarrow hcp transformation is predicted to occur at a six-fold compression ($V/V_o = 0.16$).

Electrical Resistance Measurements

The four-probe electrical resistance measurements on Pr were performed using designer diamond anvils having various flat sizes. Having multiple electrical probes gave us the flexibility to measure four-probe resistance in various regions of the sample for any nonuniformity across the sample. Six different high-pressure experiments were performed on all Pr samples to confirm the reproducibility of the electrical resistance data. In the first five experiments, the ruby fluorescence technique was employed for pressure measurements up to 56 GPa. In an ultra-high-pressure experiment to 179 GPa, pressure was calibrated using the known equation of the state of Pr and the measured volume of Pr by x-ray diffraction technique. All x-ray diffraction patterns on Pr were collected at the beam line X-17C at the NSLS - BNL with a micro-collimated beam of $10 \mu\text{m} \times 10 \mu\text{m}$.

Figure 22 shows the photomicrograph of the Pr sample in an eight-probe designer diamond anvil at a pressure of 56 GPa. One set of current and voltage leads used for the measurement are indicated along with the Pr sample, which is 80 microns in diameter. A constant current source of 1 mA supplied by the Model 2400 SourceMeter from Keithley and the Model 2182 nano-voltmeter from the same manufacturer were used to measure

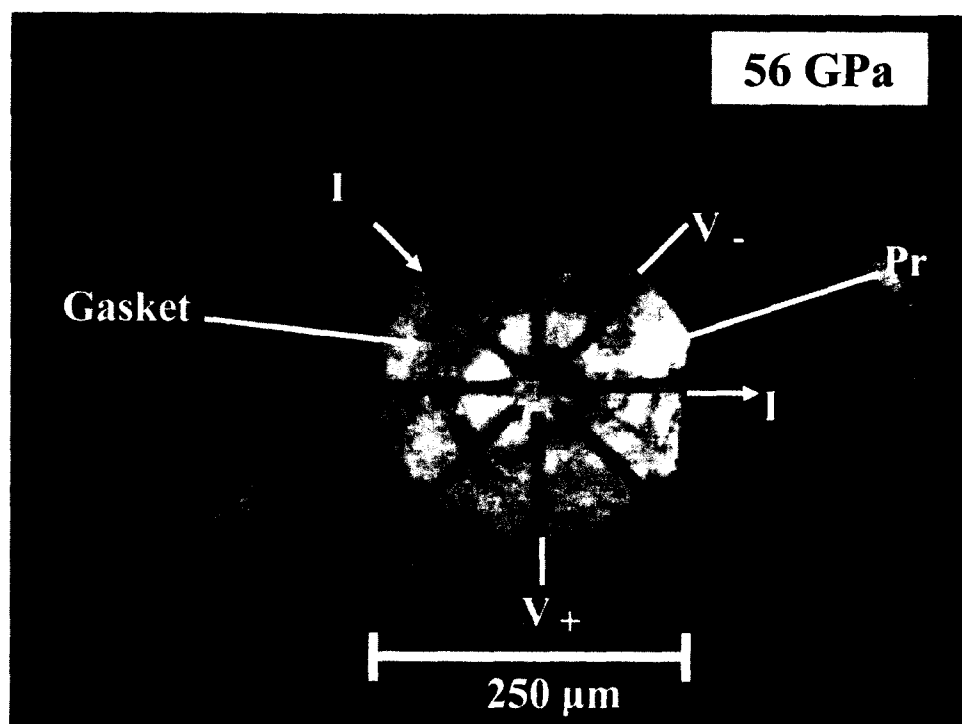


FIG. 22. Photomicrograph of the Pr sample in an eight-probe designer diamond anvil, with the direction of the current (I) flow and polarity of the voltage (V) leads of four-probe configuration.

electrical resistance, with the resistance values reported at each pressure averaged from 20 independent readings. Table 2 shows a summary of all six experiments on Pr metal in a diamond anvil cell.

Figure 23 shows the four-probe resistance of the Pr sample as a function of pressure to 179 GPa during the compression cycle in Experiment 6. In the pressure range of 0 to 10 GPa, there is an overall increase in resistance, which can be attributed largely to sample extrusion or thinning and hence a decrease in the cross-sectional area of the specimen. At 20 GPa, an abrupt drop of approximately 59% is observed in a narrow pressure range of 3 to 5 GPa at the *f*-delocalization (Fig. 23). After *f*-shell delocalization, the resistance reaches a steady value in the pressure range between 50 GPa to 130 GPa. There is a slight gradual increase in resistance above 130 GPa, and another plateau in resistance is reached in the 150 GPa to 179 GPa pressure range. This sharp drop in resistance at 20 GPa coincides with the formation of the α -U phase in Pr, as confirmed by numerous x-ray investigations. The origin of a gradual increase in resistance in the 130-150 GPa range is related to additional structural transformation in this pressure range, as will be discussed later. Since the electrical resistance data below 10 GPa during compression is invariably affected by the sample extrusion and other sample geometry considerations, decompression data can reveal absolute value of sample resistivity, as shown in Fig. 24.

Table 2 also shows the percent change in resistance for the six different experiments at the 20 GPa transition mark. The average resistance drop for the six experiments during compression was calculated to be 53%. The measured range of resistance drop varies from 43% to 59%, and this variation can be attributed to the experimental

TABLE 2. Summary of six high-pressure experiments on Pr, documenting the electrical resistance drop at 20 GPa.

	P_{MAX} (GPa)	Change in Resistance at 20 GPa
Experiment 1	32	57%
Experiment 2	30	43%
Experiment 3	56	50%
Experiment 4	30	56%
Experiment 5	30	52%
Experiment 6	179	59%

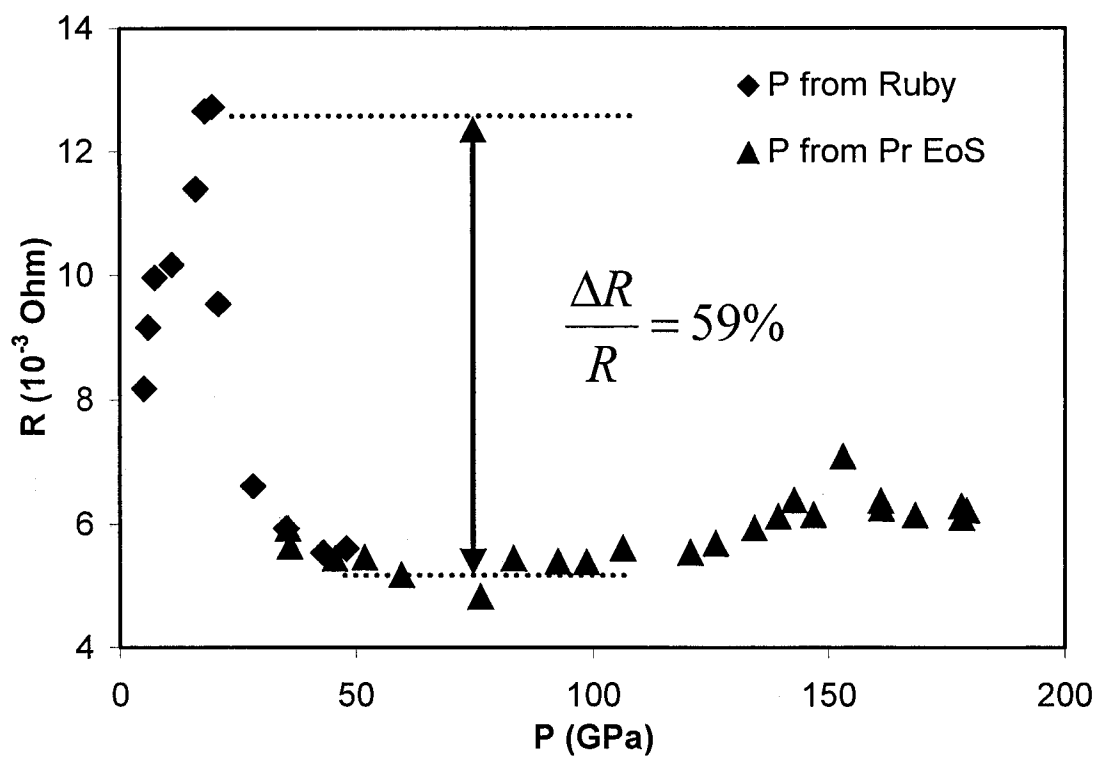


FIG. 23. Electrical resistance of Pr during compression up to 179 GPa, observed in experiment 6.

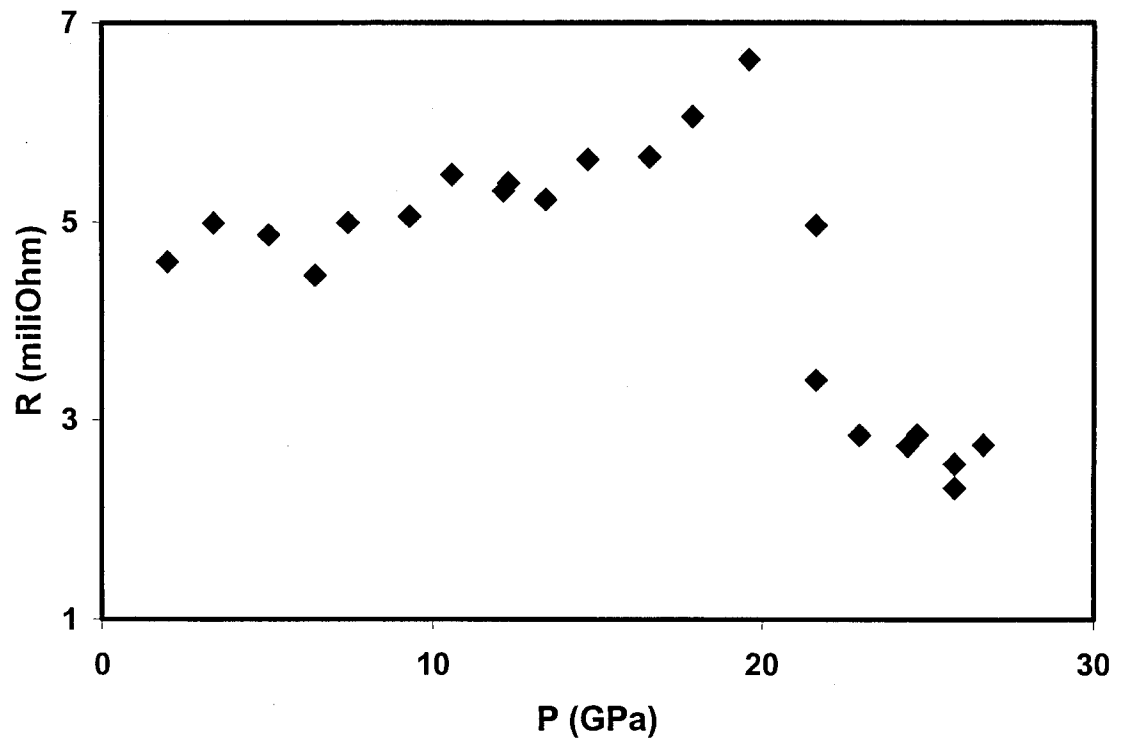


FIG. 24. Electrical resistance measured during decompression cycle of experiment 1.

uncertainties in locating the maximum in resistance before the drop at the transition (Fig. 23). The time elapsed between different pressure and conductivity measurements was similar in all experiments; however, transformation kinetics effects may somewhat effect the magnitude of resistance drop observed. It should be noted that our observed value of resistance drop is consistent with the 50% drop reported for cerium metal at the *f*-delocalization pressure of 0.7 GPa.⁷⁶

Distortion of α -U Structure

Another experiment on a Pr sample was performed in order to obtain a better understanding of the increase in electrical resistance near 150 GPa (Fig. 23) and to study the stability of the α -U phase at ultra-high pressure.

A Pr sample purchased from Alfa Aesar, having 99.9% purity, was studied using the EDXD technique at beamline X17-C at the NSLS - BNL. In this experiment, type Ia diamonds with an 8° bevel, 35- μ m central flat, and a 350- μ m culet were employed. A polycrystalline Pr sample was loaded in a preindented spring steel gasket, which has a 20 μ m drilled sample hole. Cu, which was used as a pressure marker, was also placed in the sample chamber. Due to the relative softness of Pr and in order to avoid the occurrence of an unwanted reaction of the Pr-sample with the medium, no pressure-transmitting medium was used in this experiment. An X-ray beam of 10 μ m X 12 μ m was used to study Pr under increasing pressures.

Pressure Determination

To obtain the most accurate pressure from our internal pressure marker, Birch-Murnaghan EoS, Eq. (7), was fitted to the data for Cu reported by McQueen *et al.* (Ref. 26) and Holmes *et al.* (Ref. 27) in the pressure range from 0-1000 GPa^{77,78}:

$$P = 3B_0 f_E (1 + 2f_E)^{5/2} \left\{ 1 + \frac{3}{2}(B'-4)f_E + \frac{3}{2} \left[B_0 B'' + (B'-3)(B'-3) + \frac{35}{9} \right] f_E^2 \right\} \quad (7)$$

Equation (7) is based on a fourth-order expansion of the elastic strain energy, where B_0 is the bulk modulus, B' is the first derivative of bulk modulus, and B'' is the second derivative of the bulk modulus. In the case of the third-order fit, the coefficient of f_E^2 is equal to zero and the second derivative of the bulk modulus is given by:

$$B'' = \frac{-1}{B_0} \left[(3 - B')(4 - B') + \frac{35}{9} \right]$$

and

$$f_E = \frac{\left[\left(\frac{V_0}{V} \right)^{2/3} - 1 \right]}{2}$$

for volume at room temperature-pressure, V_0 . Using $a_0=3.6148 \text{ \AA}$ for Cu (Ref. 40), third-order EoS was fitted to copper, with the following values obtained: $V_0=47.234 \text{ \AA}^3$, $B_0=121.6 \text{ GPa}$, $B'=5.583$, and $B''=-0.0656 \text{ GPa}^{-1}$ for Cu. The result of the fit to the data reported in Refs. 26 and 27 may be seen in Fig. 25. This third-order Cu-EoS fit can be used for pressure measurements to 1000 GPa, provided the volume for the fcc phase of Cu is known by x-ray diffraction methods.

α -U \rightarrow P2₁2₁2₁ Phase Transition

Figure 26 shows the EDXD spectrums recorded on increasing pressure to 313 GPa. The attention is focused on the energy range of 24 to 32 keV, in which dramatic changes in the diffraction data are observed. In an earlier study, Pr was studied to a pressure of 103 GPa at ambient temperature, and a α -U structure was observed to be stable till the highest pressure. In Fig. 26, we focus on the behavior of Pr metal above 100 GPa. The spectra shown at 103 GPa in Fig. 26 is fitted to the α -U structure (space group Cmc_m) with four atoms occupying 4c Wyckoff positions at $(0, y, \frac{1}{4})$, $(0, -y, \frac{3}{4})$, $(\frac{1}{2}, \frac{1}{2}+y, \frac{1}{4})$, and $(\frac{1}{2}, \frac{1}{2}-y, \frac{3}{4})$. Using the value of 0.1 for y gives the best fit to the spectra; we obtained $a = 2.507 \pm 0.004 \text{ \AA}$, $b = 4.959 \pm 0.017 \text{ \AA}$, and $c = 4.527 \pm 0.001 \text{ \AA}$ at 103 GPa, which is in good agreement with what was reported earlier.⁴⁵ At a pressure of 147 ± 5 GPa, a change in structure occurs with the appearance of a new diffraction peak between the (021) and (111) peaks of the orthorhombic α -U phase. This new peak is labeled as (012) peak of a primitive orthorhombic phase at 158 GPa in Fig. 26. This (012) diffraction peak is not permitted (zero intensity) in the α -U structure due to the C-centering of the unit cell, which requires that Miller indices $h + k$ to be an even number. Therefore, a new crystal structure was assigned to diffraction patterns above 147 GPa as orthorhombic, space group P2₁2₁2₁ with the four atom positions at (x, y, z) , $(\frac{1}{2}-x, -y, \frac{1}{2}+z)$, $(-x, \frac{1}{2}+y, \frac{1}{2}-z)$, and $(\frac{1}{2}+x, \frac{1}{2}-y, -z)$. The α -U and P2₁2₁2₁ structures are closely related; for example, if x and z values in P2₁2₁2₁ are both set to 0.25 and the origin is shifted by this amount along the negative x -axis, we get back the α -U structure and atomic positions as described by the 4c Wyckoff positions. This new structure should be viewed as a distorted α -U structure. Figure 27 shows the full-energy dispersive x-ray diffraction pattern at a

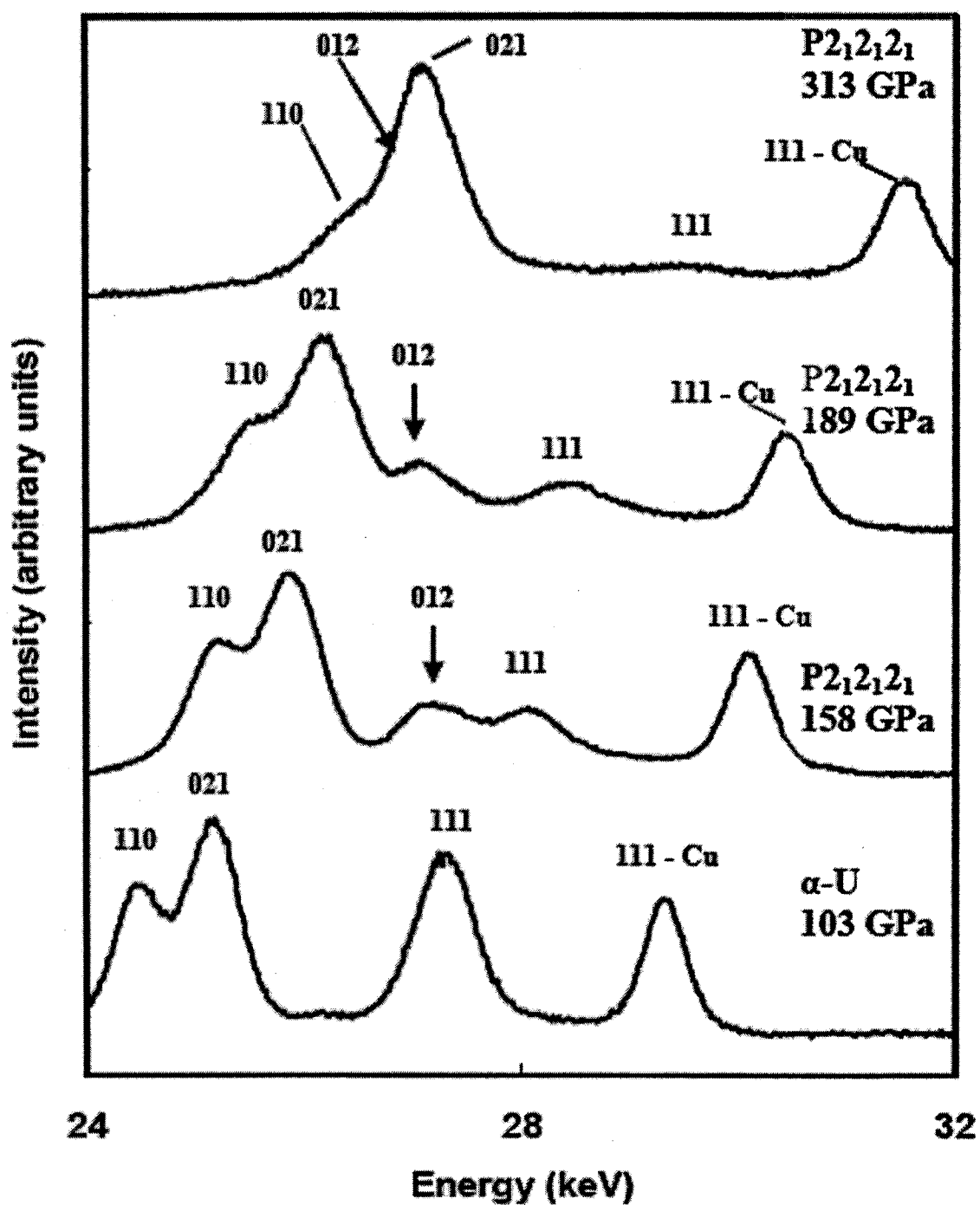


FIG. 26. Energy dispersive x-ray diffraction pattern of Pr sample and a Cu pressure marker at various pressures to 313 GPa. The diffraction angle $2\theta = 13^\circ$.

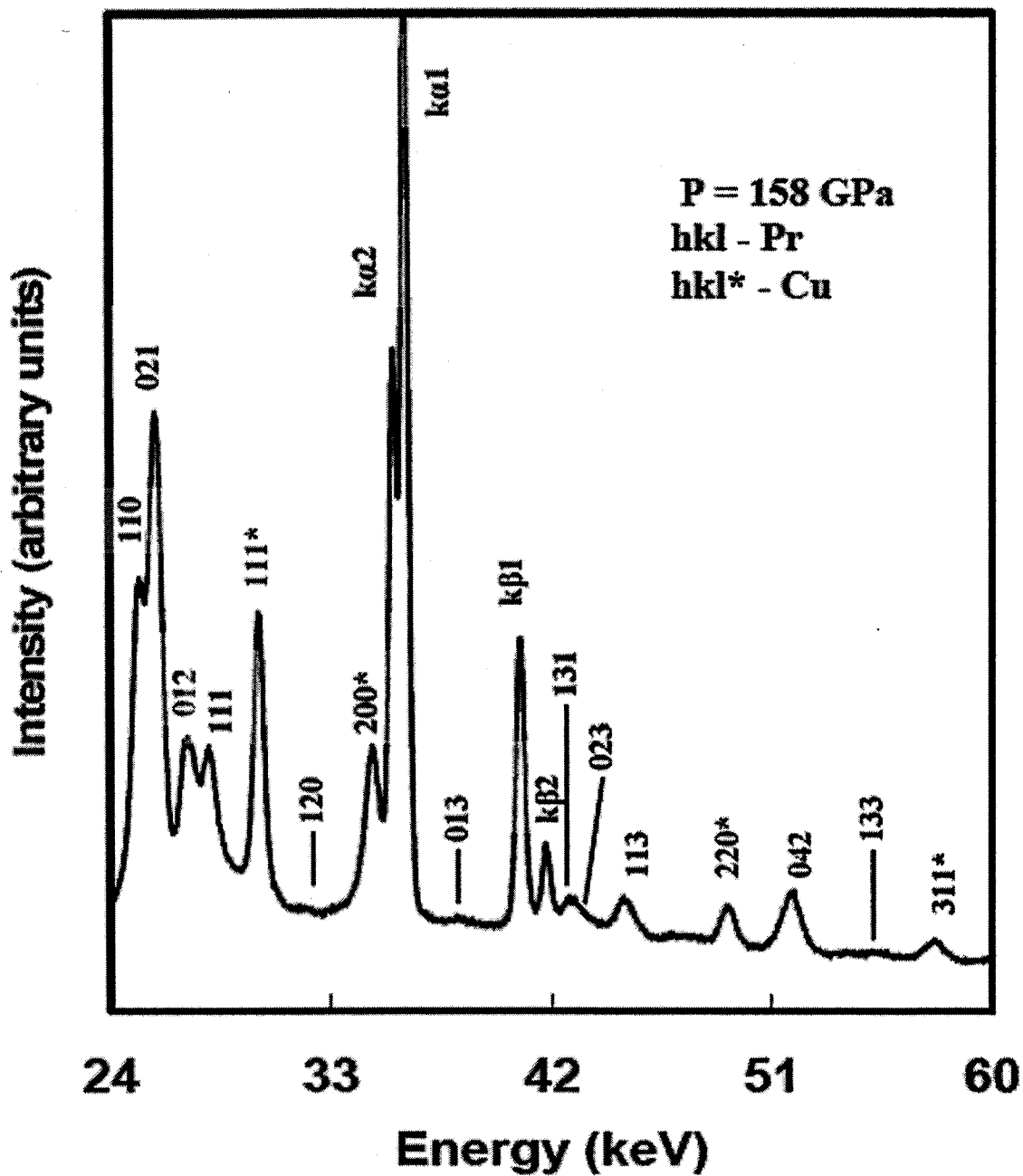


FIG. 27. The energy dispersive x-ray diffraction pattern for the Pr sample and Cu pressure marker at 158 GPa ($2\theta = 13^\circ$), in an extended energy range.

pressure of 158 GPa where eleven diffraction peaks from the Pr sample are indexed to the $P2_12_12_1$ phase and four diffraction peaks from copper pressure marker are indexed to an fcc phase.

Figure 28 shows the shift in atomic positions from α -U to $P2_12_12_1$. The blue arrows represent the shift along the c axis, and the black arrows correspond to the shift along the a-axis. When used to fit our data, we obtained $a = 2.434 \pm 0.008 \text{ \AA}$, $b = 4.813 \pm 0.005 \text{ \AA}$, and $c = 4.433 \pm 0.001 \text{ \AA}$ at 158 GPa. The values of $x = 0.2$, $y = 0.1$, and $z = 0.28$ were determined by varying the parameters so that the calculated intensities versus observed intensities are in a good agreement. A very interesting effect is observed when the pressure is increased beyond 158 GPa: The (012) diffraction peak moves slightly to the left, to lower energy, while the rest of the peaks move to the right and increase in energy with increasing pressure (Fig. 26). This implies a highly anisotropic compression of the orthorhombic unit cell, with interplaner spacing for the (012) plane increasing with increasing pressure while the interplaner spacing for the (110), (021), and (111) planes decreases with increasing pressure (Fig. 29). This anisotropic compression is clearly shown in Fig. 30, where linear compressions of the three axes above 158 GPa are plotted as a function of pressure. The lattice parameters a, b, and c have been normalized to lattice parameters at 158 GPa. The c-axis of $P2_12_12_1$ phase shows negative compressibility, while the a-axis and b-axis show positive compressibility. This anisotropic compression leads to a very interesting situation in that b-axis and c-axis of the primitive orthorhombic phase become nearly equal (Fig. 31) at a pressure of $260 \pm 7 \text{ GPa}$, and the structure can be regarded as a pseudo-tetragonal phase. However, attempts to index observed diffraction patterns above 260 GPa with a bct phase ($c/a = 1.78$), as predicted by the density

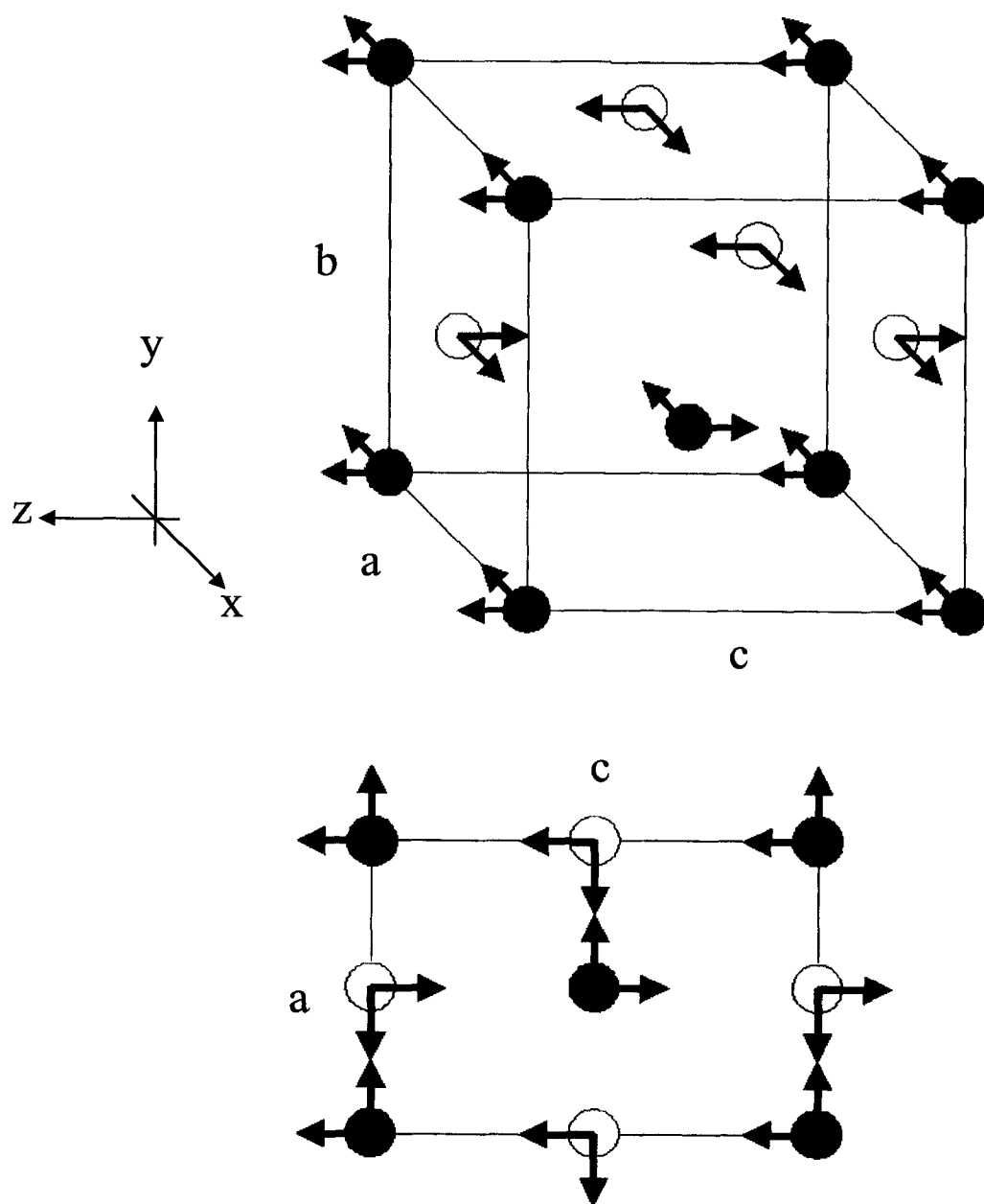


FIG. 28. Distortion of α -U structure, indicated by the blue and black arrows, that leads to a new structure $P2_12_12_1$ above 147 GPa.

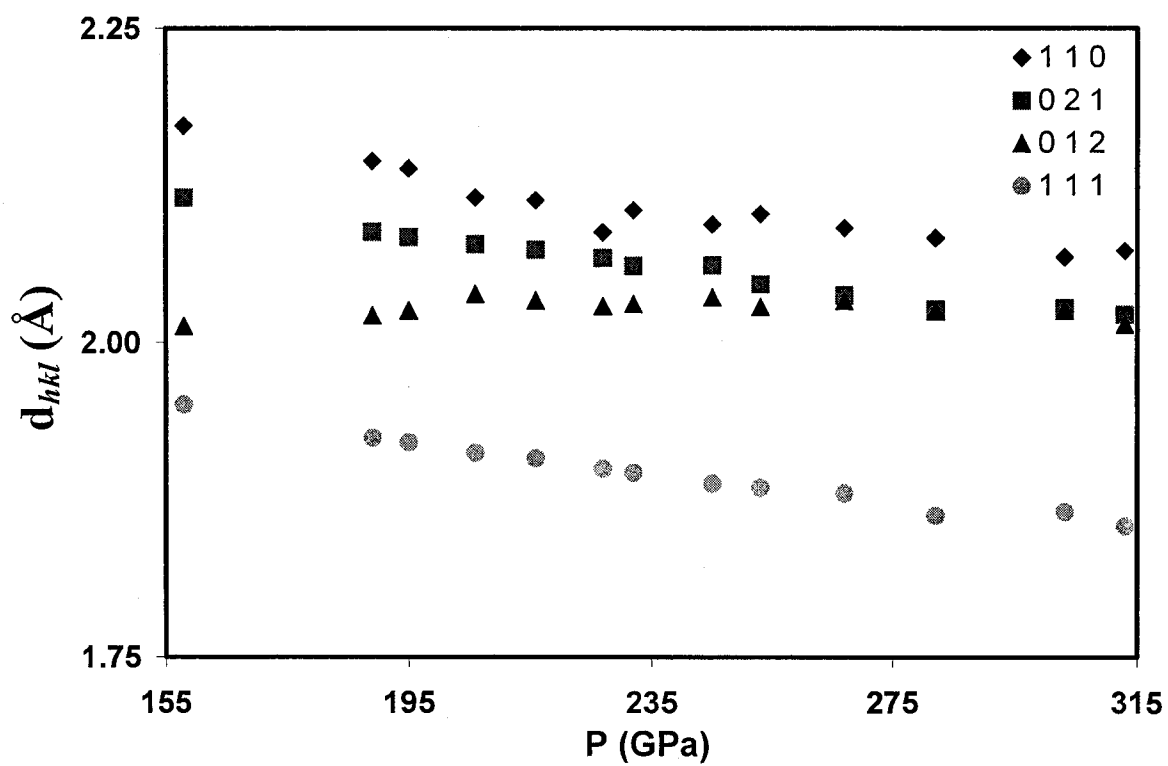


FIG. 29. Change in the interplaner spacing, d_{hkl} , of the $P2_12_1$ structure of Pr with increasing pressure, in the range of 155-315 GPa.

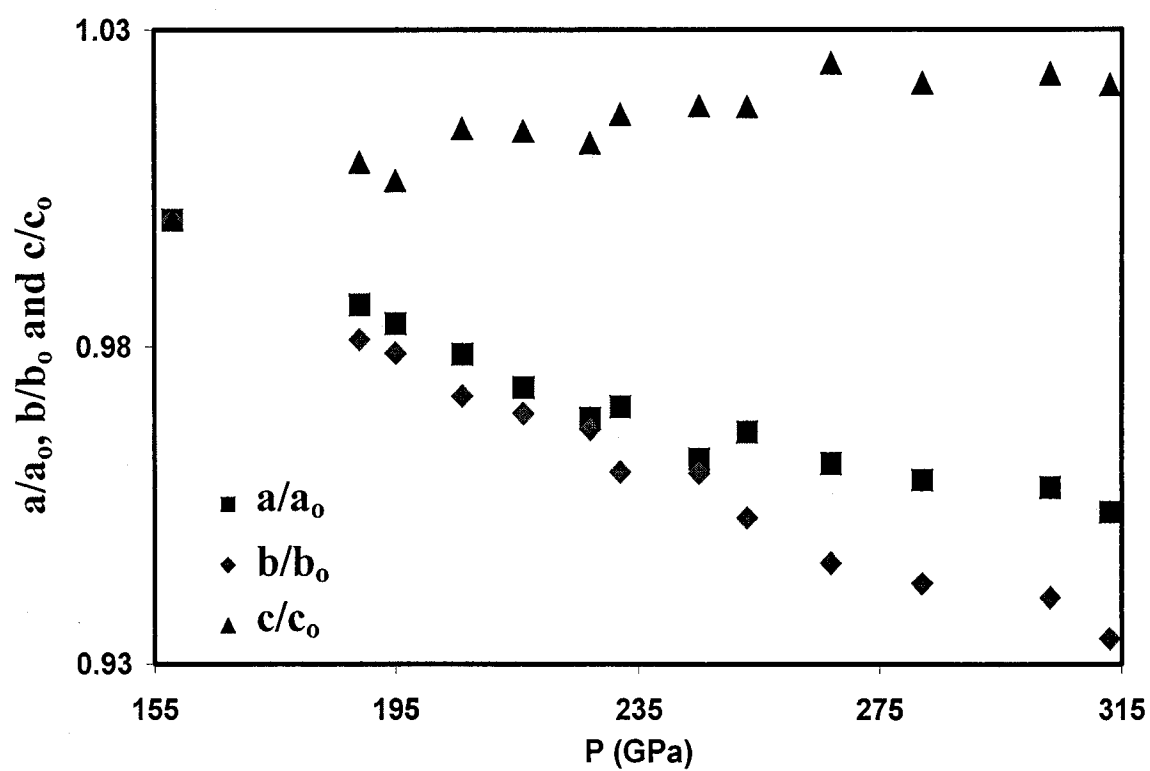


FIG. 30. Linear compression of the three axes of the $P2_12_12_1$ phase, a/a_0 , b/b_0 , and c/c_0 , normalized to lattice parameters at 158 GPa.

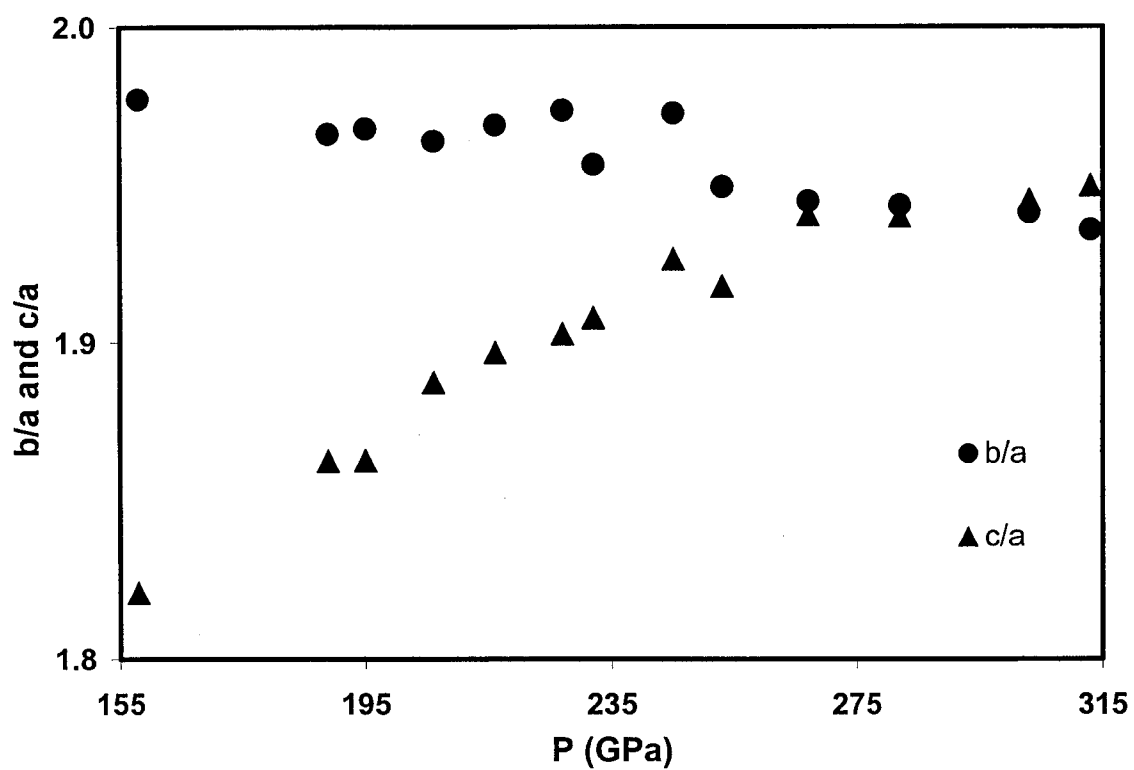


FIG. 31. Anisotropic compression of b-axis and c-axis leading to almost equal value above 260 GPa.

functional theory,⁷⁵ were not successful. The bct phase observed for Protactinium metal at ambient conditions with $c/a = 0.82$ also cannot fit our diffraction data. The measured lattice parameters for the orthorhombic phase at 267 GPa are $a = 2.341 \pm 0.013 \text{ \AA}$, $b = 4.553 \pm 0.043 \text{ \AA}$ and $c = 4.543 \pm 0.001 \text{ \AA}$. This primitive orthorhombic phase is found to be stable to the highest pressure of 313 GPa. After the pressure was increased from 313 GPa to 323 GPa, diamonds fractured during x-ray data collection, and the resulting spectra could not be recovered at this highest pressure point. The measured lattice parameters at 313 GPa are $a = 2.322 \pm 0.026 \text{ \AA}$, $b = 4.495 \pm 0.001 \text{ \AA}$, and $c = 4.528 \pm 0.001 \text{ \AA}$. and the measured volume compression is $V/V_0 = 0.343$. It should be added that there is a gradual loss of intensity of the (111) diffraction peak at ultra-high pressures above 200 GPa, which would imply additional structural rearrangements or possible orientation effects. However, due to limited diffraction data at ultra high-pressures, the $P2_12_12_1$ structure should be considered as one of the possible candidates.

The phase transformation at 147 GPa is consistent with the gradual increase in electrical resistance under high pressure in the 130-150 GPa pressure range followed by a plateau in the 150-180 GPa (Fig. 23). This change in electrical resistance can now be attributed to the structural transformation from α -U to the primitive orthorhombic structure.

Figure 32 shows the pressure-volume data along with the EoS curve of Pr to 313 GPa. Once the lattice parameters and volumes are determined, the Birch-Murnaghan EoS of the fourth order, Eq. (7), is fitted to our data in the 155 GPa to 315 GPa range, as shown in Fig. 32. Although the third-order Birch-Murnaghan EoS is a suitable fit for various pressure-volume data, as in the case of Cu mentioned earlier, Pr pressure-volume data for the $P2_12_12_1$ structure is fit more accurately using the fourth-order

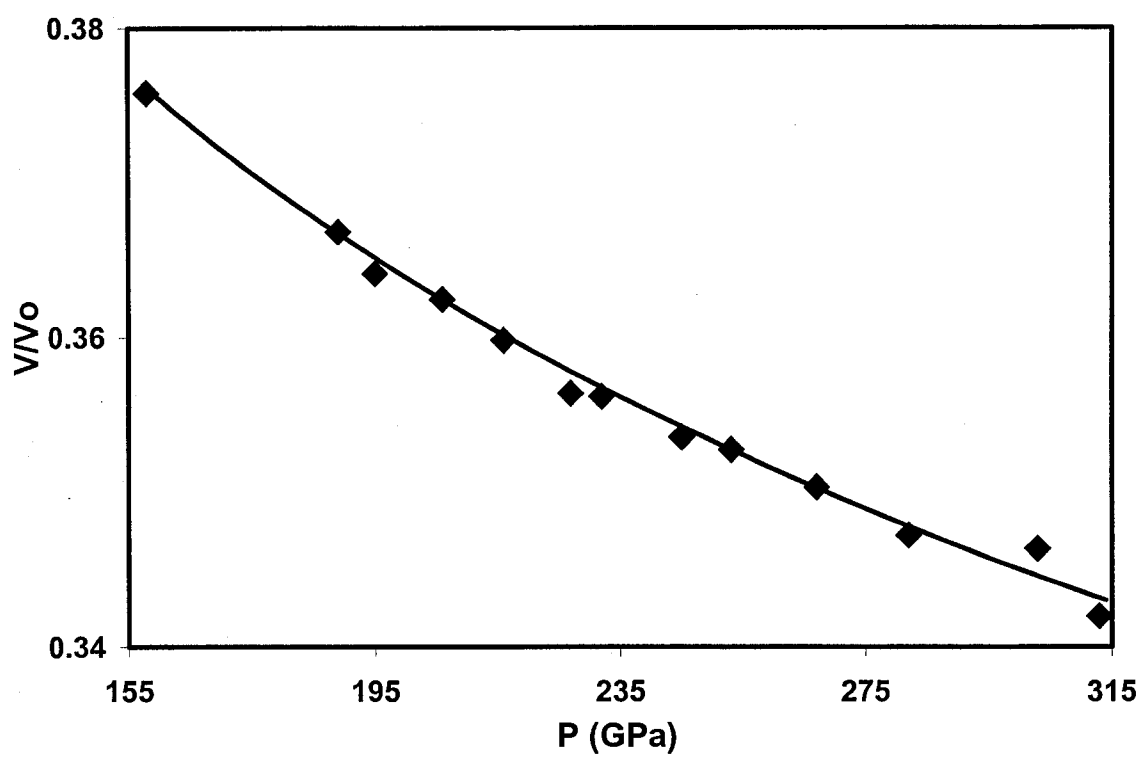


FIG. 32. The pressure-volume curve of Pr in the 155-315 GPa range. The fourth-order Birch-Murnaghan EoS fit for the $P2_12_12_1$ phase of Pr is shown by the solid curve.

Birch-Murnaghan EoS. Since the electrical resistance experiment to 176 GPa, experiment 6, had no independent pressure marker, only the data from this experiment is used in the EoS fit. The following values were obtained by the fit $V_o(P2_12_12_1) = 30.19 \text{ \AA}^3/\text{atom}$, $B_o = 177.07 \text{ GPa}$, $B_o' = 0.349$, and $B_o'' = -0.0433 \text{ GPa}^{-1}$ with $V_o(P2_12_12_1)/V_o(\text{dhcp}) = 0.874$. The resulting bulk modulus $B_o = 177.07 \text{ GPa}$ obtained for the $P2_12_12_1$ structure is substantially larger than the $B_o = 24 \text{ GPa}$ reported for the α -U structure based on a fit between 20 and 103 GPa.⁴⁵ It is interesting to point out that the $P2_12_12_1$ structure is quite incompressible, as indicated by the following parameters at 147 GPa: $V_o = 13.19 \text{ \AA}^3/\text{atom}$, $B = 926.9 \text{ GPa}$, $B' = 10.11$, and $B'' = -0.027 \text{ GPa}^{-1}$. The increase in the bulk modulus B_o is of no surprise, since the increasing participation of f electrons in bonding is expected to stiffen the lattice. As a result, the bulk modulus, B_o , obtained for our data is closer in value to that of the light actinides with delocalized f -electrons than the lanthanides at a lower pressure, which is generally below 40 GPa. It is significant to note that after a volume collapse in excess of 10% at 20 GPa, no further volume discontinuity is observed in the EoS data for Pr metal to 313 GPa. The post-collapsed phases in Pr metal show a gradual compression with increasing pressure to a nearly three-fold compression.

Conclusions

Multiple measurements, using various designer diamond anvil geometry, show an average drop of 53% in electrical resistance at 20 GPa for Pr. By comparison to the phase diagram this pressure coincides with the well-established structural phase transition to the α -U structure. This structure is believed to indicate the onset of f -electron delocali-

zation, and as additional conduction electrons become available, the electrical conductivity increases, giving rise to drop in electrical resistance. In addition to the change at 20 GPa, an additional change in electrical resistance is observed at 150 GPa as Pr undergoes a structural phase transition to a $P2_12_12_1$ structure. This structure is a distortion of the α -U structure and is found to be stable up to the highest measured pressure of 313 GPa. Observation of the $P2_12_12_1$ structure shows an additional pathway in which the α -U structure may be distorted so that the total free energy of the system is minimized.

NEODYMIUM

Introduction

Compared to Pr the transition pressure in Nd, associated with the delocalization of 4*f*-electrons and the formation of an α -U structure, is reported to occur at a much higher pressure of 113 ± 6 GPa.⁴⁰ As a result much less experimental and theoretical work has been done on Nd. For example, multiple high-pressure and temperature studies to 103 GPa and 830 K using both EDXD and ADXD^{45, 54} show the development of an α -U structure in Pr occurring in a very narrow pressure region of 2-5 GPa, with an associated volume collapse of 10%, while in Nd observation of this structure at 113 GPa is based only on EDXD data.⁴⁰ From the analysis of EDXD data a continuous transition to an α -U structure is reported, with no volume collapse, and is then stable up to the highest pressure of 155 GPa.

In order to gain a better understanding of Nd and for comparison to Pr, a Nd sample purchased from Alfa Aesar, having 99.9% purity, was studied using DAC and ADXD techniques at APS, beamline HPCAT 16ID-B. Using a six-probe designer diamond anvil with an opposing probe separation of 25 μm , an 8° bevel, a 100- μm central flat, and a 300- μm culet, simultaneous electrical resistance and x-ray studies were performed on the same sample. A polycrystalline Nd sample was loaded in a preindented spring steel gasket, which has a 50- μm drilled hole. In order to avoid the occurrence of an unwanted reaction and because electrical resistance measurements were carried out, only a Nd sample

with no pressure-transmitting medium was loaded in the gasket hole. The pressure was determined from the known P-V EoS (Ref. 40). All electrical resistance measurements were performed using the four-probe technique, while ADXD was performed on Nd during increasing pressure by using an x-ray beam with wavelength of 0.3683 Å and measuring 18 μm X 20 μm.

ADXD Study to 152 GPa

At ambient conditions Nd crystallizes in a dhcp structure with measured lattice parameters $a = 3.657 \text{ \AA}$ and $c = 11.799 \text{ \AA}$. Because the initial phase transitions are well known, pressure is increased and the first spectrum collected is indexed to the *hP3* phase of Nd. Values obtained for the *hP3*, $a = 2.8513 \pm 0.0089 \text{ \AA}$, $c = 6.8060 \pm 0.0351 \text{ \AA}$, and $V = 15.973 \text{ \AA}^3/\text{atom}$, are used to determine the pressure of 71 GPa from the EoS.⁴⁰ With further increases in pressure we are able to index three more spectra to the *hP3* phase. The last spectrum indexed to this phase is at 76 GPa, with $a = 2.8322 \pm 0.0099 \text{ \AA}$ and $c = 6.7471 \pm 0.0099 \text{ \AA}$. Although we are still able to index the spectra to the *hP3* phase, the (102) peak of this phase decreases in intensity significantly over the pressure range of 71 GPa to 76 GPa. At the same time, while the (102) peak intensity is observed to have decreased, the intensity of the (111) peak of the monoclinic, *C2/m*, phase has increased. We are able to fully index the *C2/m* (four atoms/cell) phase above 76 GPa (Fig. 33). Both the *hP3* and *C2/m* phases can be treated as distortions of an fcc structure. The relation between the *hP3* and *C2/m* phase unit-cell dimensions and the lattice parameter, a_c , of the fcc phase are $a \cong a_c / \sqrt{2}$, $c \cong \sqrt{3}a_c$, $(c/a)_{ideal} \cong \sqrt{6}$ and $a \cong \sqrt{6}a_c / 2$, $b \cong a_c / \sqrt{2}$, $c \cong \sqrt{6}a_c / 2$, $\beta \cong 109.5^\circ$, $(c/a)_{ideal} \cong 1$, $(b/a)_{ideal} \cong 0.577$, for the *hP3* and *C2/m* phases,

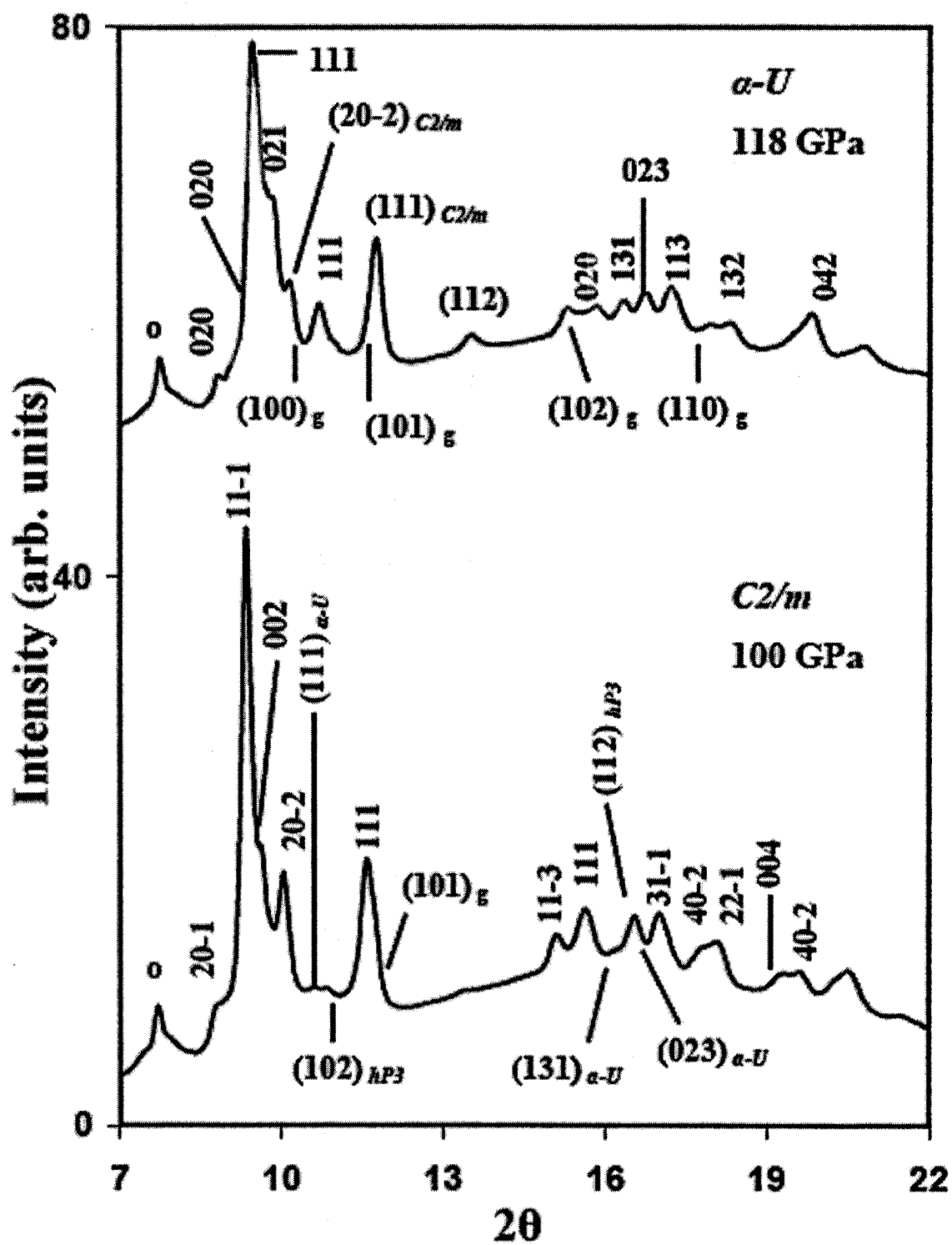


FIG. 33. ADXD spectra ($\lambda = 0.3683 \text{ \AA}$) of Nd showing the C2/m and α -U phases at 100 GPa and 118 GPa, respectively.

respectively. The four atom positions, described by the atomic positional parameter 4(i) (0.280, 0, 252) of the $C2/m$ structure, were used to obtain the following values for lattice parameters: $a = 4.8517 \pm 0.0034 \text{ \AA}$, $b = 2.7216 \pm 0.0043 \text{ \AA}$, and $c = 5.0804 \pm 0.0034 \text{ \AA}$ with $\beta = 118.38 \pm 0.01^\circ$, resulting in the calculated pressure of 88 GPa. The transition from the $hP3$ to the $C2/m$ phase above 76 GPa is consistent with what has previously been observed.⁴⁰ However, even though we are able to index the spectra with a monoclinic phase, the (102) and (112) peaks of the $hP3$ phase have not completely disappeared. Under a further pressure increase to 97 GPa, these peaks have all but disappeared, but with a slight pressure increase to 100 GPa we observe the appearance of the (111) peak of the orthorhombic (α -U) phase. The intensity of this peak continues to increase, while the intensity of such peaks as (111) and (20-2) of the $C2/m$ phase start to decrease, as pressure is increased above 100 GPa (Fig. 34).

The development of α -U phase is of particular interest due to it being the suspected point at which f -electrons change from localized to delocalized, as mentioned earlier. From the collected spectra we observe the (111) peak and other peaks not visible under the previous phase gain intensity above 100 GPa. Spectra may not be fully indexed to α -U phase yet, and we are able to continue indexing the $C2/m$ phase up to 110 GPa. As the pressure is increased above 110 GPa to 118 GPa, we are not able to get a satisfactory fit using $C2/m$ indexing, but instead we are able to index the spectra to the α -U phase (Fig. 33). Assignment of an α -U phase gives the following values for the lattice parameters: $a = 2.4660 \pm 0.0222 \text{ \AA}$, $b = 4.8733 \pm 0.0075 \text{ \AA}$, and $c = 4.4619 \pm 0.0047 \text{ \AA}$. As mentioned this is the first spectra index as α -U, which is also consistent with the previous report showing the appearance of the α -U phase at $113 \pm 6 \text{ GPa}$.⁴⁰ However, the

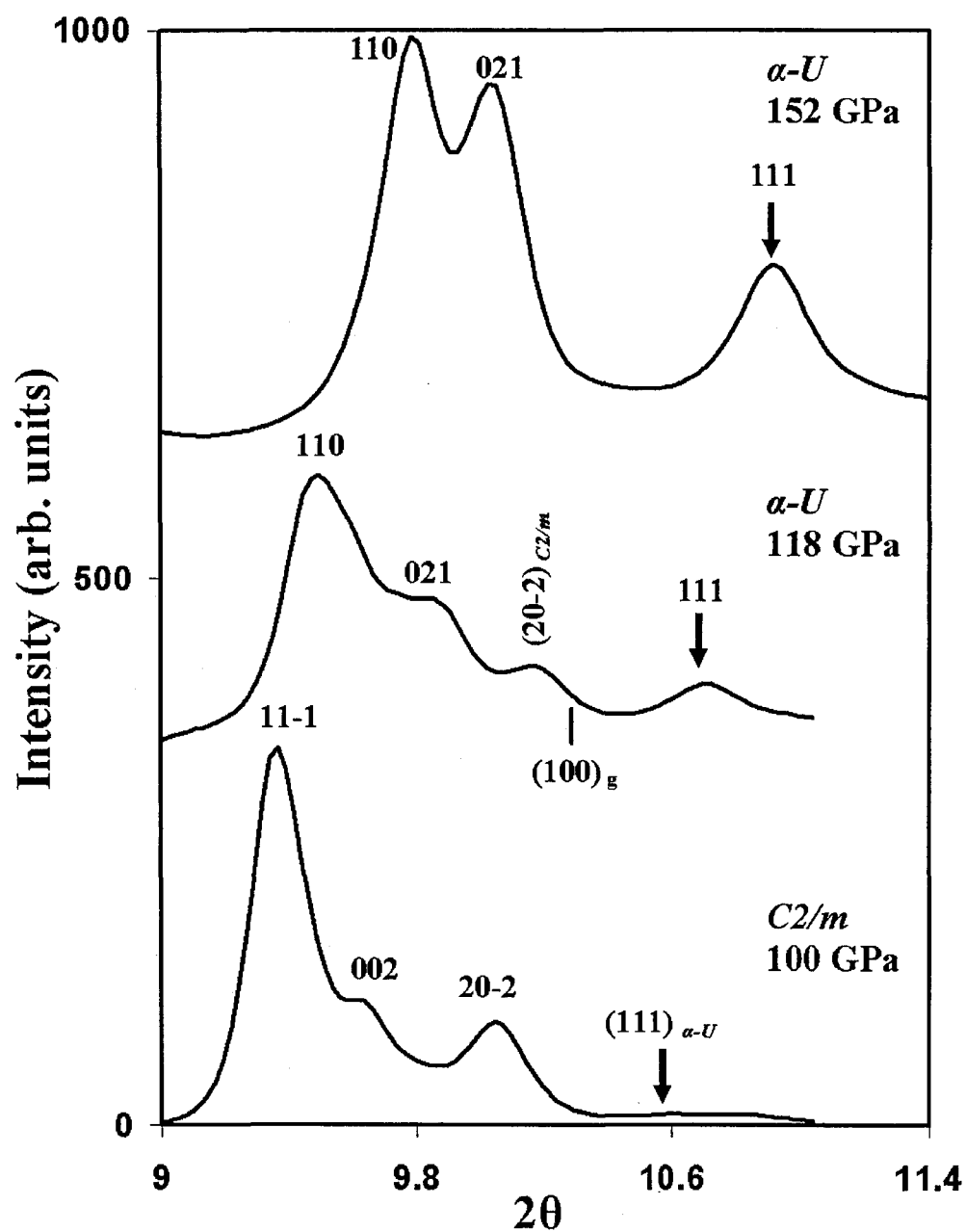


FIG. 34. Development of α -U structure of Nd above 100 GPa, as indicated by a continuous increase in the peak intensity of the (111) peak of this structure ($\lambda = 0.3683 \text{ \AA}$). The location of the (111) peak of the α -U phase is indicated by a vertical arrow.

appearance of the characteristic (111) singlet peak of the α -U phase at 100 GPa may already indicate a beginning of a delocalized f -electron state.

Electrical Resistance Measurement up to 152 GPa

Indications from the collected x-ray spectra that the f -electron delocalization may possibly be occurring at 100 GPa is consistent with the measured electrical resistance. Initially, as seen in Fig. 35, the electrical resistance measurements on Nd in the pressure range from 71 GPa to 100 GPa show a steady average value of 23.1 m Ω . During further increases in pressure, electrical resistance starts to slowly decrease, which is consistent with having more electrons in the conduction band due to the delocalization of f -electrons. The decrease in the resistance value is not sudden, but continues to decrease steadily from 23.1 m Ω at 100 GPa down to 14.6 m Ω at 152 GPa. By comparison with the x-ray spectra, the observed decrease in the electrical resistance occurs simultaneously with the appearance of the (111) peak of the α -U phase of Nd above 100 GPa. Above this pressure, a steady decrease in the electrical resistance is observed simultaneously with the development of the α -U structure, as indicated by a continuous increase in the (111) peak intensity (Fig. 34).

Continuous Development of α -U Structure

After indexing the spectra at 118 GPa to the α -U phase we are able to continue assigning all of the spectra to this phase up to the highest pressure of 152 GPa (Fig. 33). However, as the pressure is increased we also observed an increase in the intensity of the (021) peak and the (111) singlet peak of α -U structure. Figure 34 shows the observed

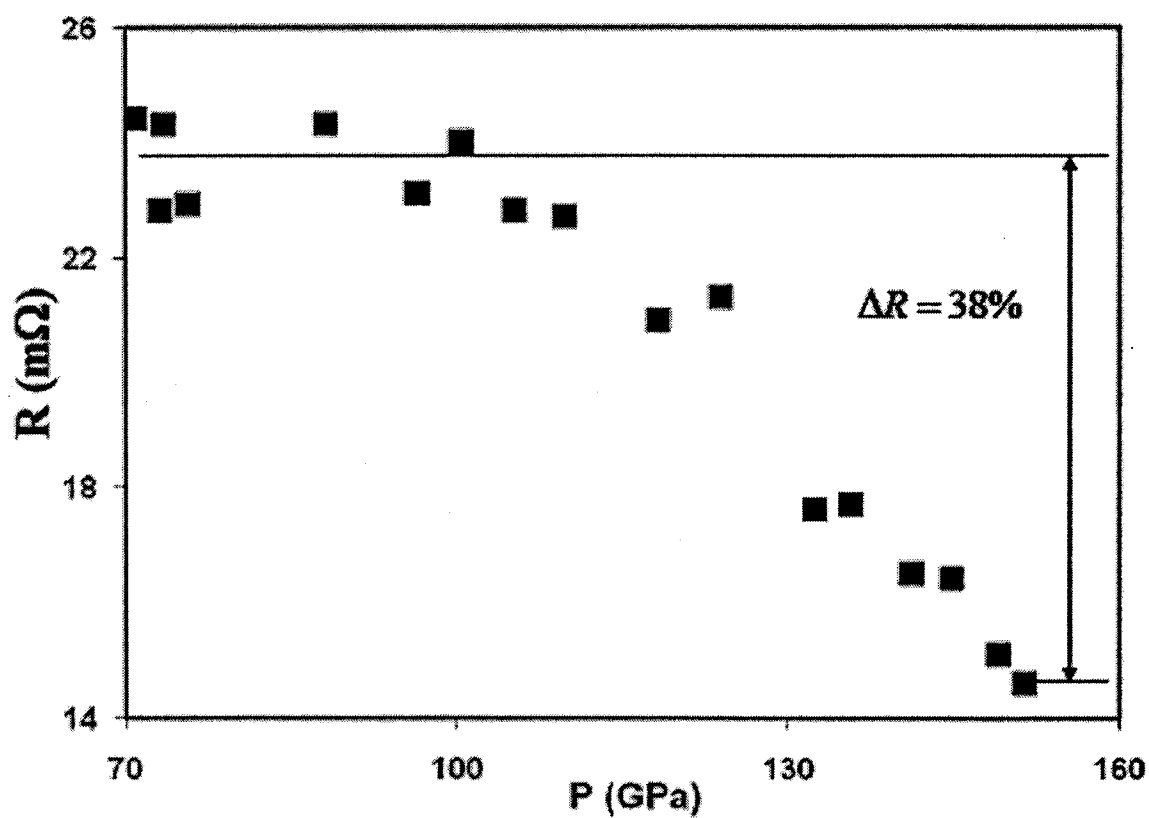


FIG. 35. Change in electrical resistance of Nd metal with increasing pressure, showing a gradual decrease of 38% in the pressure range between 100 GPa and 153 GPa.

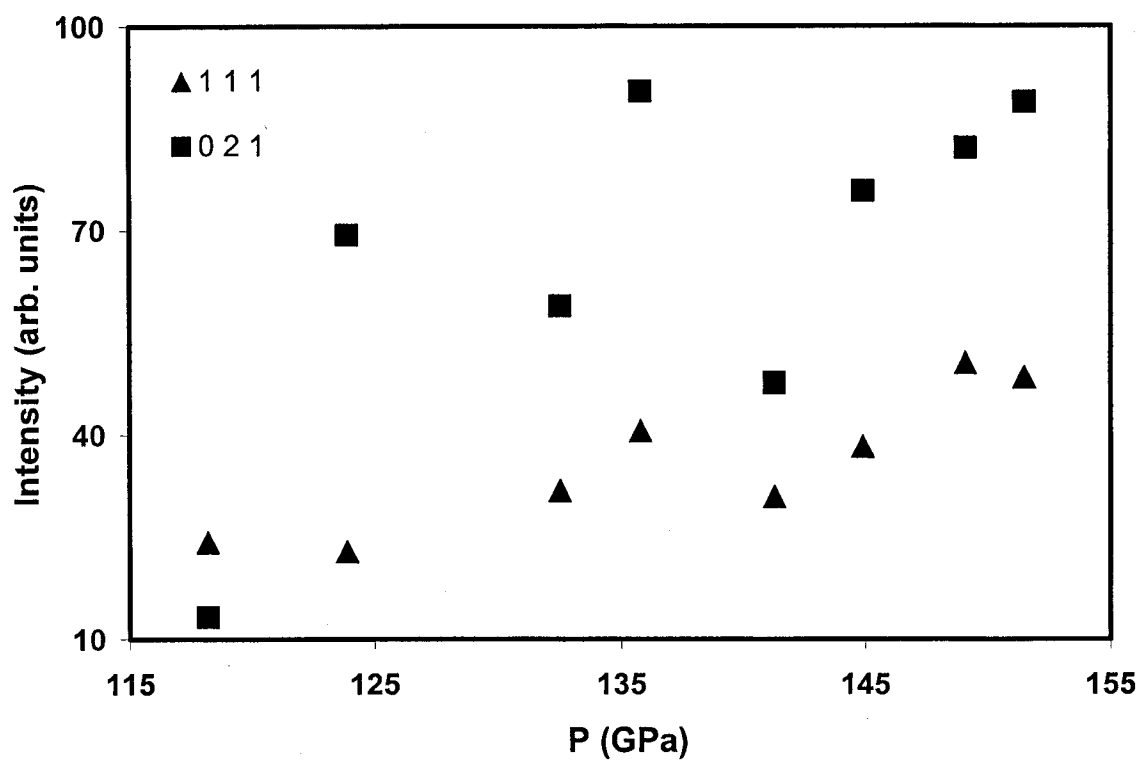


FIG. 36. Observed changes in the intensity of the (111) and (021) peaks of the α -U phase of Nd with increasing pressure.

intensity of these two peaks with increasing pressure. Although the (021) peak shows an overall increase, the (111) peak is more accurate for analysis (Fig. 36), as it is a singlet versus the (021) peak, which is a part of a triplet with the (002) and (110) peaks (Fig. 34). The change in peak intensity with increasing pressure may be attributed to the change in the y -parameter of the α -U phase.

α -U structure, space group Cmc m , is described by four atoms/cell, as discussed in previous chapters, which occupy the 4c Wyckoff positions with coordinates $(0, y, \frac{1}{4})$, $(0, -y, \frac{3}{4})$, $(\frac{1}{2}, \frac{1}{2}+y, \frac{1}{4})$, and $(\frac{1}{2}, \frac{1}{2}-y, \frac{3}{4})$. This structure is an orthorhombic distortion of an hcp structure with three lattice parameters, a , b , and c . The unit cell of α -U is related to an hcp structure, $a = a_{\text{hcp}}$, $b = \sqrt{3} a_{\text{hcp}}$, and $c = c_{\text{hcp}}$, with $y = 0.167$, $(c/a)_{\text{ideal}} = 1.633$, and $(b/a)_{\text{ideal}} = \sqrt{3}$. Previous reports suggest that setting $y=0.100$ results in a good fit for the observed peak intensity of Nd between 113 GPa and 155 GPa.⁴⁰ However, since the observed peak intensity for the α -U phase is not constant and no new peaks are seen above 118 GPa that would indicate another phase change, we are led to believe that the change in intensity is due to a changing y -parameter of the α -U phase. Figure 37 shows the change in y -parameter with increasing pressure. At 118 GPa, where the α -U phase is first indexed, the corresponding y -parameter $y = 0.070 \pm 0.005$ gives the closest match between the observed and calculated peak intensities. As the peak intensities change up to the highest pressure of 152 GPa, the corresponding y -parameter increases overall to 0.095 ± 0.005 .

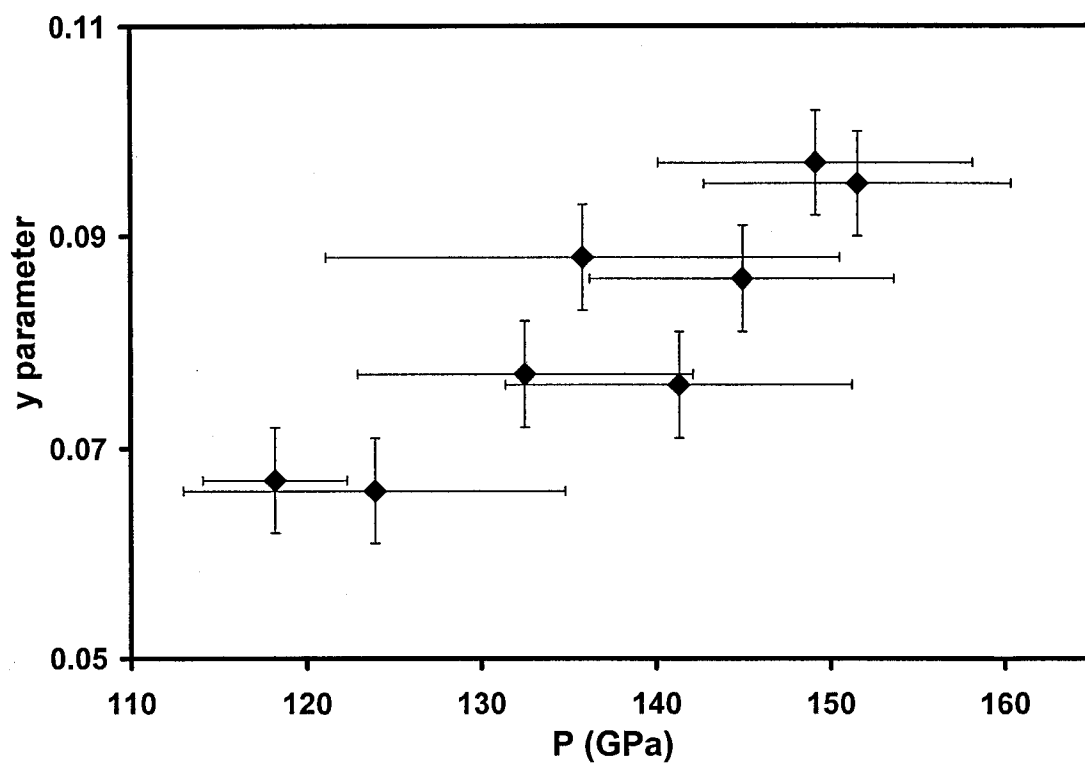


FIG. 37. Change in the y-positional parameter of the α -U phase of Nd. The y-parameter is obtained from measured x-ray diffraction intensities.

Conclusions

In the experimental range of 71-152 GPa two structural phase transitions are observed. The first transition, $hP3 \rightarrow C2/m$, occurs at 76 GPa, while the second transition, $C2/m \rightarrow \alpha-U$, is fully indexed above 110 GPa. In the pressure range of 71-100 GPa, which includes the first transition, measured electrical resistance remains constant, with an average value of 23.1 m Ω . At 100 GPa a decrease in electrical resistance is observed prior to the indexing of $\alpha-U$ structure. A closer look at the x-ray spectra at 100 GPa reveals that although the $C2/m$ phase can still be indexed, the (111) peak of the $\alpha-U$ structure has already appeared. The appearance of the (111) peak at 100 GPa and the simultaneous decrease in the electrical resistance at this pressure are consistent with the proposed correlation between the f -electron delocalization and the structural phase transition to the $\alpha-U$ structure. Furthermore, electrical resistance measurements do not indicate changes in the electronic structure as the sample undergoes the structural transition at 76 GPa and, as a result, f -electrons can still be considered localized and as not contributing to conduction or bonding prior to 100 GPa.

100 GPa is however lower than the previously proposed transition pressure of 113 GPa. One of the main reasons for this is that the latter pressure is based on the assignment of the $\alpha-U$ structure from EDXD experiments. As observed in this experiment using ADXD, the $\alpha-U$ structure continuously develops from 100 GPa up to the highest pressure of 152 GPa. Initially the $\alpha-U$ structural diffraction peaks are weak and can easily be overlooked due to a continuous transition from $C2/m$ and also due the overlap of some peak between the two phases. However, the $\alpha-U$ peak intensity increases with pressure, as most evident from the (111) singlet peak of this phase, and above 110 GPa the assign-

ment of the C2/m structure is no longer possible. The development of α -U structure is a result of a continuous shift in the atomic positions, as indicated by the change in the y -parameter describing the atomic coordinates.

These experimental high-pressure studies have clearly demonstrated the difference in $4f$ delocalization phenomenon between Pr ($4f^2$) and Nd ($4f^3$) electronic configuration. The $4f$ -shell delocalization at 20 GPa in Pr is discontinuous, as evidenced by a sudden drop in electrical resistance, along with an abrupt transformation to an α -U structure. In contrast, $4f$ delocalization in Nd occurs in a gradual manner over the pressure range of 100-152 GPa, as evidenced by a gradual drop in electrical resistance and a gradual transformation to an α -U structure.

CONCLUSIONS AND FUTURE WORK

In this thesis, I have established a clear experimental procedure for testing and validating electrical resistance data obtained with designer diamond anvils to ultra-high pressures. Starting with a few simple tests, which consist of measuring open electrical resistance and resistance through the metal gasket during preindentation, we are able to check the designer diamond anvils for any potential problems that may occur during the fabrication process. By using GaAs as a test sample, electrical resistance may be measured during increases and decreases in pressure in order to test both flat and beveled designer diamond anvils. Measured electrical resistance shows a large drop of more than six orders of magnitude at 17 GPa as the GaAs sample becomes metallic. This transition is also confirmed through simple observation of optical reflectivity in the diamond anvil cell. The relatively low transition pressure, as well as the large change observed in electrical resistance, allows for designer diamond anvils to be tested in a laboratory without a major potential of damage to the anvil. In addition to the initial test, including GaAs, flat designer diamond anvils are convenient in that they may be used multiple times in order to reproduce measured results, as is shown by the measurements performed on Pr metal. Beveled anvils on the other hand may still be tested using these methods; however, the test pressure must remain below 50 GPa in order to avoid damage to the anvil. As test cases of experimental measurements above 100 GPa, CsI and CsCl were studied for insulator to metal transitions. The main purpose of using these two wide band-gap materi-

als is that they are expected to have a continuous decrease in electrical resistance due to the closing of the electronic energy band-gap with increasing pressure. The resulting measurement on CsI shows that the sample does indeed undergo such a change and, as previously established through temperature cycling, milliohm resistance indicative of CsI metallization is measured above 115 GPa. The electrical resistance measurement of CsCl shows a similar behavior as the sample approaches the predicted metallization pressure above 280 GPa. By performing electrical resistance on CsI and CsCl, as well as GaAs, Pr, and Nd, various anvil geometries have been tested, and all of the results indicate that the mechanical strength of designer diamond anvils is not compromised by having the electrical microprobes embedded into the diamond.

Initial experiments on Pr up to 56 GPa show a large drop in electrical resistance at 20 GPa. The measured change in the electrical resistance occurs simultaneously with the structural phase transition to an α -U structure of Pr. It has been previously predicted that with increasing pressure, as the interatomic distance is decreased, the overlap of outer electron causes the delocalization of the $4f$ shell in Pr, leading to the formation of low symmetry crystal structures characteristic of f -bonded metals. Observation of α -U structure in Pr has therefore been given as evidence of this change. In recent years, due to observation of low symmetry structures, such as the monoclinic, $C2/m$, structure, occurring prior to the observed α -U structure, some doubt has been raised as to the exact pressure of f -electron delocalization. By performing electrical resistance measurements we have shown that there is no indication of a drastic change in the electronic structure prior to 20 GPa, but rather the observed change supports the predicted f -electron delocalization occurring at pressures associated with the structural phase transition to an α -U structure.

Additional electrical resistance measurement to 179 GPa indicates another change occurring in Pr at 150 GPa. There has long been speculation of post- α -U structures, including the bct structure predicted by the density-functional electronic structure calculation, that are favorable with respect to the lowering of the internal energy of the system. Further investigation above 100 GPa by EDXD shows that Pr does undergo another structural transition at 147 GPa. However, the observed structure is not bct, but rather a primitive orthorhombic structure, space group $P2_12_12_1$. The $P2_12_12_1$ structure is a distortion of the α -U structure and is shown to be stable to a nearly threefold compression at a pressure of 313 GPa. Observation of the $P2_12_12_1$ structure shows that there are additional pathways for the α -U structure to distort and lower the system energy, not just in Pr but in all f -band metals.

Transition to the α -U structure in Pr at 20 GPa is also accompanied by a 10% volume collapse. Nd, which has one more f -electron than Pr, has been reported to undergo the same structural phase transition at 113 GPa; however, the transition is continuous with no major volume collapse. In order to compare the two systems and gain further understanding of the f -electron delocalization, simultaneous electrical resistance and ADXD were performed on Nd metal to 152 GPa. The results obtained from ADXD are consistent with the reported EDXD study in that the α -U structure may be assigned to Nd above 110 GPa. Although the full spectra could only be indexed to α -U structure above 110 GPa, the (111) peak of this structure is first observed to appear at least 10 GPa below this pressure. The appearance of the (111) peak may therefore indicate the onset of f -electron delocalization. The electrical resistance measurements show that resistivity approaches a steady state value between 71-100 GPa before showing a gradual decrease

above this pressure. As the pressure is increased up to 152 GPa an overall decrease of 38% is measured for electrical resistance, while at the same time the diffraction peaks of the α -U phase continuously change in intensity. This indicates that the α -U phase develops over a much larger pressure range compared to Pr. The observed change in the (111) x-ray diffraction peak intensity is shown to be consistent with the change in the y -parameter of the α -U structure. A continuous increase in the y -parameter from 0.070 ± 0.005 at 118 GPa to 0.095 ± 0.005 at 152 GPa results in a good match between the observed and calculated diffraction peak intensities.

Electrical resistance measurements on both Pr and Nd metals give further evidence that the f -electron delocalization is signaled by the appearance of the α -U phase, as has previously been proposed. In addition to detecting the f -electron delocalization, Pr and Nd experiments also show that designer diamond anvils may be used successfully for studying materials with drastic changes in electronic properties. In order to further extend the applicability of the measured results, future work should concentrate on determining the electrical resistivity of samples from the measured electrical resistance. Since electrical resistivity is the intrinsic property of a material and independent of sample geometry and probe placement, it has a much broader implication. In order to determine resistivity from the measured resistance sample, geometry during high-pressure experiments has to be determined. One possible way of doing this is by using a single-wavelength x-ray source, such as the one used for ADXD, and measuring change in absorption with change in pressure. Absorption of incident radiation is proportional to sample thickness (i.e., sample density) and, by measuring the input versus the output beam flux, sample thickness may be deduced. Using the same x-ray beam, the sample

may also be scanned perpendicular to the beam so that the diameter may be determined. Since the sample and the gasket have different atomic numbers, the diameter can be determined by observing the point at which the x-ray absorption either increases or decreases.

In addition to determining the sample resistivity, further experiments should also be performed in order to check for additional post- $P2_12_12_1$ structures, as well as other possible post- α -U structures. Compression of Pr to 313 GPa shows an anisotropic compression, which may lead to a possible structural phase transition to a tetragonal structure above 270 GPa. However, due to the limitation of EDXD, Pr should also be studied using ADXD in this pressure range in order to investigate any possible texturing effects, such as preferred crystal orientation, that may give rise to anisotropic compression. Determining additional structural changes may not only lead to a better understanding of the behavior of f -electrons metals, but it may also provide information about the stability of various crystal structures at extreme compressions. I have demonstrated that electrical resistance changes in $4f$ -metals Pr and Nd can be clearly correlated to the crystal structural changes under high pressures as dramatic changes in transport properties are observed at the $4f$ -delocalization transition. These electrical transport measurements using designer diamond anvils can also be extended to other $4f$ and $5f$ band metals in the periodic table.

LIST OF REFERENCES

- ¹W. J. Nellis, J. A. Moriarty, A. C. Mitchell, M. Ross, R. G. Dandrea, N. W. Ashcroft, N. C. Holmes, and G. R. Gathers, *Phys. Rev. Lett.* **60**, 1414 (1988)
- ²A. Jayaraman, *Rev. Mod. Phys.* **55**, 65 (1983)
- ³J. C. Jamieson, A. W. Lawson, and N. D. Nachtrieb, *Rev. Sci. Instrum.* **30**, 1016 (1959)
- ⁴C. E. Weir, E. R. Lippincott, A. Van Valkenburg, and E. N. Bunting, *J. Res. Natl. Bur. Stand., Sec. A* **63**, 55 (1959)
- ⁵A. L. Ruoff, H. Xia, and Y. K. Vohra, *Rev. Sci. Instr.* **61**, 3830 (1990)
- ⁶Y. K. Vohra and S. T. Weir, in *Proceedings of the International School of Physics-Enrico Fermi*, edited by R. J. Hemley, G. I. Chiarotti, M. Bernasconi and L. Ulivi (IOS, Amsterdam, 2002), Course CXLVII, pp. 87-105
- ⁷R. J. Hemley and N. W. Ashcroft, *Phys. Today* **51**, 26 (1998)
- ⁸A. K. McMahan, C. Huscroft, R.T. Scalettar, and E. L. Pollock, *J. Comput.-Aided Mater. Des.* **5**, 131 (1998)
- ⁹G. J. Piermarini and S. Block, *Rev. Sci. Instrum.* **46**, 973 (1975)
- ¹⁰H. K. Mao and P. M. Bell, in *Carnegie Institution of Washington Year Book* **77**, 904 (1978)
- ¹¹L. Merrill and W. A. Bassett, *Rev. Sci. Instrum.* **45**, 290 (1974)
- ¹²G. Huber, K. Syassen, and W. B. Holzapfel, *Phys. Rev. B.* **15**, 5123 (1977)
- ¹³W. A. Bassett, T. Takahashi, and P. W. Stook, *Rev. Sci. Instr.* **38**, 37 (1967)
- ¹⁴R. A. Forman, G. J. Piermarini, J. D. Barnett, and S. Block, *Science* **176**, 184 (1972)
- ¹⁵G. J. Piermarini, S. Block, and J. S. Barnett, *J. Appl. Phys.* **44**, 5377 (1973)
- ¹⁶H. K. Mao and P. M. Bell, *Science* **200**, 1145 (1978)

- ¹⁷M. I. Eremets, *Sem. Sci. Tech.* **6**, 439 (1991)
- ¹⁸P. K. Briddon and R. Jones, *Physica B* **185**, 179 (1993)
- ¹⁹K. Asaumi and A. L. Ruoff, *Phys. Rev. B* **33**, 5633 (1986)
- ²⁰Q. Wei, N. Velisavljevic, P. Baker, and Y. K. Vohra, *Appl. Phys. Lett.* **84**, 5308 (2004)
- ²¹Q. Wei, P. Baker, N. Velisavljevic, and Y. K. Vohra, submitted for publication *J. Appl. Phys.* (August, 2005)
- ²²J. Liu and Y. K. Vohra, *J. Appl. Phys.* **79**, 1000 (1996)
- ²³H. K. Mao, P. M. Bell, J. W. Shaner, and D. J. Steinberg, *J. Appl. Phys.* **49**, 3276 (1978)
- ²⁴Z. Liu, Q. Cui, and G. Zou, *Phys. Lett. A* **143**, 79 (1990)
- ²⁵A. L. Ruoff, H. Luo, and Y. K. Vohra, *J. Appl. Phys.* **69**, 6413 (1991)
- ²⁶R. G. McQueen, S. P. Marsh, J. W. Taylor, J. M. Fritz, W. J. Carter, in *High Velocity Impact Phenomenon*, edited by R. Kinslow (Academic, New York, 1970) Chap. 7.
- ²⁷N. C. Holmes, J. A. Moriarty, G. R. Gathers, and W. J. Nellis, *J. Appl. Phys.* **66**, 2962 (1989)
- ²⁸S. Desgreniers and K. Lagarec, *J. Apply. Crystallogr.* **31**, 109 (1998)
- ²⁹A. Larson and B. Von Dreele, computer code GSAS, Los Alamos National Laboratory, 1994
- ³⁰A. Hammersley, computer code FIT2D, European Synchrotron Radiation Facility (ESRF), 1995
- ³¹T. S. McCauley and Y. K. Vohra, *Appl. Phys. Lett.* **66**, 1486 (1995)
- ³²S. T. Weir, J. Akella, C. A. Ruddle, Y. K. Vohra, and S. A. Catledge, *Appl. Phys. Lett.* **77**, 3400 (2000)
- ³³M. I. Eremets, V. V. Struzhkin, H. K. Mao, and E. Gregoryanz, *Science* **293**, 272 (2001)
- ³⁴C-S Yan, H-K Mao, W. Li, J. Qian, Y. Zhao, and R. J. Hemley, *Phys. Stat. Sol.* **201**, R25 (2004)
- ³⁵J. C. Duthie and D. G. Pettifor, *Phys. Rev. Lett.* **38**, 564 (1977)

- ³⁶A. Jayaraman, Phys. Rev. A **135**, 1056 (1964)
- ³⁷D. A. Young, *Phase Diagrams of the Elements* (University of California, 1991)
- ³⁸Y. K. Vohra, H. Olijnik, W. Grosshans, and W. B. Holzapfel, Phys. Rev. Lett. **47**, 1065 (1981)
- ³⁹B. Johansson and A. Rosengren, Phys. Rev. B. **11**, 2836 (1975)
- ⁴⁰G. N. Chesnut and Y. K. Vohra, Phys. Rev. B. **61**, R3768 (2000)
- ⁴¹G. N. Chesnut and Y. K. Vohra, Phys. Rev. Lett. **82**, 1712 (1999)
- ⁴²N. Hamaya, Y. Sakamoto, H. Fujihisa, Y. Fujii, K. Takemura, T. Kikegawa, O. Shimomura, *High Pressure Science and Technology - 1993*, edited by S. C. Schmidt *et al.*, AIP Conf. Proc. No. 309 (AIP, New York, 1994), Pt. 1, p. 457.
- ⁴³Y. K. Vohra, V. Vijayakumar, B. K. Godwal, and S. K. Sikka, Phys. Rev. B. **30**, 6205 (1984)
- ⁴⁴H. Hua, Y. K. Vohra, J. Akella, S. T. Weir, R. Ahuja, and B. Johansson, Rev. High Press. Sci. Technol. **7**, 233 (1998)
- ⁴⁵G. N. Chesnut and Y. K. Vohra, Phys. Rev. B **62**, 2965 (2000)
- ⁴⁶H. K. Mao, R. M. Hazen, P. M. Bell, and J. J. Wittig, J. Appl. Phys **52**, 4572 (1981)
- ⁴⁷W. A. Grosshans, Y. K. Vohra, and W. B. Holzapfel, J. Phys. F: Met. Phys. **13**, L147 (1983)
- ⁴⁸G. S. Smith and J. Akella, J. Appl. Phys. **53**, 9212 (1982)
- ⁴⁹G. N. Chesnut, *Dissertation* (University of Alabama at Birmingham, 2002)
- ⁵⁰R. Patterson, C. K. Saw, and J. Akella, J. Appl. Phys. **95**, 5443 (2004)
- ⁵¹M. I. McMahon and R. J. Nelmes, Phys. Rev. Lett. **78**, 3884 (1997)
- ⁵²J. Akella, S. T. Weir, Y. K. Vohra, H. Prokop, S. A. Catledge, and G. N. Chesnut, J. Phys.: Condens. Matter **11**, 6515 (1999)
- ⁵³V. P. Dmitriev, A. Yu. Kuznetsov, O. Bandilet *et al.*, Phys. Rev. B **70**, 014104 (2004)
- ⁵⁴B. J. Baer, H. Cynn, V. Iota, C. S. Yoo, and G. Shen, Phys. Rev. B **67**, 134115 (2003)

- ⁵⁵N. C. Cunningham, N. Velisavljevic, and Y. K. Vohra, Phys. Rev. B **71**, 012108 (2005)
- ⁵⁶W. A. Grosshans and W. B. Hozapfel, Phys. Rev. B **45**, 5171 (1992)
- ⁵⁷G. N. Chesnut and Y. K. Vohra, Phys. Rev. Lett. **82**, 1712 (1999)
- ⁵⁸K. Syassen, G. Wortmann, J. Feldhaus, K. H. Frank and G. Kaindl, Phys. Rev. B **26**, 4745 (1982)
- ⁵⁹J. R. Patterson, *Dissertation* (University of Alabama at Birmingham, 2002)
- ⁶⁰N. Velisavljevic, G. N. Chesnut, and Y. K. Vohra, Phys. Rev. B. **65**, 172107 (2002)
- ⁶¹S. T. Weir, Y. K. Vohra, C. A. Vanderborgh and A. L. Ruoff, Phys. Rev. B **39**, 1280 (1989)
- ⁶²J. M. Besson, J. P. Itie, A. Polian, and G. Well, Phys. Rev. B **44**, 4214 (1991)
- ⁶³S. Minomura and H. G. Drickamen, J. Phys. Chem. Solids **23**, 451 (1962)
- ⁶⁴M. A. E-G. Salem, Turk. J. Phys. **27**, 569 (2003)
- ⁶⁵AIP Handbook, 3rd Ed., McGraw-Hill, New York (1972)
- ⁶⁶E. Knittle and R. Jeanloz, Science **223**, 53 (1984)
- ⁶⁷K. Asaumi, Phys. Rev. B **29**, 1118 (1984)
- ⁶⁸M. I. Eremets, K. Shimizu, T. C. Kobayash, and K. Amaya, Science **281**, 1333 (1998)
- ⁶⁹O. K. Andersen, Phys. Rev. B **13**, 3050 (1975)
- ⁷⁰K. Hope and Y. K. Vohra, [unpublished]
- ⁷¹H. K. Mao, Y. Wu, R. J. Hemley, L. C. Chen, J. F. Shu, L. W. Finger and D. E. Cox, Phys. Rev. Lett. **64**, 1749 (1990)
- ⁷²P. Vinet, J. Ferrante, J. H. Rose, and J. R. Smith, J. Geophys. Res. **92**, 9319 (1987)
- ⁷³Y. K. Vohra, *Recent Trends in High Pressure Research*, (ed. A. K. Singh), pp.349, Oxford & IBH Publ., New Delhi (1991)
- ⁷⁴S. Satpathy, Phys. Rev. B **33**, 8706 (1986)
- ⁷⁵P. Soderlind, Phys. Rev. B **65**, 115105 (2002)

⁷⁶V. S. Egorov and I. N. Khlyustikov, in *Handbook of Physical Quantities*, edited by I. S. Grigoriev and E. Z. Meilikhov (English translation by A. A. Radzig) (CRC 1997), pp. 549-572.

⁷⁷F. Birch, *Phys. Rev.* **71**, 809 (1947)

⁷⁸R. J. Angel, *Reviews in Mineralogy and Geochemistry* **41**, 35-60, (2001)

**GRADUATE SCHOOL
UNIVERSITY OF ALABAMA AT BIRMINGHAM
DISSERTATION APPROVAL FORM
DOCTOR OF PHILOSOPHY**

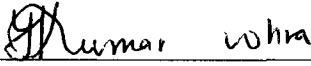
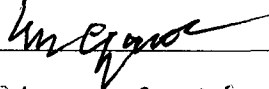
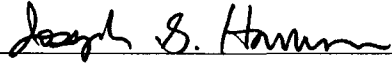
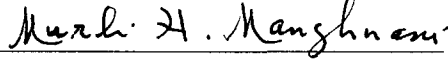
Name of Candidate Nenad Velisavljevic

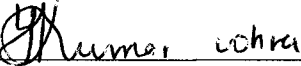
Graduate Program Physics

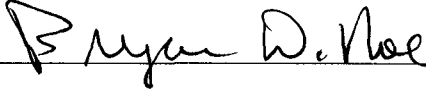
Title of Dissertation Development of the Designer Diamond Anvils and Study of
Structural and Electrical Properties of f-Electron Metals at
Ultra-High Pressures

I certify that I have read this document and examined the student regarding its content. In my opinion, this dissertation conforms to acceptable standards of scholarly presentation and is adequate in scope and quality, and the attainments of this student are such that he may be recommended for the degree of Doctor of Philosophy.

Dissertation Committee:

Name	Signature
<u>Yogesh K. Vohra</u> , Chair	<u></u>
<u>Krishan K. Chawla</u>	<u></u>
<u>Gary N. Chesnut</u>	<u></u>
<u>Joseph G. Harrison</u>	<u></u>
<u>Murli H. Manghnani</u>	<u></u>

Director of Graduate Program 

Dean, UAB Graduate School 

Date JAN 03 2006